

Several Topics for Electronics and Photonics

In the previous chapter, we introduced the principles of guided waves and learned that the mechanism of waveguiding is one in which the waves bounce obliquely between parallel planes as they progress along the structure. We studied transverse electric (TE) and transverse magnetic (TM) waves supported by plane conductors, as well as those supported by a plane dielectric slab. Thus, we restricted our study of guided waves to one-dimensional structures. In this chapter, we extend the treatment to two dimensions.

As in the previous chapter, we consider metallic waveguides, that is, those in which the TE and TM waves propagate in the medium between and parallel to the metallic boundaries of the guide, as well as optical fibers in which the supporting structure for the guided waves is a cylindrical dielectric rod surrounded by a dielectric cladding and without the presence of metallic boundaries.

We shall begin the chapter by introducing rectangular metallic waveguides, first by a geometrical extension of the parallel-plate waveguide arrangement and then by solving Maxwell's equations in two dimensions. We make use of the latter approach to study cylindrical metallic waveguides and later optical fibers. We shall also consider losses in metallic waveguides and resonators and extend our discussion of dispersion in Chapter 8 to study the phenomenon of pulse broadening, which is of particular importance in photonic systems. Finally, we shall consider the topics of interference and diffraction, and wave propagation in an anisotropic medium.

9.1 RECTANGULAR METALLIC WAVEGUIDE AND CAVITY RESONATOR

TE modes in rectangular waveguide

To introduce the rectangular metallic waveguide, we begin with TE modes in a parallel-plate waveguide. We recall that the parallel-plate waveguide is made up of two perfectly conducting sheets in the planes $x = 0$ and $x = a$, and that the electric field of the $TE_{m,0}$ mode has only a y -component with m number

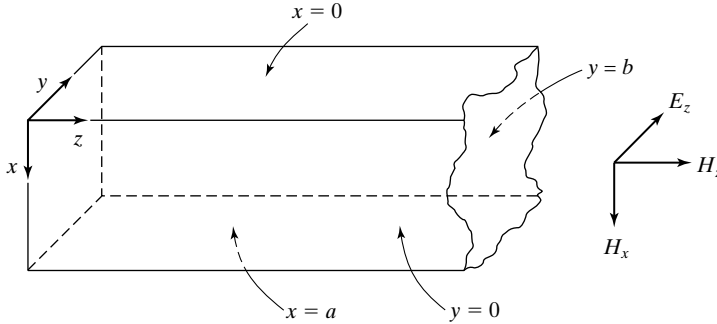


FIGURE 9.1
Rectangular waveguide.

of one-half sinusoidal variations in the x -direction and no variations in the y -direction. If we now introduce two perfectly conducting sheets in two constant- y planes, say, $y = 0$ and $y = b$, the field distribution will remain unaltered since the electric field is entirely normal to the plates, and hence the boundary condition of zero tangential electric field is satisfied for both sheets. We then have the rectangular waveguide, a metallic pipe with rectangular cross section in the xy -plane, as shown in Fig. 9.1.

Since the $TE_{m,0}$ mode field expressions derived for the parallel-plate waveguide satisfy the boundary conditions for the rectangular waveguide, those expressions as well as the entire discussion of the parallel-plate waveguide case hold also for $TE_{m,0}$ mode propagation in the rectangular waveguide case. We learned that the $TE_{m,0}$ modes can be interpreted as being due to uniform plane waves having electric field in the y -direction and bouncing obliquely between the conducting walls $x = 0$ and $x = a$, and with the associated cutoff condition characterized by bouncing of the waves back and forth normally to these walls, as shown in Fig. 9.2(a). For the cutoff condition, the dimension a is equal to m number of one-half wavelengths such that

$$\boxed{[\lambda_c]_{TE_{m,0}} = \frac{2a}{m}} \quad (9.1)$$

In a similar manner, we can have uniform plane waves having electric field in the x -direction and bouncing obliquely between the walls $y = 0$ and $y = b$, and with the associated cutoff condition characterized by bouncing of the waves back and forth normally to these walls, as shown in Fig. 9.2(b), thereby resulting in $TE_{0,n}$ modes having no variations in the x -direction and n number of one-half sinusoidal variations in the y -direction. For the cutoff condition, the dimension b is equal to n number of one-half wavelengths such that

$$\boxed{[\lambda_c]_{TE_{0,n}} = \frac{2b}{n}} \quad (9.2)$$

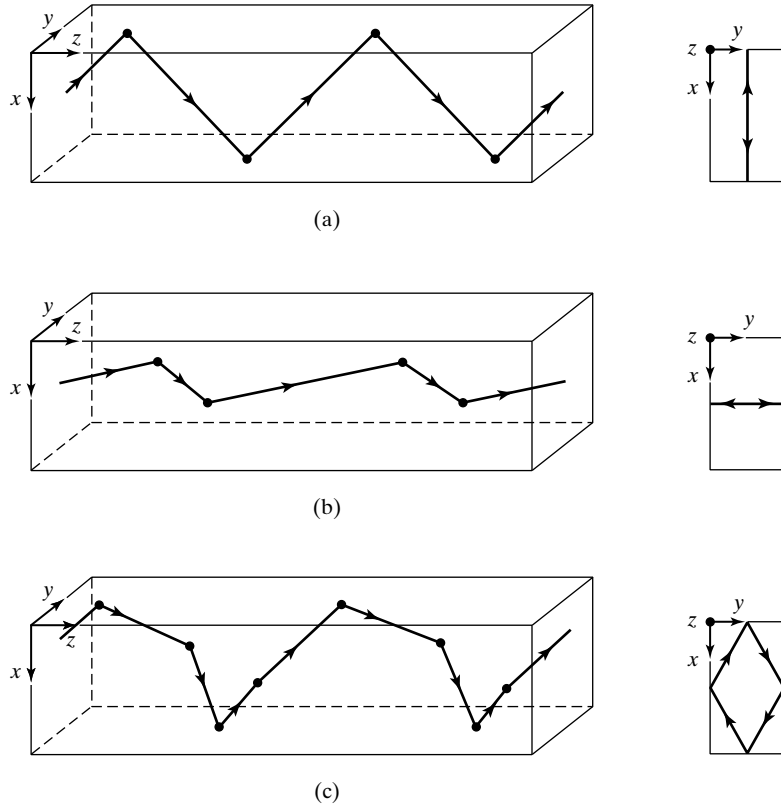


FIGURE 9.2 Propagation and cutoff of (a) $TE_{m,0}$, (b) $TE_{0,n}$, and (c) $TE_{m,n}$ modes in a rectangular waveguide.

We can even have $TE_{m,n}$ modes having m number of one-half sinusoidal variations in the x -direction and n number of one-half sinusoidal variations in the y -direction, due to uniform plane waves having both x - and y -components of the electric field and bouncing obliquely between all four walls of the guide and with the associated cutoff condition characterized by bouncing of the waves back and forth obliquely between the four walls as shown, for example, in Fig. 9.2(c). For the cutoff condition, the dimension a must be equal to m number of one-half apparent wavelengths in the x -direction, and the dimension b must be equal to n number of one-half apparent wavelengths in the y -direction such that

$$\frac{1}{[\lambda_c]_{TE_{m,n}}^2} = \frac{1}{(2a/m)^2} + \frac{1}{(2b/n)^2}$$

or

$$[\lambda_c]_{TE_{m,n}} = \frac{1}{\sqrt{(m/2a)^2 + (n/2b)^2}} \tag{9.3}$$

The discussion thus far of $TE_{m,n}$ modes in a rectangular waveguide has been based on qualitative reasoning. We shall now derive the field expressions for the TE modes. To do this, we shall first show, by making use of the expansions for the Maxwell's curl equations in Cartesian coordinates, that all transverse (x and y) field components are derivable from the longitudinal field component H_z . It is convenient to use the phasor forms of the field components and differential equations. Since all components of the fields are then dependent on t and z in the manner $e^{j[\omega t - \beta_z z]}$, we can replace $\partial/\partial t$ by $j\omega$ and $\partial/\partial z$ by $-j\beta_z$. Furthermore, $E_z = 0$ in view of TE modes and J_x, J_y , and J_z are all zero since the medium inside the waveguide is a perfect dielectric. Thus, the phasor forms of (3.12a)–(3.12c) and of the component equations of (3.22) pertinent to the discussion here are

Derivation of field expressions for TE modes

$$j\beta_z \bar{E}_y = -j\omega\mu \bar{H}_x \quad (9.4a) \quad \frac{\partial \bar{H}_z}{\partial y} + j\beta_z \bar{H}_y = j\omega\varepsilon \bar{E}_x \quad (9.4d)$$

$$-j\beta_z \bar{E}_x = -j\omega\mu \bar{H}_y \quad (9.4b) \quad -j\beta_z \bar{H}_x - \frac{\partial \bar{H}_z}{\partial x} = j\omega\varepsilon \bar{E}_y \quad (9.4e)$$

$$\frac{\partial \bar{E}_y}{\partial x} - \frac{\partial \bar{E}_x}{\partial y} = -j\omega\mu \bar{H}_z \quad (9.4c) \quad \frac{\partial \bar{H}_y}{\partial x} - \frac{\partial \bar{H}_x}{\partial y} = 0 \quad (9.4f)$$

Solving (9.4a), (9.4b), (9.4d), and (9.4e), for $\bar{E}_x, \bar{E}_y, \bar{H}_x$, and \bar{H}_y in terms of \bar{H}_z , we obtain

$$\bar{E}_x = \frac{j\omega\mu}{\beta_z^2 - \beta^2} \frac{\partial \bar{H}_z}{\partial y} \quad (9.5a)$$

$$\bar{E}_y = -\frac{j\omega\mu}{\beta_z^2 - \beta^2} \frac{\partial \bar{H}_z}{\partial x} \quad (9.5b)$$

$$\bar{H}_x = j \frac{\beta_z}{\beta_z^2 - \beta^2} \frac{\partial \bar{H}_z}{\partial x} \quad (9.5c)$$

$$\bar{H}_y = j \frac{\beta_z}{\beta_z^2 - \beta^2} \frac{\partial \bar{H}_z}{\partial y} \quad (9.5d)$$

Furthermore, by substituting (9.5a) and (9.5b) into (9.4c) and rearranging, we obtain a differential equation for \bar{H}_z as given by

$$\boxed{\frac{\partial^2 \bar{H}_z}{\partial x^2} + \frac{\partial^2 \bar{H}_z}{\partial y^2} - (\beta_z^2 - \beta^2) \bar{H}_z = 0} \quad (9.6)$$

Recall that $\beta = \omega\sqrt{\mu\varepsilon}$, so that $\beta^2 = \omega^2\mu\varepsilon$.

To solve (9.6) for \bar{H}_z , we make use of the *separation of variables* technique. This consists of assuming that the required function of the two variables x and y is the product of two functions, one of which is a function of x only and

Separation of variables technique

the second is a function of y only. Thus, denoting these functions to be \bar{X} and \bar{Y} , we have

$$\bar{H}_z(x, y, z) = \bar{X}(x)\bar{Y}(y)e^{-j\beta_z z} \quad (9.7)$$

Substituting (9.7) into (9.6), we then obtain

$$\bar{X}''(x)\bar{Y}(y) + \bar{X}(x)\bar{Y}''(y) - (\beta_z^2 - \beta^2)\bar{X}(x)\bar{Y}(y) = 0$$

or

$$\frac{\bar{X}''}{\bar{X}} + \frac{\bar{Y}''}{\bar{Y}} = \beta_z^2 - \beta^2 \quad (9.8)$$

where the primes denote differentiation with respect to the respective variables. Equation (9.8) says that a function of x only plus a function of y only is equal to a constant. For this to be satisfied, both functions must be equal to constants. Hence, we write

$$\frac{\bar{X}''}{\bar{X}} = -\beta_x^2, \text{ a constant} \quad (9.9a)$$

and

$$\frac{\bar{Y}''}{\bar{Y}} = -\beta_y^2, \text{ a constant} \quad (9.9b)$$

or

$$\frac{d^2\bar{X}}{dx^2} = -\beta_x^2\bar{X} \quad (9.10a)$$

and

$$\frac{d^2\bar{Y}}{dy^2} = -\beta_y^2\bar{Y} \quad (9.10b)$$

We have thus obtained two ordinary differential equations involving separately the two variables x and y ; hence, the technique is known as the *separation of variables* technique.

The solutions to (9.10a) and (9.10b) are given by

$$\begin{aligned} \bar{X}(x) &= \bar{A}_1 e^{j\beta_x x} + \bar{A}_2 e^{-j\beta_x x} \\ \bar{Y}(y) &= \bar{B}_1 e^{j\beta_y y} + \bar{B}_2 e^{-j\beta_y y} \end{aligned}$$

so that

$$\bar{H}_z = (\bar{A}_1 e^{j\beta_x x} + \bar{A}_2 e^{-j\beta_x x})(\bar{B}_1 e^{j\beta_y y} + \bar{B}_2 e^{-j\beta_y y})e^{-j\beta_z z} \quad (9.11)$$

where \bar{A}_1 , \bar{A}_2 , \bar{B}_1 , and \bar{B}_2 are constants. We also note from substitution of (9.9a) and (9.9b) into (9.8) that

$$-\beta_x^2 - \beta_y^2 = \beta_z^2 - \beta^2$$

or

$$\beta_z^2 = \beta^2 - \beta_x^2 - \beta_y^2 \quad (9.12)$$

Now, to determine the constants in (9.11), we make use of the boundary conditions that require that the tangential components of the electric-field intensity on all four walls of the guide be zero. Thus, we have

$$\begin{aligned} \bar{E}_x &= 0 & \text{for } y = 0, 0 < x < a \\ \bar{E}_x &= 0 & \text{for } y = b, 0 < x < a \\ \bar{E}_y &= 0 & \text{for } x = 0, 0 < y < b \\ \bar{E}_y &= 0 & \text{for } x = a, 0 < y < b \end{aligned}$$

To apply these boundary conditions to (9.11), we have to translate them into boundary conditions involving \bar{H}_z . From (9.5a) and (9.5b), these are

$$\frac{\partial \bar{H}_z}{\partial y} = 0 \quad \text{for } y = 0, 0 < x < a \quad (9.13a)$$

$$\frac{\partial \bar{H}_z}{\partial y} = 0 \quad \text{for } y = b, 0 < x < a \quad (9.13b)$$

$$\frac{\partial \bar{H}_z}{\partial x} = 0 \quad \text{for } x = 0, 0 < y < b \quad (9.13c)$$

$$\frac{\partial \bar{H}_z}{\partial x} = 0 \quad \text{for } x = a, 0 < y < b \quad (9.13d)$$

Using (9.13c) and (9.13a) in conjunction with (9.11), we get

$$\begin{aligned} \bar{A}_1 - \bar{A}_2 &= 0 & \text{or } \bar{A}_2 &= \bar{A}_1 \\ \bar{B}_1 - \bar{B}_2 &= 0 & \text{or } \bar{B}_2 &= \bar{B}_1 \end{aligned}$$

which then simplifies (9.11) to

$$\bar{H}_z = \bar{A} \cos \beta_x x \cos \beta_y y e^{-j\beta_z z} \quad (9.14)$$

where \bar{A} is a constant. Using the remaining two boundary conditions (9.13d) and (9.13b), we then obtain

$$\sin \beta_x a = 0 \quad \text{or} \quad \beta_x = \frac{m\pi}{a}, \quad m = 0, 1, 2, \dots \quad (9.15a)$$

$$\sin \beta_y b = 0 \quad \text{or} \quad \beta_y = \frac{n\pi}{b}, \quad n = 0, 1, 2, \dots \quad (9.15b)$$

Thus, the solution for \bar{H}_z for the TE_{*m,n*} mode is given by

$$\bar{H}_z = \bar{A} \cos \frac{m\pi x}{a} \cos \frac{n\pi y}{b} e^{-j\beta_z z} \quad (9.16)$$

We also note by substituting (9.15a) and (9.15b) in (9.12) that

$$\beta_z^2 = \beta^2 - \left(\frac{m\pi}{a}\right)^2 - \left(\frac{n\pi}{b}\right)^2 \quad (9.17)$$

For propagation to occur, the exponent β_z in (9.16) must be real. Hence, the cut-off condition is given by

$$\omega^2 \mu \varepsilon - \left(\frac{m\pi}{a}\right)^2 - \left(\frac{n\pi}{b}\right)^2 = 0 \quad (9.18)$$

or the cutoff frequency is given by

$$f_c = \frac{1}{\sqrt{\mu \varepsilon}} \sqrt{\left(\frac{m}{2a}\right)^2 + \left(\frac{n}{2b}\right)^2} \quad (9.19)$$

and the cutoff wavelength is

$$\begin{aligned} \lambda_c &= \frac{1}{\sqrt{\mu \varepsilon} f_c} \\ &= \frac{1}{\sqrt{(m/2a)^2 + (n/2b)^2}} \end{aligned} \quad (9.20)$$

which is the same as given by (9.3). Now, from (9.17) and (9.20), we have

$$\begin{aligned} \beta_z^2 - \beta^2 &= -\left(\frac{m\pi}{a}\right)^2 - \left(\frac{n\pi}{b}\right)^2 \\ &= -(2\pi)^2 \left[\left(\frac{m}{2a}\right)^2 + \left(\frac{n}{2b}\right)^2 \right] \\ &= -\left(\frac{2\pi}{\lambda_c}\right)^2 \end{aligned} \quad (9.21)$$

Substituting (9.16) and (9.21) into (9.5a)–(9.5d), we obtain the expressions for the transverse field components:

$$\bar{E}_x = j \frac{\omega \mu \lambda_c^2}{4\pi^2} \frac{n\pi}{b} \bar{A} \cos \frac{m\pi x}{a} \sin \frac{n\pi y}{b} e^{-j\beta_z z} \quad (9.22a)$$

$$\bar{E}_y = -j \frac{\omega \mu \lambda_c^2}{4\pi^2} \frac{m\pi}{a} \bar{A} \sin \frac{m\pi x}{a} \cos \frac{n\pi y}{b} e^{-j\beta_z z} \quad (9.22b)$$

$$\bar{H}_x = j \frac{\lambda_c^2}{2\pi\lambda_g} \frac{m\pi}{a} \bar{A} \sin \frac{m\pi x}{a} \cos \frac{n\pi y}{b} e^{-j\beta_z z} \quad (9.22c)$$

$$\bar{H}_y = j \frac{\lambda_c^2}{2\pi\lambda_g} \frac{n\pi}{b} \bar{A} \cos \frac{m\pi x}{a} \sin \frac{n\pi y}{b} e^{-j\beta_z z} \quad (9.22d)$$

Note that the sine terms in these field expressions satisfy the boundary conditions of zero tangential electric field and zero normal magnetic field at the walls of the waveguide. It can also be seen that if both m and n are equal to zero, then all transverse field components go to zero. Therefore, *for TE modes, either m or n can be zero, but both m and n cannot be zero.*

The entire procedure for the derivation of the field expressions can be repeated for TM waves by starting with the longitudinal field component \bar{E}_z . We shall not, however, pursue the derivation here; instead, we present the final expressions. This is done in Table 9.1 together with the TE mode field expressions. The upper signs of the \mp and \pm signs in these expressions refer to waves propagating in the $+z$ -direction, whereas the lower signs refer to waves propagating in the $-z$ -direction. Note from the expression for \bar{E}_z in Table 9.1

TM modes in rectangular waveguide

TABLE 9.1 Field Expressions and Associated Parameters for TE and TM Modes in a Rectangular Waveguide

Transverse electric (TE) waves	Transverse magnetic (TM) waves
Field Expressions: ($m, n = 0, 1, 2, \dots$, but not both zero)	Field Expressions: ($m, n = 1, 2, 3, \dots$)
$\bar{E}_z = 0$	$\bar{H}_z = 0$
$\bar{H}_z = \bar{A} \cos \frac{m\pi x}{a} \cos \frac{n\pi y}{b} e^{\mp j\beta_z z}$	$\bar{E}_z = \bar{A} \sin \frac{m\pi x}{a} \sin \frac{n\pi y}{b} e^{\mp j\beta_z z}$
$\bar{E}_x = j \frac{\lambda_c^2}{4\pi^2} \omega\mu \frac{n\pi}{b} \bar{A} \cos \frac{m\pi x}{a} \sin \frac{n\pi y}{b} e^{\mp j\beta_z z}$	$\bar{E}_x = \mp j \frac{\lambda_c^2}{2\pi\lambda_g} \frac{m\pi}{a} \bar{A} \cos \frac{m\pi x}{a} \sin \frac{n\pi y}{b} e^{\mp j\beta_z z}$
$\bar{E}_y = -j \frac{\lambda_c^2}{4\pi^2} \omega\mu \frac{m\pi}{a} \bar{A} \sin \frac{m\pi x}{a} \cos \frac{n\pi y}{b} e^{\mp j\beta_z z}$	$\bar{E}_y = \mp j \frac{\lambda_c^2}{2\pi\lambda_g} \frac{n\pi}{b} \bar{A} \sin \frac{m\pi x}{a} \cos \frac{n\pi y}{b} e^{\mp j\beta_z z}$
$\bar{H}_x = \mp \frac{\bar{E}_y}{\eta_g}$	$\bar{H}_x = \mp \frac{\bar{E}_y}{\eta_g}$
$\bar{H}_y = \pm \frac{\bar{E}_x}{\eta_g}$	$\bar{H}_y = \pm \frac{\bar{E}_x}{\eta_g}$
$f_c = \frac{1}{2\sqrt{\mu\epsilon}} \sqrt{\left(\frac{m}{a}\right)^2 + \left(\frac{n}{b}\right)^2}$	$f_c = \frac{1}{2\sqrt{\mu\epsilon}} \sqrt{\left(\frac{m}{a}\right)^2 + \left(\frac{n}{b}\right)^2}$
$\lambda_c = \frac{2}{\sqrt{(m/a)^2 + (n/b)^2}}$	$\lambda_c = \frac{2}{\sqrt{(m/a)^2 + (n/b)^2}}$
$\lambda_g = \frac{\lambda}{\sqrt{1 - (\lambda/\lambda_c)^2}} = \frac{\lambda}{\sqrt{1 - (f_c/f)^2}}$	$\lambda_g = \frac{\lambda}{\sqrt{1 - (\lambda/\lambda_c)^2}} = \frac{\lambda}{\sqrt{1 - (f_c/f)^2}}$
$v_{pz} = \frac{1}{\sqrt{\mu\epsilon} \sqrt{1 - (f_c/f)^2}} = \frac{1}{\sqrt{\mu\epsilon} \sqrt{1 - (\lambda/\lambda_c)^2}}$	$v_{pz} = \frac{1}{\sqrt{\mu\epsilon} \sqrt{1 - (f_c/f)^2}} = \frac{1}{\sqrt{\mu\epsilon} \sqrt{1 - (\lambda/\lambda_c)^2}}$
$\eta_g = \frac{\sqrt{\mu/\epsilon}}{\sqrt{1 - (f_c/f)^2}} = \frac{\sqrt{\mu/\epsilon}}{\sqrt{1 - (\lambda/\lambda_c)^2}}$	$\eta_g = \sqrt{\frac{\mu}{\epsilon}} \sqrt{1 - \left(\frac{f_c}{f}\right)^2} = \sqrt{\frac{\mu}{\epsilon}} \sqrt{1 - \left(\frac{\lambda}{\lambda_c}\right)^2}$

that the x - and y -variations of \bar{E}_z are sinusoidal, so that \bar{E}_z goes to zero on all four walls of the waveguide. This arises because \bar{E}_z , being longitudinal, is tangential to all four walls, and the boundary conditions require that the tangential components of \mathbf{E} be zero on the walls. It can also be seen that if either m or n is equal to zero, then $\bar{E}_z = 0$. Therefore, for *TM modes both m and n must be nonzero*. Also listed in Table 9.1 are the expressions for the cutoff frequency f_c , the cutoff wavelength λ_c , the guide wavelength λ_g , the phase velocity v_{pz} along the guide axis, and the guide characteristic impedance η_g , all of which have the same interpretations as the corresponding quantities for the parallel-plate waveguide case.

Dominant mode

The foregoing discussion of the modes of propagation in a rectangular waveguide points out that a signal of given frequency can propagate in several modes, namely, all modes for which the cutoff frequencies are less than the signal frequency or the cutoff wavelengths are greater than the signal wavelength. Waveguides are, however, designed so that only one mode, the mode with the lowest cutoff frequency (or the largest cutoff wavelength), propagates. This is known as the *dominant mode*. From Table 9.1, we can see that the dominant mode is the $\text{TE}_{1,0}$ mode or the $\text{TE}_{0,1}$ mode, depending on whether the dimension a or the dimension b is the larger of the two. By convention, the larger dimension is designated to be a , and hence the $\text{TE}_{1,0}$ mode is the dominant mode. We shall now consider an example.

Example 9.1 Finding propagating modes in a rectangular waveguide

Finding propagating modes

It is desired to determine the lowest four cutoff frequencies referred to the cutoff frequency of the dominant mode for three cases of rectangular waveguide dimensions: $b/a = 1$, $b/a = \frac{1}{2}$, and $b/a = \frac{1}{3}$. Given $a = 3$ cm, it is then desired to find the propagating mode(s) for $f = 9000$ MHz for each of the three cases.

From Table 9.1, the expression for the cutoff wavelength for a $\text{TE}_{m,n}$ mode, where $m = 0, 1, 2, 3, \dots$ and $n = 0, 1, 2, 3, \dots$ but not both m and n equal to zero, and for a $\text{TM}_{m,n}$ mode where $m = 1, 2, 3, \dots$ and $n = 1, 2, 3, \dots$, is given by

$$\lambda_c = \frac{1}{\sqrt{(m/2a)^2 + (n/2b)^2}}$$

The corresponding expression for the cutoff frequency is

$$\begin{aligned} f_c &= \frac{v_p}{\lambda_c} = \frac{1}{\sqrt{\mu\epsilon}} \sqrt{\left(\frac{m}{2a}\right)^2 + \left(\frac{n}{2b}\right)^2} \\ &= \frac{1}{2a\sqrt{\mu\epsilon}} \sqrt{m^2 + \left(n\frac{a}{b}\right)^2} \end{aligned}$$

The cutoff frequency of the dominant mode $\text{TE}_{1,0}$ is $1/2a\sqrt{\mu\epsilon}$. Hence,

$$\frac{f_c}{[f_c]_{\text{TE}_{1,0}}} = \sqrt{m^2 + \left(n\frac{a}{b}\right)^2}$$

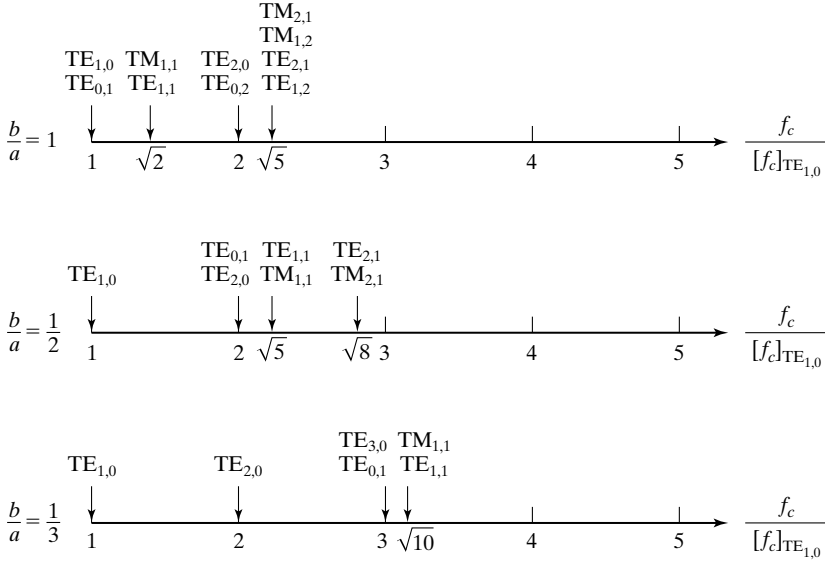


FIGURE 9.3

Lowest four cutoff frequencies referred to the cutoff frequency of the dominant mode for three cases of rectangular waveguide dimensions.

By assigning different pairs of values for m and n , the lowest four values of $f_c/[f_c]_{TE_{1,0}}$ can be computed for each of the three specified values of b/a . These computed values and the corresponding modes are shown in Fig. 9.3.

For $a = 3$ cm, and assuming free space for the dielectric in the waveguide,

$$[f_c]_{TE_{1,0}} = \frac{1}{2a\sqrt{\mu\epsilon}} = \frac{3 \times 10^8}{2 \times 0.03} = 5000 \text{ MHz}$$

Hence, for a signal of frequency $f = 9000$ MHz, all the modes for which $f_c/[f_c]_{TE_{1,0}}$ is less than 1.8 propagate. From Fig. 9.3, these are

$$\begin{array}{ll} TE_{1,0}, TE_{0,1}, TM_{1,1}, TE_{1,1} & \text{for } b/a = 1 \\ TE_{1,0} & \text{for } b/a = \frac{1}{2} \\ TE_{1,0} & \text{for } b/a = \frac{1}{3} \end{array}$$

It can be seen from Fig. 9.3 that for $b/a \leq \frac{1}{2}$, the second lowest cutoff frequency which corresponds to that of the $TE_{2,0}$ mode is twice the cutoff frequency of the dominant mode $TE_{1,0}$. For this reason, the dimension b of a rectangular waveguide is generally chosen to be less than or equal to $a/2$, in order to achieve single-mode transmission over a complete octave (factor of 2) range of frequencies.

As in the case of the parallel-plate waveguide, reflection and transmission at discontinuities in rectangular waveguides can be studied by using the transmission-line analogy. We shall illustrate this by means of an example.

Transmission-line analogy

Example 9.2 Application of transmission-line analogy to a rectangular waveguide system

A rectangular waveguide extending in the z -direction and having the dimensions $a = 4$ cm and $b = 2$ cm has a dielectric discontinuity at $z = 0$, as shown in Fig. 9.4. For $TE_{1,0}$ waves of frequency $f = 5000$ MHz incident from section 1, we wish to find (a) the transmission-line equivalent and (b) the length and the permittivity of a quarter-wave section required to achieve a match between the two sections.

- (a) First, we note that for the $TE_{1,0}$ mode, $\lambda_c = 2a = 8$ cm for both sections. For $f = 5000$ MHz, the wavelength in free space is $\lambda_1 = 6$ cm and the wavelength in a dielectric of permittivity $9\epsilon_0$ is $\lambda_2 = 2$ cm. Since λ_1 and λ_2 are both less than λ_c , the $TE_{1,0}$ mode propagates in both sections. Denoting the guide parameters associated with sections 1 and 2 by subscripts 1 and 2, respectively, we then obtain

$$\eta_{g1} = \frac{\eta_1}{\sqrt{1 - (\lambda_1/\lambda_c)^2}} = \frac{377}{\sqrt{1 - (6/8)^2}} = 570 \Omega$$

$$\eta_{g2} = \frac{\eta_2}{\sqrt{1 - (\lambda_2/\lambda_c)^2}} = \frac{377/3}{\sqrt{1 - (2/8)^2}} = 129.8 \Omega$$

Thus, the transmission-line equivalent is as shown in Fig. 9.5.

- (b) The characteristic impedance of a quarter-wave section required to achieve a match between line 1 and line 2 must be equal to $\sqrt{\eta_{g1}\eta_{g2}}$. Denoting the parameters associated with the quarter-wave section by subscript 3, we then have

$$\eta_{g3} = \frac{\eta_3}{\sqrt{1 - (\lambda_3/\lambda_c)^2}} = \sqrt{\eta_{g1}\eta_{g2}}$$

or

$$\frac{\eta_1 \sqrt{\epsilon_0/\epsilon_3}}{\sqrt{1 - (\lambda_1/\lambda_c)^2(\epsilon_0/\epsilon_3)}} = \sqrt{\eta_{g1}\eta_{g2}}$$

$$\frac{\epsilon_0/\epsilon_3}{1 - (6/8)^2(\epsilon_0/\epsilon_3)} = \frac{570 \times 129.8}{(377)^2} = 0.5205$$

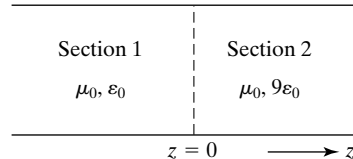
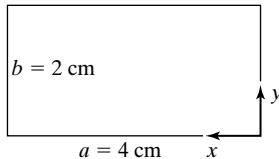


FIGURE 9.4
Rectangular waveguide discontinuity.

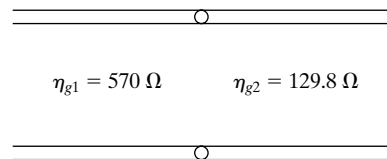


FIGURE 9.5
Transmission-line equivalent for the rectangular waveguide discontinuity of Fig. 9.4 for $TE_{1,0}$ waves of frequency 5000 MHz.

solving which we obtain $\epsilon_3 = 2.484\epsilon_0$. To find the length of the quarter-wave section, we compute

$$\begin{aligned}\lambda_{g3} &= \frac{\lambda_3}{\sqrt{1 - (\lambda_3/\lambda_c)^2}} = \frac{\lambda_1 \sqrt{\epsilon_0/\epsilon_3}}{\sqrt{1 - (\lambda_1/\lambda_c)^2 (\epsilon_0/\epsilon_3)}} \\ &= \frac{6 \times 0.6345}{\sqrt{1 - (9/16) \times 0.4026}} = 4.33 \text{ cm}\end{aligned}$$

Thus, the length of the quarter-wave section is $\lambda_{g3}/4$, or 1.0825 cm.

Let us now consider guided waves of equal amplitude propagating in the positive z - and negative z -directions in a rectangular waveguide. This can be achieved by terminating the guide by a perfectly conducting sheet in a constant- z plane, that is, a transverse plane of the guide. Due to perfect reflection from the sheet, the fields will then be characterized by standing wave nature along the guide axis, that is, in the z -direction, in addition to the standing wave nature in the x - and y -directions. The standing wave pattern along the guide axis will have nulls of transverse electric field on the terminating sheet and in planes parallel to it at distances of integer multiples of $\lambda_g/2$ from that sheet. Placing of perfect conductors in these planes will not disturb the fields, since the boundary condition of a zero tangential electric field is satisfied in those planes.

Cavity resonator

Conversely, if we place two perfectly conducting sheets in two constant- z planes separated by a distance d , then, for the boundary conditions to be satisfied, d must be equal to an integer multiple of $\lambda_g/2$. We then have a rectangular box of dimensions a , b , and d in the x -, y -, and z -directions, respectively, as shown in Fig. 9.6. Such a structure is known as a *cavity resonator* and is the counterpart of the low-frequency lumped parameter resonant circuit at microwave frequencies, since it supports oscillations at frequencies for which the foregoing condition, that is,

$$d = l \frac{\lambda_g}{2}, \quad l = 1, 2, 3, \dots \quad (9.23)$$

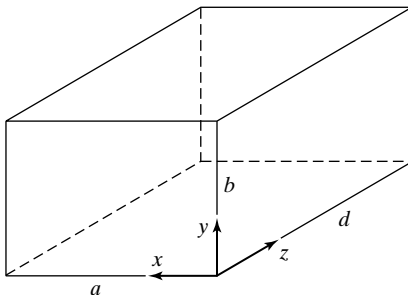


FIGURE 9.6
Rectangular cavity resonator.

is satisfied. Substituting for λ_g in (9.23) from Table 9.1 and rearranging, we obtain

$$\frac{2d}{l} = \frac{\lambda}{\sqrt{1 - (\lambda/\lambda_c)^2}}$$

or

$$\frac{1}{\lambda^2} - \frac{1}{\lambda_c^2} = \left(\frac{l}{2d}\right)^2$$

which upon substitution for λ_c gives

$$\begin{aligned} \frac{1}{\lambda^2} &= \left(\frac{m}{2a}\right)^2 + \left(\frac{n}{2b}\right)^2 + \left(\frac{l}{2d}\right)^2 \\ \lambda &= \frac{1}{\sqrt{(m/2a)^2 + (n/2b)^2 + (l/2d)^2}} \end{aligned} \quad (9.24)$$

The expression for the frequencies of oscillation is thus given by

$$f_{\text{osc}} = \frac{v_p}{\lambda} = \frac{1}{\sqrt{\mu\varepsilon}} \sqrt{\left(\frac{m}{2a}\right)^2 + \left(\frac{n}{2b}\right)^2 + \left(\frac{l}{2d}\right)^2} \quad (9.25)$$

The modes are designated by three subscripts in the manner $\text{TE}_{m,n,l}$ and $\text{TM}_{m,n,l}$. Since m , n , and l can assume combinations of integer values, an infinite number of frequencies of oscillation are possible for a given set of dimensions of the cavity resonator. Also, a given frequency of oscillation may correspond to more than one mode. We recall that for TE modes $m, n = 0, 1, 2, \dots$, but not both zero, whereas for TM modes $m, n = 1, 2, 3, \dots$. For both TE and TM modes $l = 1, 2, 3, \dots$, as given in (9.23). In addition TM modes at cutoff ($\beta_z = 0$, $\lambda_g = \infty$ and $\eta_g = 0$) satisfy the boundary conditions since then \bar{E}_x and \bar{E}_y both go to zero. Hence, for TM modes $l = 0$ is allowed. We shall now consider an example.

Example 9.3 Finding the frequencies of oscillation for a rectangular cavity resonator

The dimensions of a rectangular cavity resonator with air dielectric are $a = 4$ cm, $b = 2$ cm, and $d = 4$ cm. It is desired to determine the three lowest frequencies of oscillation and specify the mode(s) of oscillation, transverse with respect to the z -direction, for each frequency.

By substituting $\mu = \mu_0$, $\varepsilon = \varepsilon_0$, and the given dimensions for a , b , and d in (9.25), we obtain

$$\begin{aligned} f_{\text{osc}} &= 3 \times 10^8 \sqrt{\left(\frac{m}{0.08}\right)^2 + \left(\frac{n}{0.04}\right)^2 + \left(\frac{l}{0.08}\right)^2} \\ &= 3750 \sqrt{m^2 + 4n^2 + l^2} \text{ MHz} \end{aligned}$$

By assigning combinations of integer values for m , n , and l and keeping in mind the restrictions on these values as discussed, we obtain the three lowest frequencies of oscillation and the corresponding modes to be

$$\begin{aligned} 3750 \times \sqrt{2} &= 5303 \text{ MHz} && \text{for TE}_{1,0,1} \text{ mode} \\ 3750 \times \sqrt{5} &= 8385 \text{ MHz} && \text{for TE}_{0,1,1}, \text{TE}_{2,0,1}, \text{TE}_{1,0,2}, \text{and TM}_{1,1,0} \text{ modes} \\ 3750 \times \sqrt{6} &= 9186 \text{ MHz} && \text{for TE}_{1,1,1} \text{ and TM}_{1,1,1} \text{ modes} \end{aligned}$$

- K9.1.** Rectangular waveguide; TE and TM modes; Dominant mode; Cavity resonator; Frequency of oscillation.
- D9.1.** A generator of fundamental frequency 2000 MHz and rich in harmonics excites a rectangular waveguide. Find all frequencies that propagate in only TE modes for each of the following cases: **(a)** $a = 5$ cm, $b = 2.5$ cm, $\varepsilon = \varepsilon_0$; **(b)** $a = 4.5$ cm, $b = 1.5$ cm, $\varepsilon = 4\varepsilon_0$; and **(c)** $a = 6$ cm, $b = 6$ cm, $\varepsilon = \varepsilon_0$. Assume that $\mu = \mu_0$ for all cases.
Ans. **(a)** 4000, 6000 MHz; **(b)** 2000, 4000 MHz; **(c)** None.
- D9.2.** For the rectangular waveguide discontinuity of Fig. 9.4, find the power reflection coefficient for incidence from section 1 for each of the following cases: **(a)** TE_{1,0} wave of frequency $f = 10,000$ MHz; **(b)** TE_{1,1} wave of frequency $f = 10,000$ MHz; and **(c)** TM_{1,1} wave of frequency $f = 10,000$ MHz.
Ans. **(a)** 0.2756; **(b)** 0.4649; **(c)** 0.0676.
- D9.3.** The frequencies of oscillation for an air-dielectric rectangular cavity resonator of dimensions a , b , and d , in the x -, y -, and z -directions, respectively, are given for three modes as follows:

$$\begin{aligned} f_{\text{osc}} &= 3000\sqrt{5} \text{ MHz for TE}_{1,0,1} \text{ mode} \\ f_{\text{osc}} &= 3000\sqrt{26} \text{ MHz for TE}_{0,1,1} \text{ mode} \\ f_{\text{osc}} &= 3000\sqrt{30} \text{ MHz for TM}_{1,1,1} \text{ mode} \end{aligned}$$

Find the values of a , b , and d in cm.

Ans. 2.5 cm, 1 cm, 5 cm.

9.2 CYLINDRICAL METALLIC WAVEGUIDE AND CAVITY RESONATOR

Thus far in this chapter, we have been concerned with the guiding of waves between metallic boundaries involving rectangular geometries. We shall now extend the treatment to cylindrical geometry by considering the case of a cylindrical waveguide, which is simply a hollow tube of circular cross section of a radius a and extending along the z -direction, as shown in Fig. 9.7. Thus, for TM waves in a cylindrical waveguide,

$$H_z = 0 \quad E_z \neq 0$$

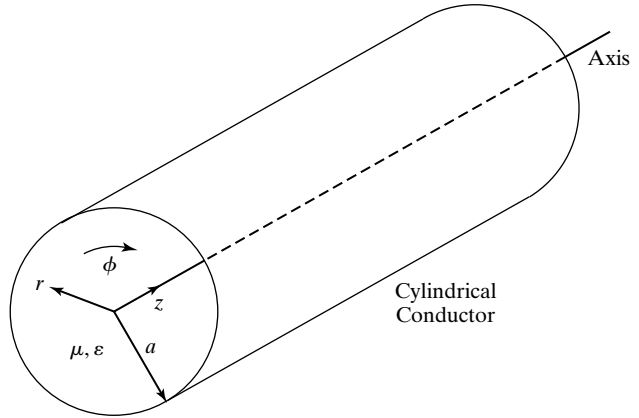


FIGURE 9.7
A cylindrical waveguide
extending in the z -direction.

and all other field components can be expressed in terms of E_z , whereas for TE waves,

$$E_z = 0 \quad H_z \neq 0$$

and all other field components can be expressed in terms of H_z .

*Solution of
Maxwell's
curl
equations in
cylindrical
coordinates*

To derive the field expressions for TM and TE modes in a cylindrical waveguide, we begin with Maxwell's curl equations in cylindrical coordinates and proceed similarly to the rectangular waveguide case, using the phasor forms of the field components in the manner $e^{j[\omega t \mp \beta_z z]}$, where the upper and lower signs represent wave propagation in the $+z$ - and $-z$ -directions, respectively. Thus, replacing $\partial/\partial t$ by $j\omega$ and $\partial/\partial z$ by $\mp j\beta_z$ in the expansions for Maxwell's curl equations in cylindrical coordinates, we have for a perfect dielectric medium inside the waveguide,

$$\frac{1}{r} \frac{\partial \bar{E}_z}{\partial \phi} \pm j\beta_z \bar{E}_\phi = -j\omega\mu \bar{H}_r \quad (9.26a)$$

$$\mp j\beta_z \bar{E}_r - \frac{\partial \bar{E}_z}{\partial r} = -j\omega\mu \bar{H}_\phi \quad (9.26b)$$

$$\frac{1}{r} \frac{\partial}{\partial r} (r \bar{E}_\phi) - \frac{1}{r} \frac{\partial \bar{E}_r}{\partial \phi} = -j\omega\mu \bar{H}_z \quad (9.26c)$$

$$\frac{1}{r} \frac{\partial \bar{H}_z}{\partial \phi} \pm j\beta_z \bar{H}_\phi = j\omega\epsilon \bar{E}_r \quad (9.26d)$$

$$\mp j\beta_z \bar{H}_r - \frac{\partial \bar{H}_z}{\partial r} = j\omega\epsilon \bar{E}_\phi \quad (9.26e)$$

$$\frac{1}{r} \frac{\partial}{\partial r} (r \bar{H}_\phi) - \frac{1}{r} \frac{\partial \bar{H}_r}{\partial \phi} = j\omega\epsilon \bar{E}_z \quad (9.26f)$$

Solving (9.26a), (9.26b), (9.26d), and (9.26e), we obtain

$$\bar{E}_r = \frac{1}{\beta_z^2 - \beta^2} \left[\pm j\beta_z \frac{\partial \bar{E}_z}{\partial r} + \frac{j\omega\mu}{r} \frac{\partial \bar{H}_z}{\partial \phi} \right] \quad (9.27a)$$

$$\bar{E}_\phi = -\frac{1}{\beta_z^2 - \beta^2} \left[\mp j\frac{\beta_z}{r} \frac{\partial \bar{E}_z}{\partial \phi} + j\omega\mu \frac{\partial \bar{H}_z}{\partial r} \right] \quad (9.27b)$$

$$\bar{H}_z = -\frac{1}{\beta_z^2 - \beta^2} \left[\frac{j\omega\varepsilon}{r} \frac{\partial \bar{E}_z}{\partial \phi} \mp j\beta_z \frac{\partial \bar{H}_z}{\partial r} \right] \quad (9.27c)$$

$$\bar{H}_\phi = \frac{1}{\beta_z^2 - \beta^2} \left[j\omega\varepsilon \frac{\partial \bar{E}_z}{\partial r} \pm j\frac{\beta_z}{r} \frac{\partial \bar{H}_z}{\partial \phi} \right] \quad (9.27d)$$

thereby expressing the transverse field components in terms of the longitudinal field components. Recall that $\beta^2 = \omega^2\mu\varepsilon$.

Now, setting $\bar{H}_z = 0$ and substituting for \bar{H}_r and \bar{H}_ϕ in (9.26f), we obtain the differential equation for \bar{E}_z for the TM-mode case

$$\frac{1}{r} \frac{\partial}{\partial r} \left(r \frac{\partial \bar{E}_z}{\partial r} \right) + \frac{1}{r^2} \frac{\partial^2 \bar{E}_z}{\partial \phi^2} - (\beta_z^2 - \beta^2) \bar{E}_z = 0 \quad (9.28a)$$

Similarly, setting $\bar{E}_z = 0$ and substituting for \bar{E}_r and \bar{E}_ϕ in (9.26c), we obtain the differential equation for \bar{H}_z for the TE-mode case

$$\frac{1}{r} \frac{\partial}{\partial r} \left[r \frac{\partial \bar{H}_z}{\partial r} \right] + \frac{1}{r^2} \frac{\partial^2 \bar{H}_z}{\partial \phi^2} - (\beta_z^2 - \beta^2) \bar{H}_z = 0 \quad (9.28b)$$

In view of the similarity of (9.28a) and (9.28b), we let $\bar{\psi}$ stand for \bar{E}_z in the case of TM waves and \bar{H}_z in the case of TE waves and consider the solution of the differential equation

$$\frac{1}{r} \frac{\partial}{\partial r} \left(r \frac{\partial \bar{\psi}}{\partial r} \right) + \frac{1}{r^2} \frac{\partial^2 \bar{\psi}}{\partial \phi^2} - (\beta_z^2 - \beta^2) \bar{\psi} = 0$$

or

$$\boxed{\frac{1}{r} \frac{\partial}{\partial r} \left[r \frac{\partial \bar{\psi}}{\partial r} \right] + \frac{1}{r^2} \frac{\partial^2 \bar{\psi}}{\partial \phi^2} - \beta_c^2 \bar{\psi} = 0} \quad (9.29)$$

where

$$\boxed{\beta_c^2 = \beta^2 - \beta_z^2} \quad (9.30)$$

To solve this equation, we make use of the separation of variables technique as in Section 9.1. Thus, letting

$$\bar{\psi} = \bar{R}(r)\bar{\Phi}(\phi)e^{\mp j\beta_z z} \quad (9.31)$$

and substituting into (9.29), we have

$$\bar{\Phi} \frac{1}{r} \frac{\partial}{\partial r} \left(r \frac{\partial \bar{R}}{\partial r} \right) + \frac{\bar{R}}{r^2} \frac{\partial^2 \bar{\Phi}}{\partial \phi^2} + \beta_c^2 \bar{R} \bar{\Phi} = 0$$

or

$$\frac{r}{\bar{\Phi}} (\bar{R}' + r \bar{R}'') + \beta_c^2 r^2 = -\frac{\bar{\Phi}''}{\bar{\Phi}} = n^2, \text{ a constant} \quad (9.32)$$

where the primes denote differentiation with respect to the respective variables, thereby obtaining the two separate differential equations

$$\bar{\Phi}'' + n^2 \bar{\Phi} = 0 \quad (9.33a)$$

$$\bar{R}'' + \frac{1}{r} \bar{R}' + \left(\beta_c^2 - \frac{n^2}{r^2} \right) \bar{R} = 0 \quad (9.33b)$$

Bessel functions

The solution for (9.33a) is of the form

$$\bar{\Phi}(\phi) = \bar{A}_n \cos n\phi + \bar{B}_n \sin n\phi \quad (9.34a)$$

where \bar{A}_n and \bar{B}_n are constants. Equation (9.33b) is a Bessel's equation that has the solution

$$\bar{R}(r) = \bar{C}_n J_n(\beta_c r) + \bar{D}_n N_n(\beta_c r) \quad (9.34b)$$

where \bar{C}_n and \bar{D}_n are constants, and

$$\begin{aligned} J_n(\beta_c r) &= \text{Bessel function of the first kind of order } n \text{ and argument } \beta_c r \\ N_n(\beta_c r) &= \text{Bessel function of the second kind of order } n \text{ and argument } \beta_c r \end{aligned}$$

The variations of $J_n(x)$ and $N_n(x)$ with their argument x are shown for a few values of n in Figs. 9.8(a) and (b), respectively. The function $N_n(x)$ has the property that $N_n(0) \rightarrow \infty$ for all orders. Since the fields must remain finite inside the guide, which includes $r = 0$ (the z -axis), it follows that \bar{D}_n must be zero. Hence, the solution for $\bar{R}(r)$ pertinent to the cylindrical waveguide problem is given by

$$\bar{R}(r) = \bar{C}_n J_n(\beta_c r)$$

The solution for $\bar{\psi}$ is thus given by

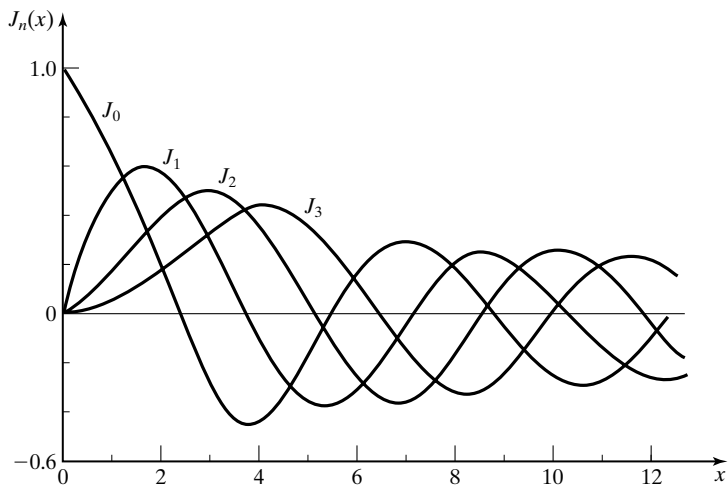
$$\bar{\psi} = J_n(\beta_c r) (\bar{A}_n \cos n\phi + \bar{B}_n \sin n\phi) e^{\mp j\beta_z z} \quad (9.35)$$

where we have absorbed \bar{C}_n into \bar{A}_n and \bar{B}_n . This is the general solution for $\bar{\psi}$, which we use for \bar{E}_z in the case of TM waves and the \bar{H}_z in the case of TE waves to obtain their particular solutions satisfying the boundary conditions.

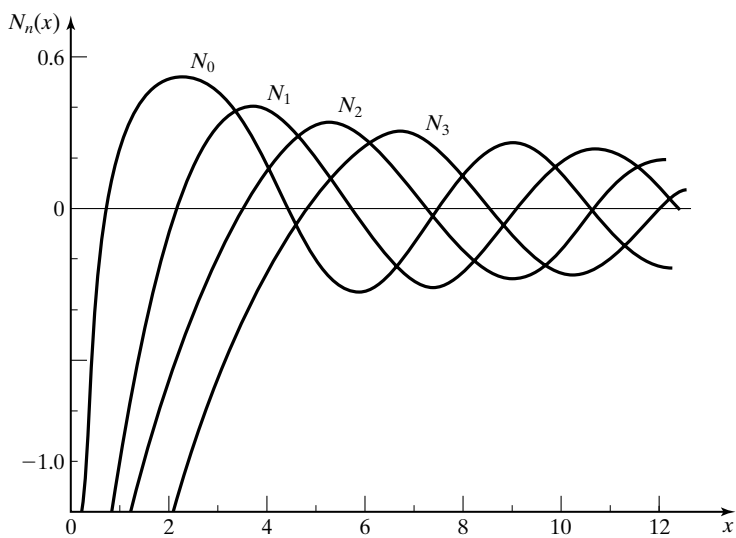
TM modes

For TM modes, $\bar{H}_z = 0$ and $\bar{\psi} = \bar{E}_z$. Hence,

$$\bar{E}_z = J_n(\beta_c r) (\bar{A}_n \cos n\phi + \bar{B}_n \sin n\phi) e^{\mp j\beta_z z} \quad (9.36)$$



(a)



(b)

FIGURE 9.8

Variations of (a) $J_n(x)$ and (b) $N_n(x)$, with the argument x for a few values of n .

Since for a cylindrical waveguide, $0 \leq \phi \leq 2\pi$ and \bar{E}_z must be a single-valued function, the solution must be periodic in ϕ with a period 2π . This requires that n be an integer. Thus,

$$n = 0, 1, 2, 3, \dots$$

The boundary condition at $r = a$ requires that the tangential component of $\bar{\mathbf{E}}$ be zero. Since \bar{E}_z is tangential, it follows that $[\bar{E}_z]_{r=a} = 0$ for all ϕ , giving us

$$0 = J_n(\beta_c a)(\bar{A}_n \cos n\phi + \bar{B}_n \sin n\phi)e^{\mp j\beta_z z}$$

or

$$\boxed{J_n(\beta_c a) = 0} \quad (9.37)$$

Note that this also makes the remaining tangential component \bar{E}_ϕ equal to zero at $r = a$ since from (9.27b), $\bar{E}_\phi \propto \partial \bar{E}_z / \partial \phi$. Equation (9.37) tells us that only certain values of $\beta_c a$ and hence of β_c are allowed. These are the values for which the Bessel function goes to zero, that is, they are the roots of the equation

$$J_n(x) = 0 \quad (9.38)$$

For a given value of n , there are an infinite number of roots as can be seen from Fig. 9.8(a). Denoting the number of the root to be m , we list in Table 9.2 the lowest three ($m = 1, 2, 3$) nonvanishing roots for the first five values of n ($n = 0, 1, 2, 3, 4$).

With the understanding that the values of $\beta_c a$ are given by those in Table 9.2, we can obtain the expressions for the transverse-field components by noting that $\bar{H}_z = 0$ and substituting (9.36) into (9.27a)–(9.27d):

$$\bar{E}_r = \mp j \frac{\beta_z}{\beta_c} J'_n(\beta_c r)(\bar{A}_n \cos n\phi + \bar{B}_n \sin n\phi)e^{\mp j\beta_z z} \quad (9.39a)$$

$$\bar{E}_\phi = \pm j \frac{\beta_z n}{\beta_c^2 r} J_n(\beta_c r)(\bar{A}_n \sin n\phi - \bar{B}_n \cos n\phi)e^{\mp j\beta_z z} \quad (9.39b)$$

$$\bar{H}_r = \mp \frac{\omega \epsilon}{\beta_z} \bar{E}_\phi \quad (9.39c)$$

$$\bar{H}_\phi = \pm \frac{\omega \epsilon}{\beta_z} \bar{E}_r \quad (9.39d)$$

In (9.39a), the prime associated with J_n denotes differentiation with respect to the argument $\beta_c r$.

The allowed values of $\beta_c a$ may be written as $(\beta_c a)_{n,m}$, where the first subscript refers to the order of the Bessel function and the second subscript denotes the m th root of the n th order Bessel function. The corresponding modes are designated as $\text{TM}_{n,m}$ modes. In terms of the field configurations, the first

TABLE 9.2 Roots of $J_n(x)$

$m \backslash n$	0	1	2	3	4
1	2.40	3.83	5.14	6.38	7.59
2	5.52	7.02	8.42	9.76	11.06
3	8.65	10.17	11.62	13.02	14.37

subscript refers to the number of complete sinusoidal variations of the field components in the ϕ direction. For example, $n = 0$ means that the field components have no variations in ϕ , $n = 1$ means that they have one sinusoidal variation in ϕ , and so on. The second subscript refers to the number of quasi half-cycle variations (except that in the case of $n = 0$, the first one is a one-quarter cycle) of the field components in the r direction in accordance with the behavior of the Bessel functions, as shown in Fig. 9.8(a), and their derivatives, depending upon the component.

For TE modes, $\bar{E}_z = 0$ and $\bar{\psi} = \bar{H}_z$. Hence,

TE modes

$$\boxed{\bar{H}_z = J_n(\beta_c r)(\bar{A}_n \cos n\phi + \bar{B}_n \sin n\phi)e^{\mp j\beta_c z}} \quad (9.40)$$

Again, n must be an integer as in the case of TM modes, since the solution must be periodic in ϕ with period 2π in order that \bar{H}_z is single-valued. Thus,

$$n = 0, 1, 2, 3, \dots$$

The boundary condition at $r = a$ requires that the tangential component of $\bar{\mathbf{E}}$ be zero. Since $\bar{E}_z = 0$ for TE modes, we need to consider \bar{E}_ϕ , which is the remaining tangential component of $\bar{\mathbf{E}}$. From (9.27b), we note that $\bar{E}_\phi \propto \partial\bar{H}_z/\partial r$. Thus, we have

$$\left[\frac{\partial\bar{H}_z}{\partial r} \right]_{r=a} = 0$$

or

$$0 = J'_n(\beta_c a)(\bar{A}_n \cos n\phi + \bar{B}_n \sin n\phi)e^{\mp j\beta_c z}$$

where the prime associated with J_n denotes the derivative of the Bessel function. It follows that

$$\boxed{J'_n(\beta_c a) = 0} \quad (9.41)$$

Equation (9.41) tells us that again in this case, only certain values of $\beta_c a$, and hence of β_c , are allowed. These are the values for which the derivative of the Bessel function goes to zero, that is, they are the roots of the equation

$$J'_n(x) = 0 \quad (9.42)$$

It can be seen by visualizing the derivatives of the graphs of the Bessel functions in Fig. 9.8(a) that for a given value of n , there are infinite number of roots for (9.42), corresponding to the points at which the slopes of the Bessel functions are zero. Denoting the number of the root to be m , we list in Table 9.3 the lowest three ($m = 1, 2, 3$) nonvanishing roots for the first five values of n ($n = 0, 1, 2, 3, 4$).

With the understanding that the values of $\beta_c a$ are given by those in Table 9.3, we can obtain the expressions for the transverse field components by noting that

TABLE 9.3 Roots of $J'_n(x)$

$m \backslash n$	0	1	2	3	4
1	3.83	1.84	3.05	4.20	5.32
2	7.02	5.33	6.71	8.02	9.28
3	10.17	8.54	9.97	11.35	12.68

$\bar{E}_z = 0$ and substituting (9.40) into (9.27a)–(9.27b):

$$\bar{E}_r = j \frac{\omega\mu n}{\beta_c^2 r} J_n(\beta_c r) (\bar{A}_n \sin n\phi - \bar{B}_n \cos n\phi) e^{\mp j\beta_z z} \quad (9.43a)$$

$$\bar{E}_\phi = j \frac{\omega\mu}{\beta_c} J'_n(\beta_c r) (\bar{A}_n \cos n\phi + \bar{B}_n \sin n\phi) e^{\mp j\beta_z z} \quad (9.43b)$$

$$\bar{H}_r = \mp \frac{\beta_z}{\omega\mu} \bar{E}_\phi \quad (9.43c)$$

$$\bar{H}_\phi = \pm \frac{\beta_z}{\omega\mu} \bar{E}_r \quad (9.43d)$$

The allowed values of $\beta_c a$ may once again be written as $(\beta_c a)_{n,m}$ and the modes designated as $\text{TE}_{n,m}$ modes. As in the case of $\text{TM}_{n,m}$ modes, the first subscript refers to the number of complete sinusoidal variations of the field components in the ϕ direction. The second subscript refers to the number of quasi-half-cycle variations (except that for $n \neq 0$, the first one is a one-quarter cycle) of the field components in the r direction.

Characteristics of TM and TE modes Let $(\beta_c)_{n,m}$ be the values of β_c for the (n,m) th mode found from the roots of $J_n(\beta_c a)$ for TM modes and of $J'_n(\beta_c a)$ for TE modes. Then recalling that

$$\beta_c^2 = \beta^2 - \beta_z^2 = \omega^2 \mu \epsilon - \beta_z^2$$

and that the cutoff condition occurs for β_z equal to zero, we note that the cutoff frequencies are given by

$$\omega^2 \mu \epsilon = (\beta_c)_{n,m}^2$$

$$(f_c)_{n,m} = \frac{(\beta_c)_{n,m}}{2\pi \sqrt{\mu \epsilon}} \quad (9.44)$$

and the cutoff wavelengths are given by

$$\begin{aligned} (\lambda_c)_{n,m} &= \frac{1}{\sqrt{\mu \epsilon} (f_c)_{n,m}} \\ &= \frac{2\pi}{(\beta_c)_{n,m}} \end{aligned} \quad (9.45)$$

Proceeding further, for the propagating range of frequencies for a given mode, we have from (9.30),

$$\begin{aligned}\beta_z^2 &= \beta^2 - \beta_c^2 \\ &= \left(\frac{2\pi}{\lambda}\right)^2 \left[1 - \left(\frac{f_c}{f}\right)^2\right] \\ &= \left(\frac{2\pi}{\lambda}\right)^2 \left[1 - \left(\frac{\lambda}{\lambda_c}\right)^2\right]\end{aligned}$$

or

$$\lambda_g = \frac{\lambda}{\sqrt{1 - (f_c/f)^2}} = \frac{\lambda}{\sqrt{1 - (\lambda/\lambda_c)^2}} \quad (9.46)$$

The phase velocity along the guide axis is given by

$$v_{pz} = \lambda_g f = \frac{1}{\sqrt{\mu\varepsilon}} \frac{1}{\sqrt{1 - (f_c/f)^2}} = \frac{1}{\sqrt{\mu\varepsilon}} \frac{1}{\sqrt{1 - (\lambda/\lambda_c)^2}} \quad (9.47)$$

Finally, by taking the ratios of appropriate pairs of transverse electric- and magnetic-field components given by (9.39a)–(9.39d) for TM modes and (9.43a)–(9.43d) for TE modes, we obtain the guide characteristic impedances to be

$$\begin{aligned}[\eta_g]_{\text{TM}} &= \frac{\bar{E}_r}{\pm \bar{H}_\phi} = \frac{\bar{E}_\phi}{\mp \bar{H}_r} = \frac{\beta_z}{\omega\varepsilon} = \frac{2\pi}{\lambda_g \omega\varepsilon} = \sqrt{\frac{\mu}{\varepsilon}} \frac{\lambda}{\lambda_g} \\ &= \sqrt{\frac{\mu}{\varepsilon}} \sqrt{1 - \left(\frac{f_c}{f}\right)^2} = \sqrt{\frac{\mu}{\varepsilon}} \sqrt{1 - \left(\frac{\lambda}{\lambda_c}\right)^2}\end{aligned} \quad (9.48a)$$

and

$$\begin{aligned}[\eta_g]_{\text{TE}} &= \frac{\bar{E}_r}{\pm \bar{H}_\phi} = \frac{\bar{E}_\phi}{\mp \bar{H}_r} = \frac{\omega\mu}{\beta_z} = \frac{\omega\mu\lambda_g}{2\pi} = \sqrt{\frac{\mu}{\varepsilon}} \frac{\lambda_g}{\lambda} \\ &= \frac{\sqrt{\mu/\varepsilon}}{\sqrt{1 - (f_c/f)^2}} = \frac{\sqrt{\mu/\varepsilon}}{\sqrt{1 - (\lambda/\lambda_c)^2}}\end{aligned} \quad (9.48b)$$

Note that the expressions (9.46)–(9.48b) are the same as the corresponding expressions for the rectangular waveguide case. We shall now consider an example.

Example 9.4 Finding propagating modes and their characteristics for a cylindrical waveguide

The radius of an air-dielectric cylindrical waveguide is given by $a = 5$ cm. It is desired to find the propagating modes and their characteristics for a signal of frequency $f = 3$ GHz.

Finding propagating modes

From Tables 9.2 and 9.3, we note that the lowest root is 1.84, corresponding to the $TE_{1,1}$ mode. Thus, $TE_{1,1}$ mode is the dominant mode and its cutoff frequency is given by

$$\begin{aligned} [f_c]_{TE_{1,1}} &= \frac{[(\beta_c a)_{1,1}]/a}{2\pi\sqrt{\mu_0\epsilon_0}} = \frac{1.84}{5 \times 10^{-2}} \times \frac{3 \times 10^8}{2\pi} \\ &= 1.757 \text{ GHz} \end{aligned}$$

In fact, by choosing the roots in increasing order of value from Tables 9.2 and 9.3 and dividing them by a and substituting in (9.44), we can find the cutoff frequencies in the increasing order. The four lowest cutoff frequencies and the corresponding modes found in this manner are listed in Table 9.4. For any given frequency f , propagation occurs in all modes for which $f > f_c$. Thus, for a signal of frequency 3 GHz, the propagating modes are $TE_{1,1}$, $TM_{0,1}$, and $TE_{2,1}$. The corresponding values of λ_c , λ_g , v_{pz} , and η_g , computed by using (9.45)–(9.48b), are also listed in Table 9.4.

TABLE 9.4 The Four Lowest Cutoff Frequencies and the Corresponding Modes for an Air-Dielectric Cylindrical Waveguide of Radius $a = 5$ cm and the Parameters for the Propagating Modes for $f = 3$ GHz

$\beta_c a$	Mode(s)	f_c (GHz)	λ_c (cm)	λ_g (cm)	v_{pz} (m/s)	η_g (ohms)
1.84	$TE_{1,1}$	1.757	17.074	12.337	3.701×10^8	465.10
2.40	$TM_{0,1}$	2.292	13.090	15.500	4.650×10^8	243.24
3.05	$TE_{2,1}$	2.913	10.300	41.827	12.548×10^8	1576.84
3.83	$TE_{0,1}, TM_{1,1}$	3.657	8.203	—	—	—

*Cylindrical
cavity
resonator*

As in the case of the rectangular waveguide, by placing two perfectly conducting sheets in two constant- z planes separated by a distance d , we can have a cylindrical cavity resonator that supports oscillations at frequencies for which

$$d = l \frac{\lambda_g}{2}, \quad l = 1, 2, 3, \dots \quad (9.49)$$

Substituting for λ_g from (9.46), we have

$$\begin{aligned} \frac{2d}{l} &= \frac{\lambda}{\sqrt{1 - (\lambda/\lambda_c)^2}} \\ \frac{1}{\lambda^2} &= \frac{1}{\lambda_c^2} + \left(\frac{l}{2d}\right)^2 \end{aligned}$$

$$\boxed{f_{\text{osc}} = \frac{v_p}{\lambda} = \frac{1}{\sqrt{\mu\epsilon}} \sqrt{\frac{1}{\lambda_c^2} + \left(\frac{l}{2d}\right)^2}} \quad (9.50)$$

The modes are designated $TE_{n,m,l}$ and $TM_{n,m,l}$, where n and m are allowed values as discussed earlier. For both TE and TM modes, $l = 1, 2, 3, \dots$, as given by (9.49). In addition, as for the rectangular waveguide case, TM modes at cutoff ($\beta_z = 0$, $\lambda_g = \infty$ and $\eta_g = 0$) satisfy the boundary conditions, since both \bar{E}_r and \bar{E}_ϕ go to zero. Hence, for TM modes $l = 0$ is allowed. Let us consider an example.

Example 9.5 Finding the frequencies of oscillation for a cylindrical cavity resonator

A cylindrical cavity resonator is formed by placing two perfectly conducting sheets 5 cm apart in the cross-sectional planes of the cylindrical waveguide of Example 9.4, so that $d = 5$ cm. It is desired to find the four lowest frequencies of oscillation and identify the mode(s) of oscillation for each frequency.

By substituting $\mu = \mu_0$, $\varepsilon = \varepsilon_0$, and $d = 5$ cm, in (9.50), we obtain

$$\begin{aligned} f_{\text{osc}} &= 3 \times 10^8 \sqrt{\frac{1}{\lambda_c^2} + \left(\frac{l}{0.1}\right)^2} \\ &= 3000 \sqrt{\left(\frac{0.1}{\lambda_c}\right)^2 + l^2} \text{ MHz} \end{aligned}$$

By using the results of Table 9.4 and assigning values to l , as discussed, we obtain the four lowest frequencies of oscillation and the corresponding modes to be

$$\begin{aligned} 3000 \times \frac{10}{13.09} &= 2292 \text{ MHz for TM}_{0,1,0} \text{ mode} \\ 3000 \sqrt{\left(\frac{10}{17.074}\right)^2 + 1} &= 3477 \text{ MHz for TE}_{1,1,1} \text{ mode} \\ 3000 \times \frac{10}{8.203} &= 3657 \text{ MHz for TM}_{1,1,0} \text{ mode} \\ 3000 \sqrt{\left(\frac{10}{13.09}\right)^2 + 1} &= 3775 \text{ MHz for TM}_{0,1,1} \text{ mode} \end{aligned}$$

- K9.2.** Cylindrical waveguide; Bessel functions; TM and TE modes; Cylindrical cavity resonator.
- D9.4.** An air-dielectric waveguide with the z -axis as its axis has a semicircular cross section of radius $a = 5$ cm, as shown in Fig. 9.9. Find the mode with the lowest cutoff frequency and the corresponding value of the cutoff frequency for **(a)** TE waves and **(b)** TM waves.
Ans. **(a)** $\text{TE}_{1,1}$, 1.757 GHz; **(b)** $\text{TM}_{1,1}$, 3.657 GHz.
- D9.5.** The resonant frequencies for the $\text{TM}_{0,1,0}$ mode and the $\text{TE}_{1,1,1}$ mode of an air-dielectric cylindrical cavity resonator are both known to be 3000 MHz. Find the values of the dimensions a and d of the resonator.
Ans. 3.82 cm; 7.79 cm.

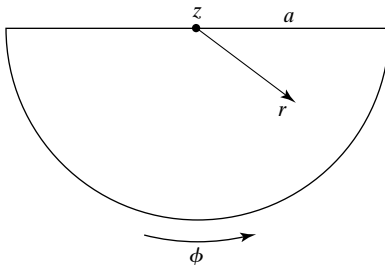


FIGURE 9.9
For Problem D9.4.

9.3 LOSSES IN METALLIC WAVEGUIDES AND RESONATORS

Loss in dielectric

In this section, we shall extend our discussion of waveguides and resonators to consider the effects of lossy materials. Power dissipation in the imperfect dielectric of a guide results in loss that follows simply from the attenuation constant for the case of a uniform plane wave propagating in the dielectric. If, for the purpose of illustration, we consider the TE or TM wave in a parallel-plate waveguide, then we know that progress of the composite TE or TM wave along the guide by a distance d involves travel of the component uniform plane waves obliquely to the plates by a distance $d/\sqrt{1 - (f_c/f)^2}$. Thus, if α'_d is the attenuation constant for uniform plane wave propagation in the dielectric, then the attenuation constant α_d for the TE or TM wave along the guide axis is $\alpha'_d/\sqrt{1 - (f_c/f)^2}$ and the attenuation $e^{\mp\alpha_d z}$ is equal to $e^{\mp[\alpha'_d/\sqrt{1 - (f_c/f)^2}]z}$. From Section 4.5, we recall that for a slightly imperfect dielectric ($\sigma/\omega\epsilon \ll 1$),

$$\alpha'_d \approx \frac{\sigma}{2} \sqrt{\frac{\mu}{\epsilon}} \left(1 - \frac{\sigma^2}{8\omega^2\epsilon^2} \right) \approx \frac{\sigma}{2} \sqrt{\frac{\mu}{\epsilon}}$$

Basis for analysis of loss in conductors

Unlike the case of the imperfect dielectric, attenuation of the wave due to power flow into the imperfect conductors of a guide as the wave propagates down the guide involves an elaborate treatment. Since the conductors are only slightly imperfect ($\sigma/\omega\epsilon \gg 1$), the procedure is based on considering the situation as though a plane wave having the same magnetic field components as those given by the appropriate tangential magnetic field components on that wall for the perfect conductor case propagates normally into the conductor and then computing the power flow into the wall (assumed to be of infinite depth in view of the rapid attenuation of fields as they propagate into a good conductor). Now, for a tangential magnetic field $\bar{\mathbf{H}}_t$ on a given wall, the electric-field vector of a uniform plane wave propagating into the wall (designated to be in the direction \mathbf{a}_n) is $\bar{\eta}_c \bar{\mathbf{H}}_t \times \mathbf{a}_n$, where $\bar{\eta}_c$ is the intrinsic impedance of the conductor. The complex Poynting vector is

$$\begin{aligned} \bar{\mathbf{P}} &= \frac{1}{2} \bar{\mathbf{E}} \times \bar{\mathbf{H}}^* = \frac{1}{2} \bar{\eta}_c (\bar{\mathbf{H}}_t \times \mathbf{a}_n) \times \bar{\mathbf{H}}_t^* \\ &= \frac{1}{2} \bar{\eta}_c [\mathbf{a}_n (\bar{\mathbf{H}}_t \cdot \bar{\mathbf{H}}_t^*) - \bar{\mathbf{H}}_t (\mathbf{a}_n \cdot \bar{\mathbf{H}}_t^*)] \\ &= \frac{1}{2} \bar{\eta}_c \bar{\mathbf{H}}_t \cdot \bar{\mathbf{H}}_t^* \mathbf{a}_n \end{aligned} \quad (9.51)$$

The time-average power flowing into the conductor of conductivity σ for a length Δz along the guide is given by

$$\begin{aligned} \Delta \langle P_d \rangle &= \int_l (\text{Re } \bar{\mathbf{P}}) \cdot dl \Delta z \mathbf{a}_n \\ &= \int_l \text{Re} \left(\frac{1}{2} \bar{\eta}_c \bar{\mathbf{H}}_t \cdot \bar{\mathbf{H}}_t^* \right) dl \Delta z \\ &= \frac{\Delta z}{2\sigma\delta} \int_l \bar{\mathbf{H}}_t \cdot \bar{\mathbf{H}}_t^* dl \end{aligned} \quad (9.52)$$

where $\delta(= 1/\sqrt{\pi f \mu \sigma})$ is the skin depth at the frequency of operation f , dl is the differential length element along the transverse dimension, and \int_l denotes integration performed along the transverse dimension. We shall illustrate the application of (9.52) by means of an example.

Example 9.6 Attenuation constant for TE_{1,0} mode in a rectangular guide with imperfect conductors

Let us consider the propagation of TE_{1,0} mode in a rectangular waveguide and obtain the expression for the attenuation constant α_c associated with it due to imperfect, but good, conductors making up the walls of the guide.

To obtain the attenuation constant α_c , we note that since for a given mode the fields are attenuated in the manner $e^{-\alpha_c z}$ where the z -direction is assumed to be the guide axis, the time-average power flow $\langle P_f \rangle$ down the guide varies in the manner $e^{-2\alpha_c z}$. The time-average power dissipated over an infinitesimal distance Δz at any value of z along the guide is then given by

$$\begin{aligned}\Delta \langle P_d \rangle &= -\frac{\partial \langle P_f \rangle}{\partial z} \Delta z \\ &= 2\alpha_c \langle P_f \rangle \Delta z\end{aligned}$$

so that

$$\alpha_c = \frac{1}{2\langle P_f \rangle} \frac{\Delta \langle P_d \rangle}{\Delta z} \quad (9.53)$$

Thus, the attenuation constant is one-half the ratio of the time-average power dissipated per unit distance at any value of z along the guide to the time-average power flow down the guide at that value of z . In fact, this is a general result applicable for any lossy traveling wave. The procedure for computing α_c for a given mode therefore consists of evaluating $\Delta \langle P_d \rangle$ and $\langle P_f \rangle$ for that mode.

To find $\Delta \langle P_d \rangle$, we consider the different walls of the waveguide separately. For each wall, we compute the time-average power flowing into the conductor over a surface made up of distance Δz along the guide axis and the entire transverse dimension of that wall by using (9.52). To proceed further, we substitute $m = 1$ and $n = 0$ in the TE mode field expressions given in Table 9.1, and considering the (+) wave only, we obtain the TE_{1,0} mode field components in a lossless waveguide to be

$$\bar{E}_z = \bar{E}_x = \bar{H}_y = 0 \quad (9.54a)$$

$$\bar{H}_z = \bar{A} \cos \frac{\pi x}{a} e^{-j\beta z} \quad (9.54b)$$

$$\bar{E}_y = -j \frac{\lambda_c^2}{4\pi^2} \omega \mu \frac{\pi}{a} \bar{A} \sin \frac{\pi x}{a} e^{-j\beta z} \quad (9.54c)$$

$$\bar{H}_x = -\frac{\bar{E}_y}{\eta_g} = j \frac{2a}{\lambda_g} \bar{A} \sin \frac{\pi x}{a} e^{-j\beta z} \quad (9.54d)$$

where a and b are the dimensions of the guide in the x - and y -directions, respectively, as shown in Fig. 9.10. For the lossy case, the field components are multiplied by $e^{-\alpha_c z}$. Since

Attenuation constant for TE_{1,0} mode in a rectangular waveguide

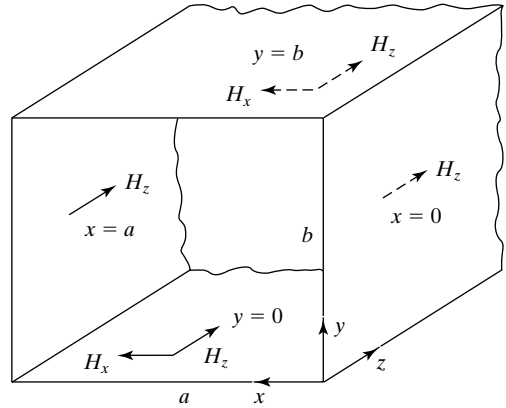


FIGURE 9.10

Rectangular waveguide with imperfectly conducting walls and showing the tangential magnetic field components on the walls for the $TE_{1,0}$ mode.

we compute the quantities $\Delta\langle P_d \rangle$ and $\langle P_f \rangle$ at some particular value of z , say, z_0 , we can absorb the factors $e^{-\alpha_c z_0}$ and $e^{-j\beta_z z_0}$ into the constant \bar{A} . Also, each nonzero tangential component of magnetic field on a given wall will be accompanied by a tangential electric field perpendicular to it so as to produce power flow into the conductor. Since some of these tangential electric-field components are longitudinal, the mode is no longer exactly TE mode. However, these components are very small in magnitude; hence, the mode is almost a TE mode.

We shall now consider the different walls and compute the corresponding values of $\Delta\langle P_d \rangle$ with the aid of Fig. 9.10.

RIGHT SIDE WALL ($x = 0$)

$$\begin{aligned}\bar{\mathbf{H}}_t &= \bar{A} \mathbf{a}_z \\ \bar{\mathbf{H}}_t \cdot \bar{\mathbf{H}}_t^* &= |\bar{A}|^2 \\ \Delta\langle P_d \rangle &= \frac{\Delta z}{2\sigma\delta} \int_{y=0}^b |\bar{A}|^2 dy \\ &= \frac{|\bar{A}|^2 b}{2\sigma\delta} \Delta z\end{aligned}\quad (9.55a)$$

LEFT SIDE WALL ($x = a$)

Same as for the right side wall.

$$\Delta\langle P_d \rangle = \frac{|\bar{A}|^2 b 2\sigma\delta}{\Delta z} \quad (9.55b)$$

BOTTOM WALL ($y = 0$)

$$\begin{aligned}\bar{\mathbf{H}}_t &= \bar{A} \left(j \frac{2a}{\lambda_g} \sin \frac{\pi x}{a} \mathbf{a}_x + \cos \frac{\pi x}{a} \mathbf{a}_z \right) \\ \bar{\mathbf{H}}_t \cdot \bar{\mathbf{H}}_t^* &= |\bar{A}|^2 \left(\frac{4a^2}{\lambda_g^2} \sin^2 \frac{\pi x}{a} + \cos^2 \frac{\pi x}{a} \right)\end{aligned}$$

$$\begin{aligned}
 \Delta \langle P_d \rangle &= \frac{\Delta z}{2\sigma\delta} \int_{x=0}^a |\bar{A}|^2 \left(\frac{4a^2}{\lambda_g^2} \sin^2 \frac{\pi x}{a} + \cos^2 \frac{\pi x}{a} \right) dx \\
 &= \frac{|\bar{A}|^2 \Delta z}{4\sigma\delta} \left(\frac{4a^3}{\lambda_g^2} + a \right)
 \end{aligned} \tag{9.55c}$$

TOP WALL ($y = b$)

Same as for the bottom wall.

$$\Delta \langle P_d \rangle = \frac{|\bar{A}|^2 \Delta z}{4\sigma\delta} \left(\frac{4a^3}{\lambda_g^2} + a \right) \tag{9.55d}$$

Adding up the contributions from all four walls, we obtain the total time-average power dissipated over an infinitesimal length Δz along the guide to be

$$\begin{aligned}
 \Delta \langle P_d \rangle &= \frac{|\bar{A}|^2}{2\sigma\delta} \left(\frac{4a^3}{\lambda_g^2} + a + 2b \right) \Delta z \\
 &= \frac{|\bar{A}|^2}{2\sigma\delta} \left[\frac{4a^3}{\lambda^2} \left(1 - \frac{\lambda^2}{4a^2} \right) + a + 2b \right] \Delta z \\
 &= \frac{|\bar{A}|^2}{\sigma\delta} \left(\frac{2a^3}{\lambda^2} + b \right) \Delta z
 \end{aligned} \tag{9.56}$$

Now, to find the time-average power transmitted down the guide, we note that the time-average Poynting vector is given by

$$\begin{aligned}
 \langle \mathbf{P} \rangle &= \frac{1}{2} \text{Re } \bar{\mathbf{E}} \times \bar{\mathbf{H}}^* \\
 &= -\frac{1}{2\eta_g} \bar{E}_y \bar{E}_y^* \mathbf{a}_z \\
 &= \frac{1}{2\eta_g} \frac{\lambda_c^4}{16\pi^4} \omega^2 \mu^2 \frac{\pi^2}{a^2} |\bar{A}|^2 \sin^2 \frac{\pi x}{a} \mathbf{a}_z \\
 &= \frac{\omega^2 \mu^2 a^2}{2\eta_g \pi^2} |\bar{A}|^2 \sin^2 \frac{\pi x}{a} \mathbf{a}_z
 \end{aligned} \tag{9.57}$$

The time-average power transmitted down the guide is then given by

$$\begin{aligned}
 \langle P_f \rangle &= \int_{y=0}^b \int_{x=0}^a \langle \mathbf{P} \rangle \cdot dx dy \mathbf{a}_z \\
 &= \frac{\omega^2 \mu^2 a^2}{2\eta_g \pi^2} |\bar{A}|^2 \int_{y=0}^b \int_{x=0}^a \sin^2 \frac{\pi x}{a} dx dy \\
 &= \frac{\omega^2 \mu^2 a^2 b}{4\eta_g \pi^2} |\bar{A}|^2
 \end{aligned} \tag{9.58}$$

Finally, the attenuation constant is given by

$$\begin{aligned}
 \alpha_c &= \frac{\Delta \langle P_d \rangle}{2 \langle P_f \rangle \Delta z} \\
 &= \frac{|\bar{A}|^2}{2\sigma\delta} \left(\frac{2a^3}{\lambda^2} + b \right) \frac{4\eta_g \pi^2}{\omega^2 \mu^2 a^3 b |\bar{A}|^2} \\
 &= \frac{1}{\sigma\delta} \left(1 + \frac{b\lambda^2}{2a^3} \right) \frac{\eta\epsilon}{\mu b \sqrt{1 - (f_c/f)^2}} \\
 &= \frac{1}{\sigma\delta} \left[1 + \frac{2b}{a} \left(\frac{\lambda}{\lambda_c} \right)^2 \right] \frac{1}{b\eta \sqrt{1 - (f_c/f)^2}}
 \end{aligned}$$

or

$$\alpha_c = \frac{1}{\alpha\delta b\eta \sqrt{1 - (f_c/f)^2}} \left[1 + \frac{2b}{a} \left(\frac{f_c}{f} \right)^2 \right] \quad (9.59)$$

Note that for $f \rightarrow f_c$, $\alpha_c \rightarrow \infty$. For $f \ll f_c$, $\alpha_c \approx 1/\sigma\delta b\eta \propto \sqrt{f}$, so that for $f \rightarrow \infty$, $\alpha_c \rightarrow \infty$. Thus, as f varies from f_c to infinity, α_c varies from infinity to some minimum value and then increases to infinity. The minimum value of α_c occurs for

$$\left(\frac{f}{f_c} \right)^2 = \left(1.5 + \frac{3b}{a} \right) + \sqrt{\left(1.5 + \frac{3b}{a} \right)^2 - \frac{2b}{a}} \quad (9.60)$$

For example, for $b/a = 1/2$, the minimum value occurs for $f/f_c \approx 2.4142$.

Q factor of a resonator

To proceed further, let us now consider the walls of a cavity resonator to be imperfect but good conductors. Then we can talk of the quality, or Q factor, of the resonator and derive the expression for it. The Q factor, which is a measure of the frequency selectivity of the resonator, is defined as

$$\begin{aligned}
 Q &= 2\pi \frac{\text{energy stored in the resonator}}{\text{energy dissipated per cycle}} \\
 &= 2\pi f \frac{\text{energy stored in the resonator}}{\text{time average power dissipated}}
 \end{aligned} \quad (9.61)$$

Since the conductors are good conductors, the power dissipated in them can be computed by analysis, as in Example 9.6 for the waveguide case. As for the energy stored in the cavity, it is distributed between the electric and magnetic fields at any arbitrary instant of time. But there are particular values of time at which the electric field is maximum and the magnetic field is zero, and vice versa. At these values of time, the entire energy is stored in one of the two fields.

This can be taken advantage of to obtain the stored energy. We shall illustrate the determination of the Q factor by means of an example.

Example 9.7 Q factor for $TE_{1,0,1}$ mode in a rectangular cavity resonator with imperfect conductors

Let us consider the $TE_{1,0,1}$ mode of oscillation in the rectangular cavity resonator of Fig. 9.6 and obtain the expression for the Q factor associated with it due to imperfect, but good, conductors making up the walls of the resonator.

First, we obtain the expressions for $TE_{1,0,1}$ mode field components by superimposing the (+) and (-) wave field components for the $TE_{1,0}$ waves from Table 9.1 and satisfying the boundary conditions of zero tangential electric fields at the ends $z = 0$ and $z = d$. Thus, we have

$$\bar{E}_z = \bar{E}_x = \bar{H}_y = 0 \quad (9.62a)$$

$$\bar{H}_z = \cos \frac{\pi x}{a} [\bar{A}_1 e^{-j\beta_z z} + \bar{A}_2 e^{j\beta_z z}] \quad (9.62b)$$

$$\bar{E}_y = -j \frac{\lambda_c^2}{4\pi^2} \omega \mu \frac{\pi}{a} \sin \frac{\pi x}{a} [\bar{A}_1 e^{-j\beta_z z} + \bar{A}_2 e^{j\beta_z z}] \quad (9.62c)$$

$$\bar{H}_x = j \frac{1}{\eta_g} \frac{\lambda_c^2}{4\pi^2} \omega \mu \frac{\pi}{a} \sin \frac{\pi x}{a} [\bar{A}_1 e^{-j\beta_z z} - \bar{A}_2 e^{j\beta_z z}] \quad (9.62d)$$

$$[\bar{E}_y]_{z=0} = [\bar{E}_y]_{z=d} = 0 \quad (9.63)$$

so that

$$\bar{A}_1 + \bar{A}_2 = 0 \quad \text{or} \quad \bar{A}_2 = -\bar{A}_1 \quad (9.64a)$$

$$\sin \beta_z d = 0 \quad \text{or} \quad \beta_z = \pi/d \quad (9.64b)$$

giving us the required field components

$$\bar{E}_z = \bar{E}_x = \bar{H}_y = 0 \quad (9.65a)$$

$$\bar{H}_z = \bar{A} \cos \frac{\pi x}{a} \sin \frac{\pi z}{d} \quad (9.65b)$$

$$\bar{E}_y = -j \bar{A} \frac{\omega \mu a}{\pi} \sin \frac{\pi x}{a} \sin \frac{\pi z}{d} \quad (9.65c)$$

$$\bar{H}_x = -\bar{A} \frac{a}{d} \sin \frac{\pi x}{a} \cos \frac{\pi z}{d} \quad (9.65d)$$

where $\bar{A} = -2j\bar{A}_1$ and we have also substituted $\lambda_c = 2a$ and $\omega \mu / \eta_g = 2\pi / \lambda_g = \pi / d$.

To find the energy stored in the cavity, we shall make use of the electric field. Noting that the amplitude of the only electric field component E_y , which is the value of E_y at the instant of time the magnetic field throughout the cavity is zero, is given by

$$|\bar{E}_y| = |\bar{A}| \frac{\omega \mu a}{\pi} \sin \frac{\pi x}{a} \sin \frac{\pi z}{d} \quad (9.66)$$

*Q factor for
TE_{1,0,1} mode
of a
rectangular
cavity
resonator*

and integrating the energy density throughout the volume of the cavity, we obtain the energy stored in the cavity to be

$$\begin{aligned}
 W_{\text{stored}} &= \int_{x=0}^a \int_{y=0}^b \int_{z=0}^d \frac{1}{2} \varepsilon |\bar{E}_y|^2 dv \\
 &= \frac{1}{2} \varepsilon |\bar{A}|^2 \frac{\omega^2 \mu^2 a^2}{\pi^2} \int_{x=0}^a \int_{y=0}^b \int_{z=0}^d \sin^2 \frac{\pi x}{a} \sin^2 \frac{\pi z}{d} dx dy dz \quad (9.67) \\
 &= |\bar{A}|^2 \frac{\omega^2 \mu^2 \varepsilon}{8\pi^2} a^3 bd
 \end{aligned}$$

To find the time-average power dissipated in the walls of the cavity, we note from the application of (9.51) that for a given wall, the time-average power dissipated is

$$\begin{aligned}
 \langle P_d \rangle &= \int_S (\text{Re } \bar{\mathbf{P}}) \cdot d\mathbf{S} \mathbf{a}_n \\
 &= \int_S \text{Re} \left(\frac{1}{2} \bar{\eta}_c \bar{\mathbf{H}}_t \cdot \bar{\mathbf{H}}_t^* \right) dS \quad (9.68) \\
 &= \frac{1}{2\sigma\delta} \int_S \bar{\mathbf{H}}_t \cdot \bar{\mathbf{H}}_t^* dS
 \end{aligned}$$

where S is the surface of the wall. Applying this result to the different walls of the cavity, we compute the corresponding values of $\langle P_d \rangle$ with the aid of Fig. 9.11.

RIGHT SIDE WALL ($x = 0$)

$$\begin{aligned}
 \bar{\mathbf{H}}_t &= \bar{A} \sin \frac{\pi z}{d} \mathbf{a}_z \\
 \bar{\mathbf{H}}_t \cdot \bar{\mathbf{H}}_t^* &= |\bar{A}|^2 \sin^2 \frac{\pi z}{d} \\
 \langle P_d \rangle &= \frac{1}{2\sigma\delta} \int_{y=0}^b \int_{z=0}^d \bar{\mathbf{H}}_t \cdot \bar{\mathbf{H}}_t^* dy dz \quad (9.69a) \\
 &= \frac{|\bar{A}|^2 bd}{4\sigma\delta}
 \end{aligned}$$

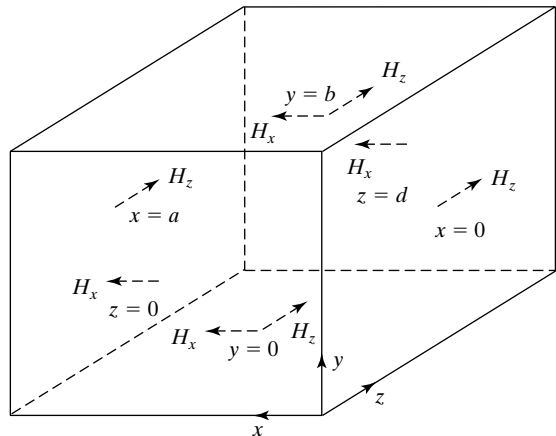


FIGURE 9.11

Rectangular cavity resonator with imperfectly conducting walls and showing the tangential magnetic field components on the walls for the $\text{TE}_{1,0,1}$ mode.

LEFT SIDE WALL ($x = a$)

Same as for right side wall.

$$\langle P_d \rangle = \frac{|\bar{A}|^2 bd}{4\sigma\delta} \quad (9.69b)$$

BOTTOM WALL ($y = 0$)

$$\begin{aligned} \bar{\mathbf{H}}_t &= \bar{A} \left[-\frac{a}{d} \sin \frac{\pi x}{a} \cos \frac{\pi z}{d} \mathbf{a}_x + \cos \frac{\pi x}{a} \sin \frac{\pi z}{d} \mathbf{a}_z \right] \\ \bar{\mathbf{H}}_t \cdot \bar{\mathbf{H}}_t^* &= |\bar{A}|^2 \left[\left(\frac{a}{d} \right)^2 \sin^2 \frac{\pi x}{a} \cos^2 \frac{\pi z}{d} + \cos^2 \frac{\pi x}{a} \sin^2 \frac{\pi z}{d} \right] \\ \langle P_d \rangle &= \frac{1}{2\sigma\delta} \int_{x=0}^a \int_{z=0}^d \bar{\mathbf{H}}_t \cdot \bar{\mathbf{H}}_t^* dx dz \\ &= \frac{|\bar{A}|^2}{8\sigma\delta} \left(\frac{a^3}{d} + ad \right) \end{aligned} \quad (9.69c)$$

TOP WALL ($y = b$)

Same as for bottom wall.

$$\langle P_d \rangle = \frac{|\bar{A}|^2}{8\sigma\delta} \left(\frac{a^3}{d} + ad \right) \quad (9.69d)$$

FRONT WALL ($z = 0$)

$$\begin{aligned} \bar{\mathbf{H}}_t &= -\bar{A} \frac{a}{d} \sin \frac{\pi x}{a} \mathbf{a}_x \\ \bar{\mathbf{H}}_t \cdot \bar{\mathbf{H}}_t^* &= |\bar{A}|^2 \left(\frac{a}{d} \right)^2 \sin^2 \frac{\pi x}{a} \\ \langle P_d \rangle &= \frac{1}{2\sigma\delta} \int_{x=0}^a \int_{y=0}^b \bar{\mathbf{H}}_t \cdot \bar{\mathbf{H}}_t^* dx dy \\ &= \frac{|\bar{A}|^2 a^3 b}{4\sigma\delta d^2} \end{aligned} \quad (9.69e)$$

BACK WALL ($z = d$)

Same as for front wall.

$$\langle P_d \rangle = \frac{|\bar{A}|^2 a^3 b}{4\sigma\delta d^2} \quad (9.69f)$$

Adding up the contributions from all six walls, we obtain the total time-average power dissipated to be

$$\langle P_d \rangle = \frac{|\bar{A}|^2}{2\sigma\delta} \left(bd + \frac{a^3}{2d} + \frac{ad}{2} + \frac{a^3b}{d^2} \right) \quad (9.70)$$

Substituting (9.67) and (9.70) into (9.61), we obtain

$$\begin{aligned} Q &= \omega \frac{\omega^2 \mu \epsilon a^3 b d / 8\pi^2}{\frac{1}{2\sigma\delta} \left(bd + \frac{a^3}{2d} + \frac{ad}{2} + \frac{a^3b}{d^2} \right)} \\ &= \frac{\omega^3 \mu^2 \epsilon \sigma \delta}{4\pi^2} \frac{2a^3 b d^3}{2bd^3 + a^3d + ad^3 + 2a^3b} \end{aligned} \quad (9.71)$$

From (9.25), the resonant frequency ω for the $\text{TE}_{1,0,1}$ mode is, however, given by

$$\omega = \frac{\pi}{\sqrt{\mu\epsilon}} \left[\left(\frac{1}{a} \right)^2 + \left(\frac{1}{d} \right)^2 \right]^{1/2} \quad (9.72)$$

Thus, (9.71) reduces to

$$Q = \frac{\pi\sigma\delta\eta}{2} \frac{b(a^2 + d^2)^{3/2}}{ad(a^2 + d^2) + 2b(a^3 + d^3)} \quad (9.73)$$

For a numerical example, for the $\text{TE}_{1,0,1}$ mode of Example 9.3 and with the walls of the cavity made of copper ($\sigma = 5.80 \times 10^7 \text{ S/m}$), $\delta = 9.075 \times 10^{-7} \text{ m}$ and the value of Q is about 11,020.

- K9.3.** Attenuation constant; $\text{TE}_{1,0}$ mode in a rectangular waveguide; Q factor; $\text{TE}_{1,0,1}$ mode in a rectangular cavity resonator.
- D9.6.** For each of the following cases of $\text{TE}_{1,0}$ waves propagating in a rectangular waveguide with copper walls, find the frequency of operation for which the attenuation constant α_c is a minimum and the minimum value of α_c : **(a)** $a = 3 \text{ cm}$, $b = 1.5 \text{ cm}$, and air-dielectric and **(b)** $a = b = 3 \text{ cm}$, and dielectric of $\epsilon = 4\epsilon_0$ and $\mu = \mu_0$.
Ans. **(a)** 12.0711 GHz, 0.00653; **(b)** 7.4045 GHz, 0.0047.
- D9.7.** Find Q for $\text{TE}_{1,0,1}$ mode for each of the following cases of a rectangular cavity resonator with copper walls: **(a)** $a = b = d = 5 \text{ cm}$, air-dielectric; **(b)** $a = 2.5 \text{ cm}$, $b = 2 \text{ cm}$, $d = 5 \text{ cm}$, air-dielectric; **(c)** $a = b = d = 5 \text{ cm}$; dielectric with $\epsilon = 2.25\epsilon_0$ and $\mu = \mu_0$.
Ans. **(a)** 16,434; **(b)** 10,160; **(c)** 13,417.

9.4 OPTICAL FIBER

Thus far in this chapter, we have discussed the guiding of waves between metallic boundaries. We now turn our attention to the optical fiber. An optical fiber, so called because of its filamentary appearance, consists typically of a core and a cladding with circular cross sections, as shown in Fig. 9.12(a). The core is made up of a material of permittivity greater than that of the cladding, so that a critical angle exists for waves inside the core incident on the interface between the core and the cladding, and hence waveguiding is made possible in the core by total internal reflection. The phenomenon of guiding may be visualized by considering a longitudinal cross section of the fiber through its axis, shown in Fig. 9.12(b), and comparing it with that of the slab waveguide, shown in Fig. 8.22. Whereas this situation corresponds to meridional rays, skewed rays whose paths lie in planes offset from the fiber axis also explain the guiding mechanism. Although the cladding is not essential for the purpose of waveguiding in the core since the permittivity of the core material is greater than that of free space, the cladding serves two useful purposes: (1) It avoids scattering and field distortion by the supporting structure of the fiber since the field decays exponentially outside the core and hence is negligible outside the cladding; (2) it allows a single-mode propagation for a larger value of the radius of the core than permitted in the absence of the cladding.

Description

To simplify analysis of waveguiding in an optical fiber, we shall consider the cladding region to extend to infinity, so that the geometry is one of a cylindrical dielectric rod of permittivity greater than that of the surrounding medium, as shown in Fig. 9.13. In addition, we shall consider the permittivity of the core to be uniform, thereby corresponding to the case of a step-index fiber. To carry out the field analysis, we make use of our previous experience with the cylindrical metallic waveguide and the dielectric slab waveguide. First, we know that the transverse field components can be expressed in terms of the longitudinal field components E_z and H_z . We shall, however, find that the modes do not all separate into TE and TM modes and that the situation leads to the so-called hybrid modes. Second, we know in analogy with the case of the slab guide that radially decaying fields can be expected outside the core.

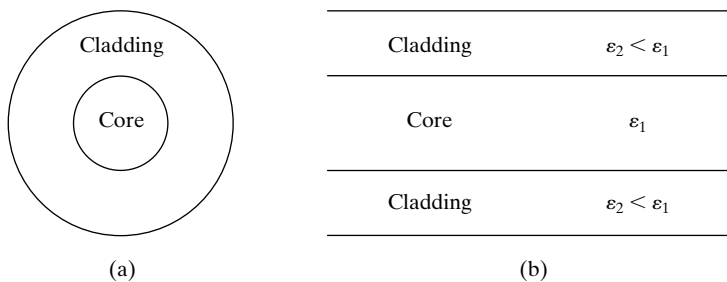


FIGURE 9.12

(a) Transverse and (b) longitudinal cross sections of an optical fiber.

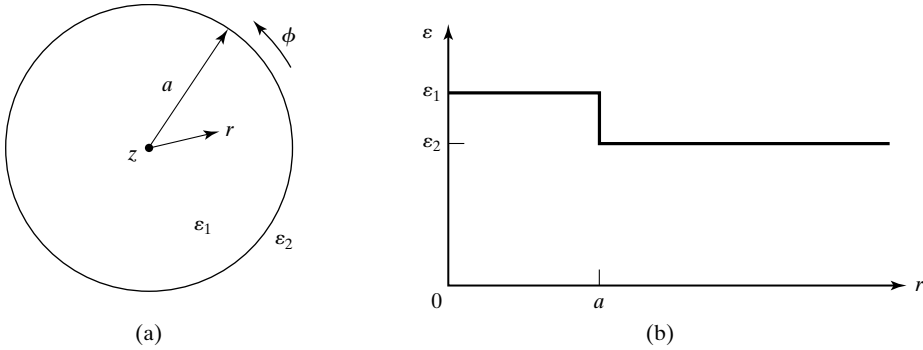


FIGURE 9.13

(a) Cross section of a cylindrical dielectric rod surrounded by a cladding region extending to infinity. (b) Permittivity profile for the arrangement of (a).

We recall from Section 9.2 that the differential equation to be satisfied by the fields for the cylindrical geometry is that given by (9.29)

$$\frac{1}{r} \frac{\partial}{\partial r} \left(r \frac{\partial \bar{\psi}}{\partial r} \right) + \frac{1}{r^2} \frac{\partial^2 \bar{\psi}}{\partial \phi^2} + \beta_c^2 \bar{\psi} = 0 \quad (9.74)$$

where $\bar{\psi}$ stands for \bar{E}_z or \bar{H}_z and

$$\beta_c^2 = \omega^2 \mu \epsilon - \left(\frac{2\pi}{\lambda_g} \right)^2 = \beta^2 - \beta_z^2 \quad (9.75)$$

We also learned that (9.74) is separable into a differential equation involving r only and one involving ϕ only. The solution for the r -variation is a superposition of the Bessel functions $J_l(\beta_c r)$ and $N_l(\beta_c r)$, whereas the solutions for the ϕ -variation are sinusoidal ($\cos l\phi$ and $\sin l\phi$). The sinusoidal variations in ϕ require l to be an integer. The behaviors of the Bessel functions for real arguments are shown in Fig. 9.8.

Field solution in the core

Inside the core, $\beta = \beta_1 = \omega \sqrt{\mu \epsilon_1}$, $\beta_{c1}^2 = \beta_1^2 - \beta_z^2 > 0$, and β_c is real. The solutions for the r -variation are J_l and N_l with real arguments. But since N_l has the property that $N_l(0) \rightarrow \infty$ for all orders, we rule it out. Thus,

$$\bar{\psi}(r, \phi, z) = \bar{A} J_l(\beta_{c1} r) \begin{cases} \cos l\phi \\ \sin l\phi \end{cases} e^{-j\beta_z z} \quad \text{for } r < a \quad (9.76)$$

where we consider only the (+) wave, for simplicity. Defining $u = \beta_{c1}a$, we can write the longitudinal components and then the transverse field components by using (9.27a)–(9.27d) as follows:

$$\bar{E}_{z1} = \bar{A}J_l\left(u\frac{r}{a}\right)\left\{\begin{array}{l} \cos l\phi \\ \sin l\phi \end{array}\right\}e^{-j\beta_z z} \quad (9.77a)$$

$$\bar{H}_{z1} = \bar{B}J_l\left(u\frac{r}{a}\right)\left\{\begin{array}{l} \sin l\phi \\ \cos l\phi \end{array}\right\}e^{-j\beta_z z} \quad (9.77b)$$

$$\bar{E}_{r1} = \left[-\frac{j\beta_z a}{u}\bar{A}J'_l\left(u\frac{r}{a}\right) \mp \frac{j\omega\mu a^2 l}{u^2 r}\bar{B}J_l\left(u\frac{r}{a}\right)\right]\left\{\begin{array}{l} \cos l\phi \\ \sin l\phi \end{array}\right\}e^{-j\beta_z z} \quad (9.77c)$$

$$\bar{H}_{r1} = \left[\mp \frac{j\omega\varepsilon_1 a^2 l}{u^2 r}\bar{A}J_l\left(u\frac{r}{a}\right) - \frac{j\beta_z a}{u}\bar{B}J'_l\left(u\frac{r}{a}\right)\right]\left\{\begin{array}{l} \sin l\phi \\ \cos l\phi \end{array}\right\}e^{-j\beta_z z} \quad (9.77d)$$

$$\bar{E}_{\phi 1} = \left[\pm \frac{j\beta_z a^2 l}{u^2 r}\bar{A}J_l\left(u\frac{r}{a}\right) + \frac{j\omega\mu a}{u}\bar{B}J'_l\left(u\frac{r}{a}\right)\right]\left\{\begin{array}{l} \sin l\phi \\ \cos l\phi \end{array}\right\}e^{-j\beta_z z} \quad (9.77e)$$

$$\bar{H}_{\phi 1} = \left[-\frac{j\omega\varepsilon_1 a}{u}\bar{A}J'_l\left(u\frac{r}{a}\right) \mp \frac{j\beta_z a^2 l}{u^2 r}\bar{B}J_l\left(u\frac{r}{a}\right)\right]\left\{\begin{array}{l} \cos l\phi \\ \sin l\phi \end{array}\right\}e^{-j\beta_z z} \quad (9.77f)$$

In (9.77a)–(9.77f), the upper functions and signs go together and the lower functions and signs go together. Note that when $\bar{E}_{z1} \propto \cos l\phi$, $\bar{H}_{z1} \propto \sin l\phi$. This is because when a given transverse component is proportional to \bar{E}_z (or \bar{H}_z), it is proportional to $\partial\bar{H}_z/\partial\phi$ (or $\partial\bar{E}_z/\partial\phi$).

In the cladding, $\beta = \beta_2 = \omega\sqrt{\mu\varepsilon_2}$, $\beta_{c2}^2 = \beta_2^2 - \beta_z^2 < 0$, and β_c is imaginary. The solutions for the r -variations are J_l and N_l with imaginary arguments jwr/a , where $w^2 = -\beta_{c2}^2 a^2$. It is common practice then to represent the solution in terms of the modified Bessel functions I_l and K_l with real arguments wr/a . The behaviors of these functions for a few values of l are shown in Fig. 9.14. Since I_l has the property that $I_l(\infty) \rightarrow \infty$ for all orders, we rule it out. We can thus write the solutions for the field components as follows:

$$\bar{E}_{z2} = \bar{C}K_l\left(w\frac{r}{a}\right)\left\{\begin{array}{l} \cos l\phi \\ \sin l\phi \end{array}\right\}e^{-j\beta_z z} \quad (9.78a)$$

$$\bar{H}_{z2} = \bar{D}K_l\left(w\frac{r}{a}\right)\left\{\begin{array}{l} \sin l\phi \\ \cos l\phi \end{array}\right\}e^{-j\beta_z z} \quad (9.78b)$$

$$\bar{E}_{r2} = \left[\frac{j\beta_z a}{w}\bar{C}K'_l\left(w\frac{r}{a}\right) \pm \frac{j\omega\mu a^2 l}{w^2 r}\bar{D}K_l\left(w\frac{r}{a}\right)\right]\left\{\begin{array}{l} \cos l\phi \\ \sin l\phi \end{array}\right\}e^{-j\beta_z z} \quad (9.78c)$$

$$\bar{H}_{r2} = \left[\mp \frac{j\omega\varepsilon_2 a^2 l}{w^2 r}\bar{C}K_l\left(w\frac{r}{a}\right) + \frac{j\beta_z a}{w}\bar{D}K'_l\left(w\frac{r}{a}\right)\right]\left\{\begin{array}{l} \sin l\phi \\ \cos l\phi \end{array}\right\}e^{-j\beta_z z} \quad (9.78d)$$

$$\bar{E}_{\phi 2} = \left[\mp \frac{j\beta_z a^2 l}{w^2 r}\bar{C}K_l\left(w\frac{r}{a}\right) - \frac{j\omega\mu a}{w}\bar{D}K'_l\left(w\frac{r}{a}\right)\right]\left\{\begin{array}{l} \sin l\phi \\ \cos l\phi \end{array}\right\}e^{-j\beta_z z} \quad (9.78e)$$

$$\bar{H}_{\phi 2} = \left[\frac{j\omega\varepsilon_2 a}{w}\bar{C}K'_l\left(w\frac{r}{a}\right) \pm \frac{j\beta_z a^2 l}{w^2 r}\bar{D}K_l\left(w\frac{r}{a}\right)\right]\left\{\begin{array}{l} \cos l\phi \\ \sin l\phi \end{array}\right\}e^{-j\beta_z z} \quad (9.78f)$$

*Field solution
in the
cladding*

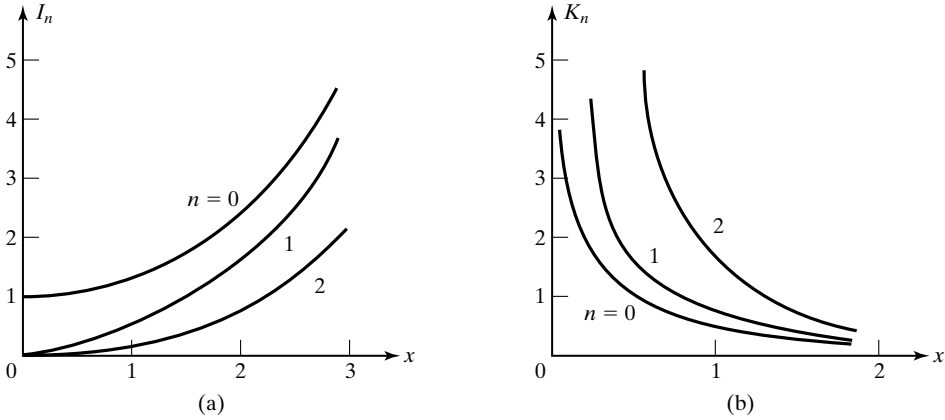


FIGURE 9.14

Behaviors of the modified Bessel functions (a) $I_n(x)$ and (b) $K_n(x)$.

Guidance condition

To obtain the guidance condition, we need to satisfy the boundary conditions for the field components. We now see that, for $l = 0$, the set of equations separates into two groups: $\bar{E}_{z1,2}$, $\bar{E}_{r1,2}$, and $\bar{H}_{\phi1,2}$, involving the constants \bar{A} and \bar{C} ; and $\bar{H}_{z1,2}$, $\bar{H}_{r1,2}$, and $\bar{E}_{\phi1,2}$, involving the constants \bar{B} and \bar{D} . The first group corresponds to the TM case, and the characteristic equation obtained by setting $\bar{E}_{z1}/\bar{H}_{\phi1} = \bar{E}_{z2}/\bar{H}_{\phi2}$ at $r = a$ is

$$\frac{J_1(u)}{J_0(u)} = -\frac{\varepsilon_2 u}{\varepsilon_1 w} \frac{K_1(w)}{K_0(w)} \quad (9.79)$$

where we have used the property that $J'_0(u) = -J_1(u)$ and $K'_0(w) = -K_1(w)$. The second group corresponds to the TE case, and the characteristic equation obtained by setting $\bar{E}_{\phi1}/\bar{H}_{z1} = \bar{E}_{\phi2}/\bar{H}_{z2}$ at $r = a$ is

$$\frac{J_1(u)}{J_0(u)} = -\frac{u}{w} \frac{K_1(w)}{K_0(w)} \quad (9.80)$$

For $l \neq 0$, the boundary conditions cannot be satisfied by the two separate groups, and hence the fields can no longer be separated into TM and TE modes, but instead are known as *hybrid modes*. The characteristic equation obtained by setting $\bar{E}_{z1} = \bar{E}_{z2}$, $\bar{H}_{z1} = \bar{H}_{z2}$, $\bar{E}_{z1}/\bar{H}_{\phi1} = \bar{E}_{z2}/\bar{H}_{\phi2}$, and $\bar{E}_{\phi1}/\bar{H}_{z1} = \bar{E}_{\phi2}/\bar{H}_{z2}$ at $r = a$ is then given by (see Problem P9.20)

$$\left[\frac{J'_l(u)}{uJ_l(u)} + \frac{K'_l(w)}{wK_l(w)} \right] \left[\frac{\beta_1^2 J'_l(u)}{uJ_l(u)} + \frac{\beta_2^2 K'_l(w)}{wK_l(w)} \right] = \frac{\beta_z^2 l^2 V^4}{u^4 w^4} = l^2 \left(\frac{1}{u^2} + \frac{1}{w^2} \right) \left(\frac{\beta_1^2}{u^2} + \frac{\beta_2^2}{w^2} \right) \quad (9.81)$$

where

$$V^2 = u^2 + w^2 = (\beta_1^2 - \beta_2^2)a^2 \quad (9.82)$$

Note that

$$\begin{aligned} V &= \sqrt{\beta_1^2 - \beta_2^2} a = \frac{2\pi a}{\lambda_0} = \sqrt{\varepsilon_{r1} - \varepsilon_{r2}} \\ &= \frac{2\pi a}{\lambda_0} \sqrt{n_1^2 - n_2^2} = \frac{2\pi a}{\lambda_0} (\text{NA}) \end{aligned} \quad (9.83)$$

where

$$\text{NA} = \sqrt{n_1^2 - n_2^2} \quad (9.84)$$

is known as the *numerical aperture*, an important parameter of physical significance (see Problem P9.22).

Determination of the characteristics of the modes for a given value of l requires the solution of (9.79) or (9.80) for $l = 0$ (TM and TE modes) and (9.81) for $l \neq 0$ (hybrid modes), all with the constraint (9.82), from a knowledge of the values of ω , ε_1 , ε_2 , and a . It is convenient to replace the derivatives of the Bessel functions by the Bessel functions themselves, using the recursive formulas

$$J_{l-1}(x) + J_{l+1}(x) = \frac{2l}{x} J_l(x) \quad (9.85a)$$

$$J_{l-1}(x) - J_{l+1}(x) = 2J'_l(x) \quad (9.85b)$$

$$K_{l-1}(x) + K_{l+1}(x) = -2K'_l(x) \quad (9.85c)$$

$$K_{l-1}(x) - K_{l+1}(x) = \frac{2l}{x} K_l(x) \quad (9.85d)$$

and express (9.81) in the manner (see Problem P9.23)

$$(J^+ + K^+)(\beta_1^2 J^- - \beta_2^2 K^-) + (J^- - K^-)(\beta_1^2 J^+ + \beta_2^2 K^+) = 0 \quad (9.86)$$

where

$$J^\pm = \frac{J_{l\pm 1}(u)}{uJ_l(u)} \quad \text{and} \quad K^\pm = \frac{K_{l\pm 1}(w)}{wK_l(w)} \quad (9.87)$$

Let us first consider the hybrid modes. A method of solution consists of plotting (9.82) and (9.86) in the uw -plane and looking for the points of intersection. To do this, we note that (9.82) is simply the equation of a circle in the uw -plane, whereas (9.86) results in many branches. The approximate plot of Fig. 9.15 shows the nature of the first three branches for $l = 1$ and the circle for $V = 2$. The designations $\text{HE}_{l,m}$ and $\text{EH}_{l,m}$ for the hybrid modes denote that, although

Hybrid modes

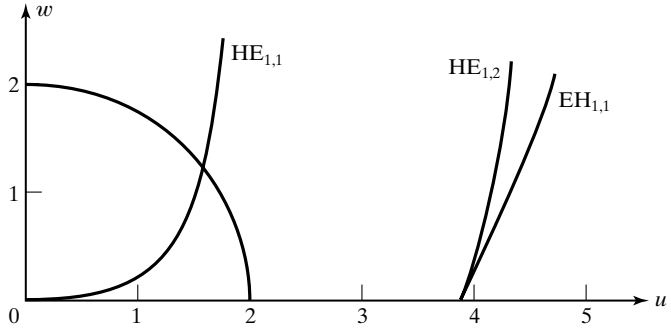


FIGURE 9.15 For illustrating the nature of solution of the characteristic equation for guided modes in an optical fiber.

hybrid, H_z is predominant for HE modes and E_z is predominant for EH modes. The subscript m denotes the number of the solution for the particular value of l . It can be seen that for the situation shown in Fig. 9.15 $HE_{1,2}$ and $EH_{1,1}$ are cut off, whereas a solution exists for $HE_{1,1}$. In fact, since the branch for $HE_{1,1}$ originates at $(0, 0)$, that mode has no cutoff. Thus, $HE_{1,1}$ mode is the dominant mode. As ω increases, V increases, and more and more points of intersection with the V -circle occur, corresponding to higher-order modes.

Single-mode operation

The modes with the lowest nonzero cutoff frequency are the TM and TE modes governed by the characteristic equations (9.79) and (9.80), respectively. Therefore, to determine the condition for single-mode operation, we consider these equations. Since the cutoff occurs for $w = 0$ (condition of fields extending to infinity in medium 2) and $K_1/K_0 = \infty$ for $w = 0$, we get $J_1(u) = 0$ or $u = 2.405$ for both modes. Also for $w = 0$, $V = \sqrt{u^2 + w^2} = u$. Thus, for single-mode operation, V must be less than 2.405.

Example 9.8 Minimum free-space wavelength for single-mode propagation in an optical fiber

A fiber with core and cladding refractive indices $n_1 = 1.45$ and $n_2 = 1.44$, respectively, has a core radius of $a = 25 \mu\text{m}$. We wish to find the minimum free-space wavelength, λ_0 , for single-mode operation.

For $n_1 = 1.45$ and $n_2 = 1.44$,

$$NA = \sqrt{(1.45)^2 - (1.44)^2} = 0.17$$

Thus, λ_0 is given by

$$\begin{aligned} V &= \frac{2\pi a}{\lambda_0}(NA) < 2.405 \\ \lambda_0 &> \frac{2\pi a(NA)}{2.405} \\ &= \frac{2\pi \times 25 \times 0.17}{2.405} \mu\text{m} \\ &= 11.1033 \mu\text{m} \end{aligned}$$

For most practical fibers, the refractive indices of the core and the cladding are nearly equal ($\varepsilon_1 \approx \varepsilon_2$), corresponding to weak guidance. The rays are then paraxial and the longitudinal components of the fields are much smaller than the transverse components, so that the waves are almost TEM, the simplest such waves being linearly polarized along two orthogonal axes. The associated modes are designated as $LP_{l,m}$ modes, formed in general by superpositions of the exact modes. The $LP_{0,1}$ mode, which corresponds to just the $HE_{1,1}$ mode, is the dominant mode with no cutoff. Thus, in terms of LP modes, single-mode operation refers to the $LP_{0,1}$ mode and it is ensured for $V < 2.405$.

*Weak
guidance and
LP modes*

K9.4. Core; Cladding; Field solutions; Hybrid modes; $HE_{1,1}$ mode; LP modes.

D9.8. A fiber has core radius $a = 10 \mu\text{m}$. Find the following for single-mode propagation at $\lambda_0 = 10 \mu\text{m}$: **(a)** maximum allowable value of the numerical aperture; **(b)** minimum allowable value of the cladding refractive index n_2 , if the core refractive index $n_1 = 1.5$; and **(c)** maximum allowable value of the core refractive index n_1 , if the difference between the core and cladding refractive indices is 0.04.

Ans. **(a)** 0.3828; **(b)** 1.4503; **(c)** 1.8513.

9.5 PULSE BROADENING IN DISPERSIVE MEDIUM

In Section 8.4, we introduced the phenomenon of dispersion resulting from the variation of phase velocity of a wave with frequency. We learned that for a signal comprising a band of frequencies, the field patterns of the different frequency components do not maintain the same phase relationships as they travel down the propagation medium, and hence they disperse. For the case of a narrow-band signal, it is then meaningful to associate a group velocity, which determines the travel time of the signal. In this section, we consider another consequence of dispersion, which is the broadening of a pulse as it travels down the propagation medium. Although this characteristic is pertinent to any dispersive medium, it is particularly important for propagation of pulses in an optical fiber, because of its predominant contribution to the limitations in signal bandwidths that can be transmitted over long distances.

A heuristic explanation of pulse broadening can be provided by considering the dispersion diagram of Fig. 8.14. The slope of the curve at a point on the dispersion curve represents the group velocity at the frequency corresponding to that point. If we consider two frequencies ω_1 and ω_2 ($> \omega_1$), then we note that the group velocity at the higher frequency is greater than that at the lower frequency. Thus, a positive group velocity differential exists between the two frequencies. Now, we know that a signal having a pulse envelope has a certain bandwidth associated with it. The narrower the pulse, the greater is the bandwidth. For a given distance, the lower frequencies undergo a greater group delay than for the higher frequencies, or the higher frequencies “run away” from the lower frequencies, thereby causing loss of bandwidth and hence broadening of the pulse. In fact, the wider the bandwidth of the signal, the greater is the group

delay spread within the bandwidth, so that the narrower the pulse envelope of the signal, the more pronounced is the pulse broadening.

Signal with Gaussian envelope

For a quantitative discussion of pulse broadening due to dispersion, we shall consider the propagation of an amplitude-modulated signal consisting of a carrier frequency signal modulated by a pulse having a Gaussian distribution with time, that is, a carrier frequency signal with a Gaussian envelope. Thus, let the electric field at the input ($z = 0$) of the dispersive channel be

$$E(0, t) = E_0 e^{-(t/T_0)^2} \cos \omega_0 t \tag{9.88}$$

where ω_0 is the carrier frequency, so that the phasor electric field is

$$\bar{E}(0, t) = E_0 e^{-(t/T_0)^2} e^{j\omega_0 t} \tag{9.89}$$

In (9.89), the function $e^{-(t/T_0)^2}$ corresponds to Gaussian distribution with 1/e half-width equal to T_0 , as shown in Fig. 9.16(a).

Analysis for signal with Gaussian envelope

To analyze the propagation of the pulse, we need to use the Fourier technique, which consists of following the Fourier spectrum of (9.89) as it propagates down the medium and examine the inverse Fourier transform at the distant location. The Fourier transform of (9.89) is given by

$$\begin{aligned} \bar{E}(0, \omega) &= \int_{-\infty}^{\infty} \bar{E}(0, t) e^{-j\omega t} dt \\ &= E_0 \int_{-\infty}^{\infty} e^{-(t/T_0)^2} e^{-j(\omega - \omega_0)t} dt \\ &= 2E_0 \int_0^{\infty} e^{-(t/T_0)^2} \cos(\omega - \omega_0)t dt \end{aligned}$$

or

$$\bar{E}(0, \omega) = \sqrt{\pi} E_0 T_0 e^{-(1/4)(\omega - \omega_0)^2 T_0^2} \tag{9.90}$$

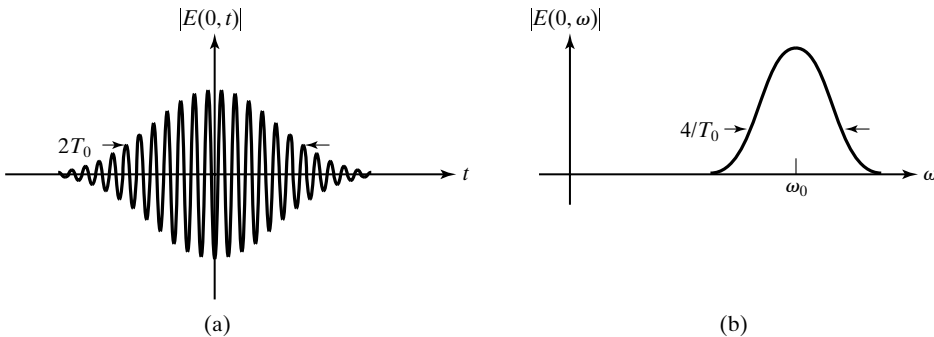


FIGURE 9.16

(a) Amplitude-modulated signal with Gaussian envelope, and (b) its Fourier spectrum.

Note that the Fourier transform is also Gaussian, with half-width $2/T_0$, and centered at the carrier frequency ω_0 , as shown in Fig. 9.16(b).

In traveling by a distance z from the input, each frequency component of the Fourier spectrum undergoes a phase change $e^{-j\beta_z z}$, where it is understood that β_z , the phase constant along the direction of propagation, is a function of ω . Assuming lossless medium, the Fourier transform of the signal at that location is then given by

$$\boxed{\bar{E}(z, \omega) = \bar{E}(0, \omega) e^{-j\beta_z z}} \quad (9.91)$$

Taking the inverse Fourier transform of (9.91), we obtain the propagated signal to be

$$\begin{aligned} \bar{E}(z, t) &= \frac{1}{2\pi} \int_{-\infty}^{\infty} \bar{E}(z, \omega) e^{j\omega t} d\omega \\ &= \frac{1}{2\pi} \int_{-\infty}^{\infty} \bar{E}(0, \omega) e^{-j\beta_z z} e^{j\omega t} d\omega \end{aligned} \quad (9.92)$$

To evaluate (9.92), we consider the pulse to be narrow-band and β_z to be a slowly varying function of ω , so that we can expand β_z in Taylor's series about the carrier frequency ω_0 and keep the first three terms:

$$\begin{aligned} \beta_z(\omega) &= \beta_z(\omega_0) + (\omega - \omega_0) \left. \frac{d\beta_z}{d\omega} \right|_{\omega_0} + \frac{1}{2} (\omega - \omega_0)^2 \left. \frac{d^2\beta_z}{d\omega^2} \right|_{\omega_0} \\ &= \beta_z^{(0)} + (\omega - \omega_0) \beta_z^{(1)} + \frac{1}{2} (\omega - \omega_0)^2 \beta_z^{(2)} \end{aligned} \quad (9.93)$$

where $\beta_z^{(0)}$, $\beta_z^{(1)}$, and $\beta_z^{(2)}$ are β_z , $d\beta_z/d\omega$, and $d^2\beta_z/d\omega^2$, respectively, evaluated at $\omega = \omega_0$. Substituting (9.93) into (9.92), we have

$$\begin{aligned} \bar{E}(z, t) &= \frac{1}{2\pi} \int_{-\infty}^{\infty} \bar{E}(0, \omega) e^{-j\beta_z^{(0)} z - j(\omega - \omega_0) \beta_z^{(1)} z - j(1/2)(\omega - \omega_0)^2 \beta_z^{(2)} z} e^{j\omega t} d\omega \\ &= \frac{1}{2\pi} \int_{-\infty}^{\infty} \bar{E}(0, \omega') e^{-j\beta_z^{(0)} z + j\omega'(t - t_0) - j(1/2)\omega'^2 \beta_z^{(2)} z} e^{j\omega_0 t} d\omega' \end{aligned} \quad (9.94)$$

where

$$\boxed{t_0 = z\beta_z^{(1)} = \frac{z}{[v_g]_{\omega_0}} = \text{group delay at } \omega_0} \quad (9.95)$$

and $\omega' = \omega - \omega_0$. Proceeding further, we obtain

$$\begin{aligned}
 \bar{E}(z, t) &= \frac{E_0 T_0}{2\sqrt{\pi}} e^{j[\omega_0 t - \beta_z^{(0)} z]} \\
 &\quad \cdot \int_{-\infty}^{\infty} e^{-(1/4)\omega'^2 T_0^2} e^{j\omega'(t-t_0) - j(1/2)\omega'^2 \beta_z^{(2)} z} d\omega' \\
 &= \frac{E_0 T_0}{2\sqrt{\pi}} e^{j[\omega_0 t - \beta_z^{(0)} z]} \\
 &\quad \cdot \int_{-\infty}^{\infty} e^{-(1/4)\omega'^2 [T_0^2 + j2\beta_z^{(2)} z]} e^{j\omega'(t-t_0)} d\omega' \\
 &= \frac{E_0 T_0}{2\sqrt{\pi}} e^{j[\omega_0 t - \beta_z^{(0)} z]} \int_{-\infty}^{\infty} e^{-(1/4)\omega'^2 T_0^2 [1 + j(S/T_0)]} e^{j\omega'(t-t_0)} d\omega'
 \end{aligned}$$

or

$$\boxed{\bar{E}(z, t) = \frac{E_0 e^{j[\omega_0 t - \beta_z^{(0)} z]}}{\sqrt{1 + j(S/T_0)}} e^{-\{(t-t_0)^2 [1 - j(S/T_0)]\} / (T_0^2 + S^2)}} \quad (9.96)$$

where

$$\boxed{
 \begin{aligned}
 S &= \frac{2}{T_0} \beta_z^{(2)} z = \frac{2}{T_0} \frac{\partial t_0}{\partial \omega} \\
 &= \text{half-bandwidth of the pulse at } z = 0 \text{ times} \\
 &\quad \text{group delay per unit frequency} \\
 &= \text{group delay for the entire half-bandwidth}
 \end{aligned}
 } \quad (9.97)$$

*Pulse
broadening
parameter*

The result that we have obtained for the transmitted pulse tells us that the pulse envelope is $e^{-(t-t_0)^2 / (T_0^2 + S^2)}$. Thus, it reaches a peak at $t = t_0$, which is simply the group delay at the carrier frequency ω_0 , and its half-width is broadened from the initial value T_0 to $T(z) = \sqrt{T_0^2 + S^2}$. The quantity S , which has the physical meaning given by (9.97), is known as the “pulse broadening parameter.” It is of interest to discuss this further since it governs the pulse spread. In fact, for $|S| \gg T_0$, the pulse half-width is approximately equal to $|S|$. From (9.97), it can be seen that the value of S is influenced by three factors: (1) the bandwidth, $2/T_0$, of the input pulse; (2) dispersion, through the factor $\beta_z^{(2)}$; and (3) the distance, z , traveled by the signal. Figure 9.17 depicts the pulse broadening as a function of distance. Note from the plot of T versus z that for large distances the half-width of the pulse increases approximately linearly with distance at the rate of $|S|/z$, or $(2/T_0)|\beta_z^{(2)}|$, which is inversely proportional to the initial half-width T_0 .

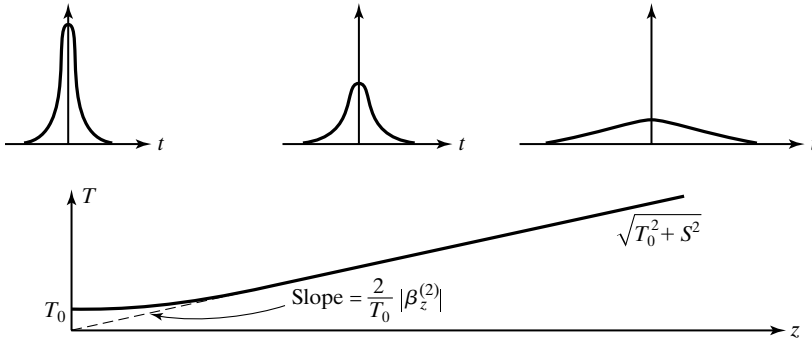


FIGURE 9.17

Broadening of the Gaussian envelope of a signal as a function of distance in a dispersive medium.

Example 9.9 Broadening of a signal with Gaussian envelope in a dispersive medium

Consider the propagation of a signal with Gaussian pulse envelope of half-width T_0 in a dispersive medium having the dispersion relation

$$\omega = \omega_p \left(1 + \frac{a^2 \beta_z^2}{2} \right)$$

where ω_p and a are constants. It is desired to investigate the broadening of the transmitted pulse.

For the given dispersion relation,

$$\begin{aligned} \frac{d\omega}{d\beta_z} &= \omega_p a^2 \beta_z \\ \frac{d^2\omega}{d\beta_z^2} &= \omega_p a^2 \end{aligned}$$

From (9.97), the pulse broadening parameter is given by

$$S = \frac{2}{T_0} \omega_p^2 a^2 z$$

and the half-width of the transmitted pulse is

$$\begin{aligned} \sqrt{T_0^2 + S^2} &= \sqrt{T_0^2 + \left(\frac{2}{T_0} \omega_p^2 a^2 z \right)^2} \\ &= T_0 \sqrt{1 + \left(\frac{2}{T_0^2} \omega_p^2 a^2 z \right)^2} \end{aligned}$$

Note that for large distances from the input, the half-width is approximately equal to $(2/T_0)\omega_p^2 a z$.

Having discussed the phenomenon of pulse spreading due to dispersion, we shall now turn to causes of dispersion in optical waveguides. In optical waveguides,

Causes of Dispersion

dispersion is influenced by three factors: (1) waveguide dispersion, (2) intermodal dispersion, and (3) material dispersion. Waveguide dispersion is due to the fact that the phase velocity of propagation of the wave along the guide axis is a function of the wave frequency. This is the same as in metallic waveguides, which led to the introduction of the topic of dispersion in Section 8.4. Intermodal dispersion results from different travel times of rays corresponding to different modes, as discussed in Section 8.7. Material dispersion results from the frequency dependence of the refractive index of optical materials. We shall here elaborate on this.

*Material
dispersion*

For a plane wave propagating in a uniform material medium having the refractive index n , the phase constant is given by

$$\beta = \frac{\omega}{v_p} = \frac{\omega n}{c} \quad (9.98)$$

To investigate pulse broadening due to material dispersion, we need to evaluate $\beta^{(2)} = d^2\beta/d\omega^2$. First, we note that

$$\frac{d\beta}{d\omega} = \frac{1}{c} \left(n + \omega \frac{dn}{d\omega} \right)$$

Since it is common practice to deal with n as a function of free-space wavelength λ_0 , we make use of the relationship

$$f\lambda_0 = c$$

and obtain

$$\frac{dn}{d\omega} = \frac{dn}{d\lambda_0} \cdot \frac{d\lambda_0}{d\omega} = \frac{dn}{d\lambda_0} \left(-\frac{2\pi c}{\omega^2} \right)$$

so that

$$\frac{d\beta}{d\omega} = \frac{1}{c} \left(n - \lambda_0 \frac{dn}{d\lambda_0} \right)$$

Note that the group velocity is

$$v_g = \frac{d\omega}{d\beta} = \frac{c}{n - \lambda_0(dn/d\lambda_0)} \quad (9.99)$$

The quantity $[n - \lambda_0(dn/d\lambda_0)]$, denoted N , is known as the *group refractive index*. Proceeding further, we obtain

$$\begin{aligned} \frac{d^2\beta}{d\omega^2} &= \frac{d}{d\lambda_0} \left(\frac{d\beta}{d\omega} \right) \cdot \frac{d\lambda_0}{d\omega} \\ &= -\frac{\lambda_0}{c} \frac{d^2n}{d\lambda_0^2} \cdot \frac{d\lambda_0}{d\omega} \end{aligned} \quad (9.100)$$

The pulse broadening parameter is given by

$$\begin{aligned}
 S &= \text{half-bandwidth of the pulse} \times \beta^{(2)}z \\
 &= -\frac{\lambda_0}{c} \frac{d^2n}{d\lambda_0^2} \frac{d\lambda_0}{d\omega} (\Delta\omega)z \\
 &= -\left(\frac{\lambda_0}{c} \frac{d^2n}{d\lambda_0^2}\right) (\Delta\lambda_0)z
 \end{aligned}
 \tag{9.101}$$

where $\Delta\omega$ is the half-bandwidth of the pulse and $\Delta\lambda_0 = (d\lambda_0/d\omega) \Delta\omega$ is the half-spectral width, that is, the half-bandwidth in the wavelength domain.

The quantity $[(\lambda_0/c)(d^2n/d\lambda_0^2)]$ is known as the *dispersion coefficient*, denoted D_λ , usually given in units of ps/km-nm, where the pulse broadening is measured in picoseconds, the length of the medium in kilometers, and the source spectral width in nanometers. The wavelength dependences of n , N , and D_λ for fused silica are shown plotted in Fig. 9.18. For $\lambda_0 < 1.312 \mu\text{m}$, $D_\lambda < 0$ and the dispersion is normal. For $\lambda_0 > 1.312 \mu\text{m}$, $D_\lambda > 0$ and the dispersion is anomalous. For $\lambda_0 \approx 1.312 \mu\text{m}$, D_λ is zero and dispersion is negligible.

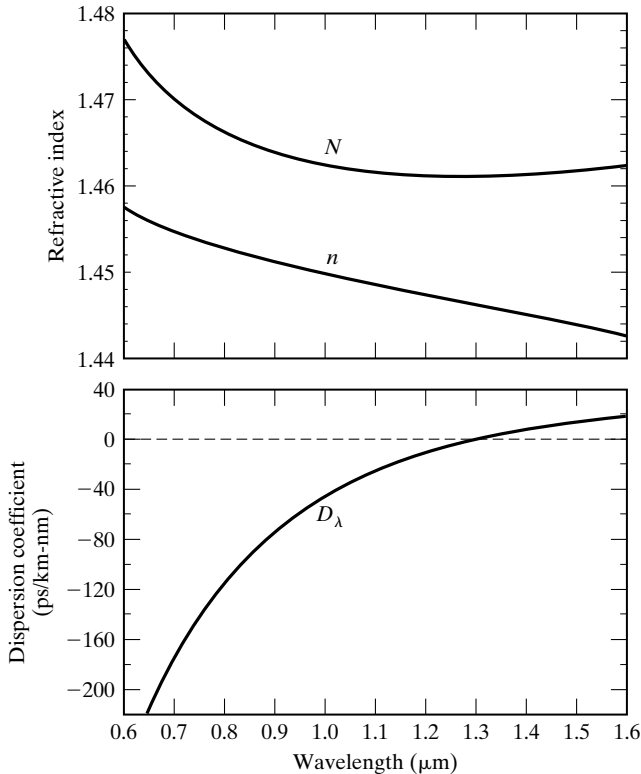


FIGURE 9.18
Wavelength dependences of n , N , and D_λ for fused silica.

- K9.5.** Signal with Gaussian envelope; Pulse broadening parameter; Dispersion in optical guides; Material dispersion; Dispersion coefficient.
- D9.9.** The phase refractive index of an optical material used in a single-mode fiber can be approximated as

$$n(\lambda_0) = 1.58 + \frac{1.46 \times 10^{-14}}{\lambda_0^2}$$

Obtain the following for λ_0 equal to $0.5 \mu\text{m}$: **(a)** the phase refractive index; **(b)** the group refractive index; and **(c)** the dispersion coefficient.

Ans. **(a)** 1.6384; **(b)** 1.7552; **(c)** 2,336 ps/km-nm.

9.6 INTERFERENCE AND DIFFRACTION

Interference explained

In this section, we turn our attention to two related topics that are based on the superposition of waves. When two or more waves are superimposed, the resulting distribution of intensity is in general not merely the sum of the distributions of the intensities of the individual waves; instead, it varies between maxima, which exceed the sum of the individual intensities, and minima, which may go to zero. This phenomenon is called *interference*. In the terminology of light, intensity means the time-average power crossing a unit area perpendicular to the direction of power flow, that is, the time-average Poynting vector, which is proportional to the square of the amplitude of the electric field. Thus, denoting intensity by the symbol I , we have

$$I = k\langle \mathbf{E} \cdot \mathbf{E} \rangle = k\langle E^2 \rangle \quad (9.102)$$

where k is the constant of proportionality, dependent on the medium. For free space, k is equal to $1/2\eta_0$.

Let us now consider two uniform plane waves whose electric fields at a point P are \mathbf{E}_1 and \mathbf{E}_2 , respectively. Then the intensities of the individual waves are

$$I_1 = k\langle E_1^2 \rangle \quad \text{and} \quad I_2 = k\langle E_2^2 \rangle \quad (9.103)$$

The intensity of the superposition of the two waves is

$$\begin{aligned} I &= k\langle (\mathbf{E}_1 + \mathbf{E}_2) \cdot (\mathbf{E}_1 + \mathbf{E}_2) \rangle \\ &= k\langle E_1^2 \rangle + k\langle E_2^2 \rangle + 2k\langle \mathbf{E}_1 \cdot \mathbf{E}_2 \rangle \\ &= I_1 + I_2 + 2k\langle E_1 E_2 \cos \alpha \rangle \end{aligned} \quad (9.104)$$

where α is the angle between the directions of \mathbf{E}_1 and \mathbf{E}_2 . The third term on the right side is seen to be the interference term. Depending on the sign of this term, it can be seen that the intensity of the composite wave can be greater than or less than the sum of the individual intensities. It is equal to the sum of the two intensities only if $\cos \alpha$ is equal to zero, which occurs when \mathbf{E}_1 and \mathbf{E}_2 are perpendicular. Thus, two waves whose fields are polarized perpendicular to each other do not produce interference.

An experimental demonstration of interference of light was first performed by Thomas Young. Young's experiment consisted of light from a monochromatic point source S_0 , behind a screen containing two pinholes separated by a distance on the order of a millimeter, passing through the pinholes, thereby giving rise to two light beams creating an interference pattern on an observation screen located at a distance R of the order of several meters beyond the pinholes, as shown in Fig. 9.19.

The two waves generated at the pinholes are spherical waves and in phase. At a point P on the observation screen, the waves can be approximated as plane waves. The interference phenomenon can therefore be analyzed by superimposing two traveling waves propagating at the angles θ_1 and θ_2 to the vertical. Because of the large value of R , the difference between these angles is small so that the two lines S_1P and S_2P can be considered to be parallel and $(r_2 - r_1) \approx d \cos \theta$. As the point P moves vertically on the observation screen, the path difference $d \cos \theta$ varies and hence the phase difference between the two waves varies, creating the interference pattern.

Assuming equal amplitudes and zero phase angle at the slits, the individual electric fields of the two beams can be written as

$$E_1 = \frac{A}{r_1} \cos(\omega t - \beta_{r_1}) \quad (9.105a)$$

$$E_2 = \frac{A}{r_2} \cos(\omega t - \beta_{r_2}) \quad (9.105b)$$

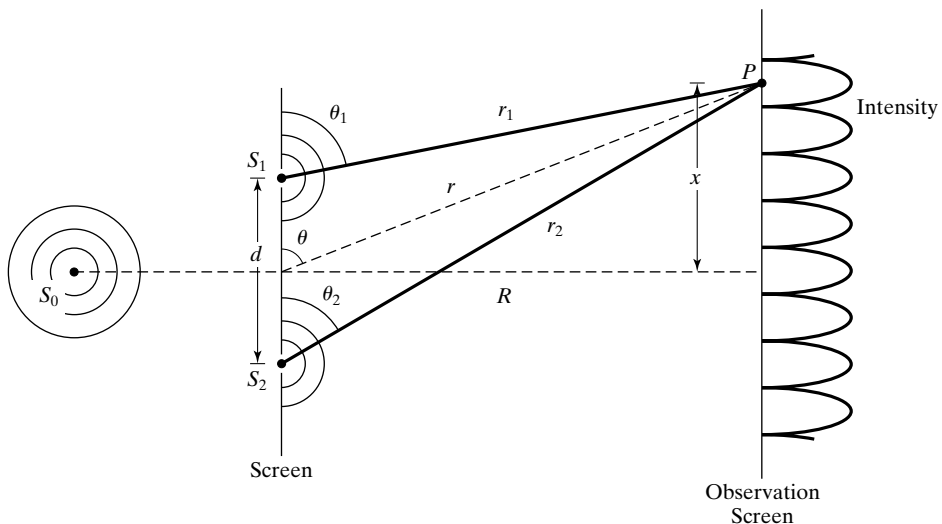


FIGURE 9.19

Experimental arrangement of Thomas Young to demonstrate interference of light.

Setting $r_1 \approx r_2 \approx r$ in the amplitude factors, we obtain the total electric field to be

$$E = E_1 + E_2 \approx \frac{A}{r} [\cos(\omega t - \beta r_1) + \cos(\omega t - \beta r_2)] \quad (9.106)$$

The intensity of the beam on the screen is therefore given by

$$\begin{aligned} I &= k \langle E^2 \rangle \\ &= \frac{kA^2}{r^2} \langle \cos^2(\omega t - \beta r_1) + \cos^2(\omega t - \beta r_2) \\ &\quad + 2 \cos(\omega t - \beta r_1) \cos(\omega t - \beta r_2) \rangle \\ &= \frac{KA^2}{r^2} \left[\frac{1}{2} + \frac{1}{2} + \cos \beta(r_2 - r_1) \right] \\ &= \frac{2kA^2}{r^2} \cos^2 \frac{\beta(r_2 - r_1)}{2} \\ &= \frac{2kA^2}{r^2} \cos^2 \frac{\beta d \cos \theta}{2} \end{aligned} \quad (9.107)$$

Thus, the intensity varies between zero and $2kA^2/r^2$. In terms of the distance x , we can write $\cos \theta = x/r = x/\sqrt{R^2 + x^2}$. Furthermore, for $x \ll R$, we can set $\sqrt{R^2 + x^2} \approx R$, so that we obtain

$$I \approx \frac{2kA^2}{R^2} \cos^2 \frac{\pi dx}{\lambda R} \quad (9.108)$$

Thus, the maxima of the intensity occur for $x = n\lambda R/d$, $n = 0, \pm 1, \pm 2, \dots$, and the minima occur for $x = (2n + 1)\lambda R/d$, $n = 0, \pm 1, \pm 2, \dots$. The separation between the maxima and the minima is a constant, equal to $\Delta x = \lambda R/d$. For a numerical example, for $d = 0.1$ mm, $R = 2$ m, and $\lambda = 0.5$ μ m, $\Delta x = 1$ cm.

Conversely to the preceding, if λ is unknown, it can be computed from a measurement of Δx and the known values of R and d . For two beams, the sharpness of the interference fringes is not sufficient to permit accurate measurement of Δx , but by using a large number of beams the sharpness can be increased. We shall not pursue the multiple-source problem here, but we will consider it in connection with antenna arrays in Section 10.4. We shall, however, include here an example of a similar phenomenon resulting from multiple reflections and transmissions of waves from a single source.

Example 9.10 Multiple-beam interference in a plane dielectric slab

Multiple-beam interference

Let us consider a uniform plane wave of electric field \bar{E}_i and wavelength λ_0 , incident at an angle θ_i on a plane dielectric slab of thickness d and refractive index n , as shown in Fig. 9.20. For simplicity, we shall consider the medium on either side of the dielectric slab

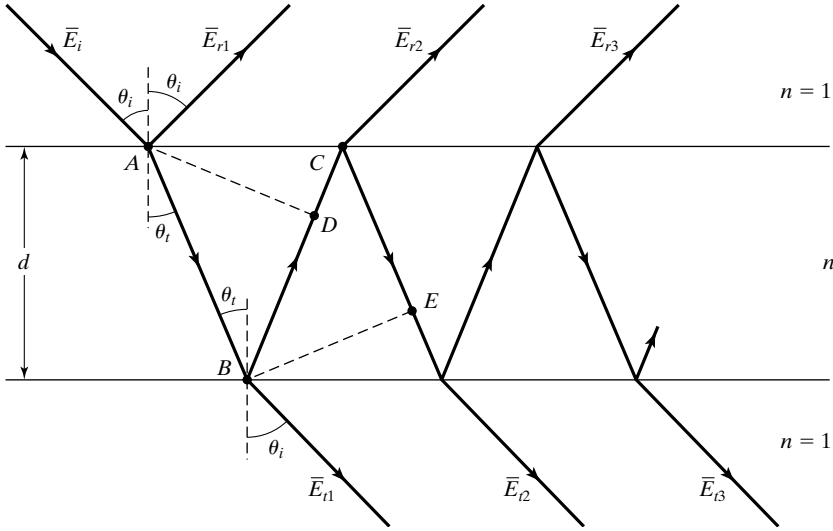


FIGURE 9.20

Multiple reflections and transmissions for plane wave incidence on a plane dielectric slab.

to be free space. We wish to investigate the interference resulting from the (infinite) number of waves produced by reflections and transmissions at the two interfaces, a few of which are shown in Fig. 9.20.

With reference to the notation shown in Fig. 9.20, and denoting Γ and τ to be the reflection and transmission coefficients, respectively, for incidence from free space on to the dielectric, and Γ' and τ' to be the reflection and transmission coefficients, respectively, for incidence from the dielectric on to free space, we can write the expressions for the successively reflected and transmitted wave electric fields as follows:

$$\bar{E}_{r1} = \bar{E}_i \Gamma \quad (9.109a) \quad \bar{E}_{t1} = \bar{E}_i \tau \tau' \quad (9.109d)$$

$$\bar{E}_{r2} = \bar{E}_i \tau \Gamma' \tau' e^{-j\delta} \quad (9.109b) \quad \bar{E}_{t2} = \bar{E}_i \tau (\Gamma')^2 \tau' e^{-j\delta} \quad (9.109e)$$

$$\bar{E}_{r3} = \bar{E}_i \tau (\Gamma')^3 \tau' e^{-j2\delta} \quad (9.109c) \quad \bar{E}_{t3} = \bar{E}_i \tau (\Gamma')^4 \tau' e^{-j2\delta} \quad (9.109f)$$

where

$$\begin{aligned} \delta &= \frac{2\pi n}{\lambda_0} (AB + BD) = \frac{2\pi n}{\lambda_0} (BC + CE) \\ &= \frac{2\pi n}{\lambda_0} \frac{d}{\cos \theta_t} (1 + \cos 2\theta_t) \\ &= \frac{4\pi n d}{\lambda_0} \cos \theta_t \end{aligned} \quad (9.110)$$

is the additional phase shift undergone by successive reflected (or transmitted) waves. Summing up all the reflected wave fields, we obtain the total reflected wave field to be

$$\begin{aligned}\bar{E}_r &= \bar{E}_i \{ \Gamma + \tau\tau'\bar{\Gamma}'e^{-j\delta}[1 + (\Gamma')^2e^{-j\delta} + \dots] \} \\ &= \bar{E}_i \left[\Gamma + \frac{\tau\tau'\Gamma'e^{-j\delta}}{1 - (\Gamma')^2e^{-j\delta}} \right]\end{aligned}\quad (9.111a)$$

Similarly, the total transmitted wave field is given by

$$\begin{aligned}\bar{E}_t &= \bar{E}_i\tau\tau'[1 + (\Gamma')^2e^{-j\delta} + \dots] \\ &= \bar{E}_i \left[\frac{\tau\tau'}{1 - (\Gamma')^2e^{-j\delta}} \right]\end{aligned}\quad (9.111b)$$

Although the specific expressions for Γ , Γ' , τ , and τ' depend on the polarization of \mathbf{E}_i and are given in Section 8.5 by the Fresnel coefficients, we can write, regardless of polarization (see Problem P9.28), that

$$\boxed{\Gamma' = -\Gamma}\quad (9.112a)$$

and

$$\boxed{\tau\tau' + \Gamma^2 = 1}\quad (9.112b)$$

Substituting (9.112a) and (9.112b) into (9.111a) and (9.111b), we obtain

$$\bar{E}_r = \bar{E}_i \left[\frac{\Gamma(1 - e^{-j\delta})}{1 - \Gamma^2e^{-j\delta}} \right]\quad (9.113a)$$

$$\bar{E}_t = \bar{E}_i \frac{1 - \Gamma^2}{1 - \Gamma^2e^{-j\delta}}\quad (9.113b)$$

The fractions of the incident intensity that are reflected and transmitted are given, respectively, by

$$\frac{I_r}{I_i} = \frac{|\bar{E}_r|^2}{|\bar{E}_i|^2} = \frac{4F^2 \sin^2(\delta/2)}{\pi^2 + 4F^2 \sin^2(\delta/2)}\quad (9.114a)$$

$$\frac{I_t}{I_i} = \frac{|\bar{E}_t|^2}{|\bar{E}_i|^2} = \frac{\pi^2}{\pi^2 + 4F^2 \sin^2(\delta/2)}\quad (9.114b)$$

where

$$\boxed{F = \frac{\pi|\Gamma|}{1 - \Gamma^2}}\quad (9.115)$$

is called the *finesse*. Note that the sum of right sides of (9.114a) and (9.114b) is equal to unity, as it should be.

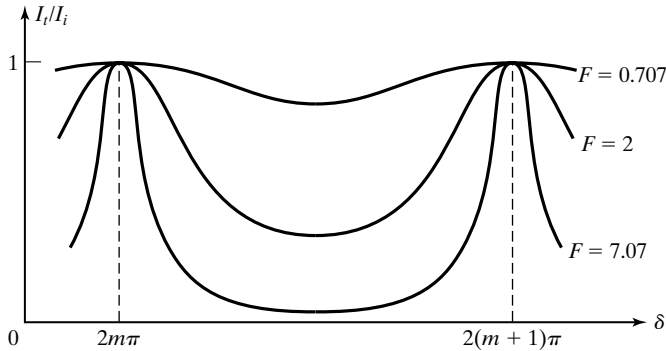


FIGURE 9.21

Plots of the transmission characteristics of the arrangement of Fig. 9.20 for several values of F .

The transmission characteristic of the arrangement of Fig. 9.20, a model for the *Fabry-Perot etalon*, or interferometer, can now be discussed with the aid of the plot of the right side of (9.114b) versus δ , which is shown in Fig. 9.21, for several values of F and hence Γ . It can be seen that maximum transmission of unity occurs for

$$\delta = \frac{4\pi nd}{\lambda_0} \cos \theta_t = 2m\pi, \quad m = 1, 2, 3, \dots \quad (9.116)$$

with the sharpness of the maxima increasing with F . For given values of λ_0 , d , and n , the plot can be thought of as variation of I_t/I_0 with θ_t (and hence θ_i), thereby corresponding to the interference pattern. For fixed values of d , n , and θ_t , the peaks in Fig. 9.21 correspond to two adjacent frequencies at which I_t/I_i is unity. From (9.116), this frequency separation can be seen to be equal to $c/(2nd \cos \theta_t)$. Also, for given values of d and n , different values of λ_0 (and hence f) give rise to interference patterns of different periodicities, thereby allowing resolution of closely spaced frequencies for high values of F (see Problem P9.29).

Fabry-Perot etalon

When an object is placed between a source of light and an observation screen, the shadow on the screen contains a fine structure of interference fringes in the vicinity of the boundary separating the dark shadow from the rest of the brightly illuminated screen, as compared to a simple sharp boundary between the dark and bright regions. This phenomenon, which occurs due to the *bending* of a portion of the beam, is known as *diffraction*. Just as interference is a manifestation of the superposition of light beams, diffraction is also a manifestation of the superposition of light beams. Interference usually applies to the interaction of only a few beams with one another, whereas diffraction usually pertains to the superposition of a large number, even a continuous distribution of beams, although the distinction is not sharp. The phenomenon of diffraction is in contrast to the principle of geometrical optics, which has to do with light traveling in straight lines, except for bending by reflection and refraction, and which is strictly valid under certain conditions: (a) The dimensions of the object in the path of light are very large compared to the wavelength and (b) the region of importance is not close to the boundary of the shadow.

Diffraction explained

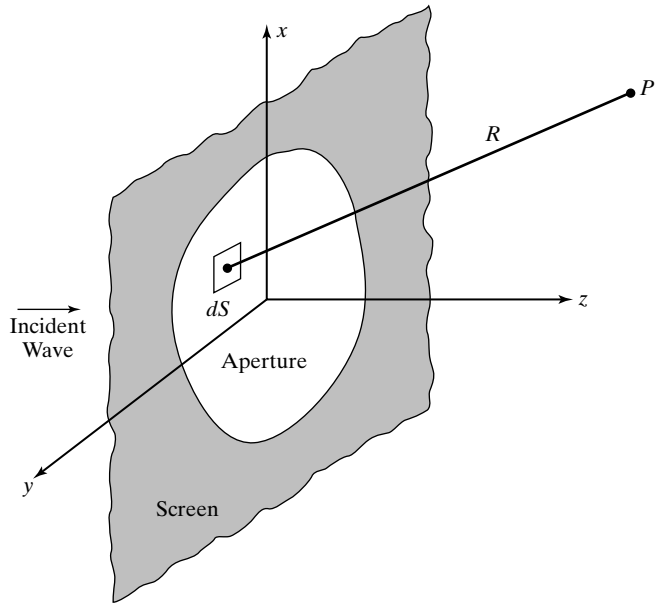


FIGURE 9.22
Geometry pertinent to
diffraction by an aperture
on a screen.

*Huygens–
Fresnel
principle*

Although the exact treatment of the phenomenon of diffraction involves solution as a boundary value problem and is very difficult, it can be studied in approximate but sufficiently accurate terms by using the Huygens–Fresnel principle, as long as the distance from the diffracting object to the point of observation is more than about ten wavelengths. To explain this principle, let us consider a plane monochromatic wave that is incident normally on a screen in the xy -plane with an aperture cut into it, as shown in Fig. 9.22. Then, according to this principle, the incident wave may be thought of as giving rise to secondary (spherical) waves that emanate from every point in the aperture and interfere with one another to the right of the screen. The scalar field at a point P is approximately given by

$$\bar{E}(P) \approx \frac{j\beta}{2\pi} \int_S \frac{\bar{E}(x', y', 0)}{R} e^{-j\beta R} dS \quad (9.117)$$

where S is the area of the aperture, and $\bar{E}(x', y', 0)$ is the scalar field in the aperture. We shall illustrate the application of (9.117) by means of an example.

Example 9.11 Diffraction of a uniform plane wave by a circular aperture

*Diffraction
by a circular
aperture*

Let us assume that the aperture of Fig. 9.22 is a circular hole of radius a having its center at the origin and illuminated by a uniform plane wave of electric-field intensity E_0 at the aperture, as shown in Fig. 9.23. We wish to investigate the diffracted field along the z -axis.

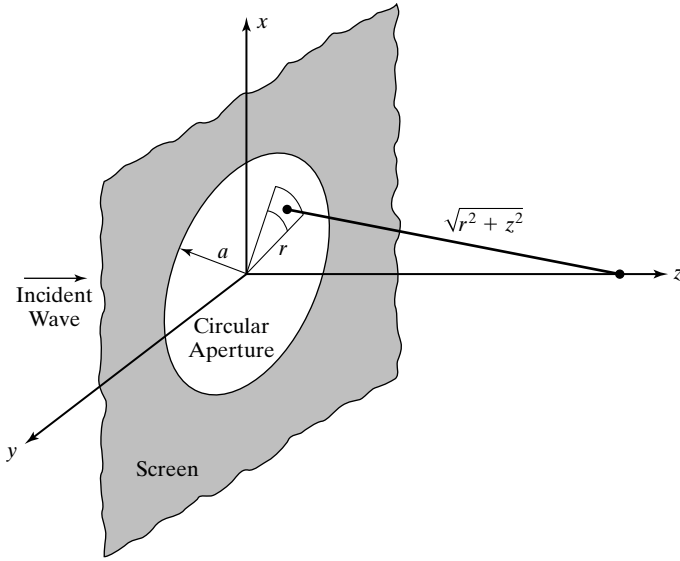


FIGURE 9.23

Geometry pertinent to diffraction by a circular aperture illuminated by a plane wave.

Applying (9.117) to the geometry in Fig. 9.23 and noting the circular symmetry about the z -axis, we obtain

$$\bar{E}(0, 0, z) = \frac{j\beta}{2\pi} \int_{r=0}^a \int_{\phi=0}^{2\pi} \frac{E_0}{\sqrt{r^2 + z^2}} e^{-j\beta\sqrt{r^2 + z^2}} r \, dr \, d\phi \quad (9.118)$$

Making the change of variable $R = \sqrt{r^2 + z^2}$, and hence $dR = (r \, dr)/R$, we obtain

$$\begin{aligned} \bar{E}(0, 0, z) &= j\beta E_0 \int_z^{\sqrt{a^2 + z^2}} e^{-j\beta R} \, dR \\ &= -E_0 e^{-j\beta\sqrt{a^2 + z^2}} + E_0 e^{-j\beta z} \end{aligned} \quad (9.119)$$

Proceeding further, the intensity is given by

$$\begin{aligned} I &= \frac{1}{2\eta_0} |\bar{E}|^2 = \frac{1}{2\eta_0} \bar{E} \bar{E}^* \\ &= \frac{E_0^2}{2\eta_0} [2 - 2 \cos \beta(\sqrt{a^2 + z^2} - z)] \\ &= \frac{E_0^2}{\eta_0} \sin^2 \frac{\beta(\sqrt{a^2 + z^2} - z)}{2} \end{aligned} \quad (9.120)$$

For $z \gg a$, (9.120) reduces to

$$\boxed{I \approx \frac{2E_0^2}{\eta_0} \sin^2 \frac{\beta a^2}{4z} = \frac{2E_0^2}{\eta_0} \sin^2 \frac{\pi a^2}{2\lambda z}} \quad (9.121)$$

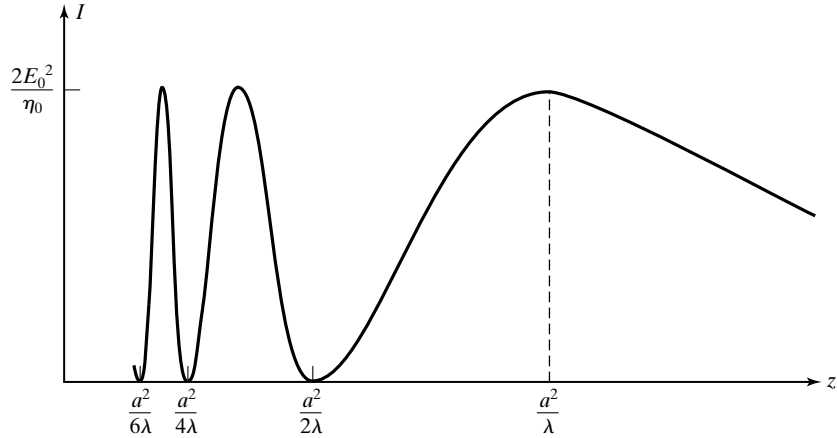


FIGURE 9.24

Variation of the intensity along the z -axis for the arrangement of Fig. 9.23.

*Fresnel vs.
Fraunhofer
diffraction*

A sketch of the result given by (9.121) is shown in Fig. 9.24. It can be seen that for $z < a^2/\lambda$, the intensity fluctuates between maxima of $2E_0^2/\eta_0$ and minima of zero, corresponding to constructive and destructive interference, respectively, of the spherical waves. The situation is said to correspond to *Fresnel diffraction*. For $z > a^2/\lambda$, the intensity decreases monotonically. For $z \gg a^2/\lambda$, the diffraction is known as *Fraunhofer diffraction*, and the evaluation of the integral in (9.117) becomes easier, because waves arriving at P from the aperture approach plane waves, thereby permitting the simplifying plane wave approximation in the integrand. We shall not pursue the topic here, however; instead, we defer the consideration to Section 10.6, where the determination of the far field due to an aperture distribution is identical to that of the solution for Fraunhofer diffraction. In practice, the boundary between the Fresnel and Fraunhofer diffraction regions is taken to be $2D^2/\lambda$, where D is the diameter of the circular aperture, or in the case of a noncircular aperture it is its maximum linear dimension. (See Problem P9.30.)

K9.6. Intensity; Two-beam interference; Multiple-beam interference; Finesse; Fabry–Perot etalon; Diffraction; Huygens–Fresnel principle; Circular aperture; Fresnel diffraction; Fraunhofer diffraction.

D9.10. For a uniform plane wave incident from free space onto a plane dielectric slab of thickness $d = 5.1\lambda_0$ and refractive index $n = 4$ at an angle $\theta_i = 60^\circ$, find F and I_r/I_i for each of the two polarizations: **(a)** perpendicular and **(b)** parallel.

Ans. **(a)** 6.034, 0.2113; **(b)** 1.226, 0.8665.

9.7 WAVE PROPAGATION IN ANISOTROPIC MEDIUM

*Linear
characteristic
polarizations*

In Section 4.2, we learned that for certain dielectric materials known as *anisotropic dielectric materials*, \mathbf{D} is not in general parallel to \mathbf{E} and the relationship between \mathbf{D} and \mathbf{E} is expressed by means of a permittivity tensor consisting of a 3×3 matrix.

Let us consider an anisotropic dielectric medium characterized by the simple \mathbf{D} to \mathbf{E} relationship given by

$$\begin{bmatrix} D_x \\ D_y \\ D_z \end{bmatrix} = \begin{bmatrix} \varepsilon_x & 0 & 0 \\ 0 & \varepsilon_y & 0 \\ 0 & 0 & \varepsilon_z \end{bmatrix} \begin{bmatrix} E_x \\ E_y \\ E_z \end{bmatrix} \quad (9.122)$$

and having the permeability μ_0 . It is easy to see that the characteristic polarizations for this case are all linear directed along the coordinate axes and having the effective permittivities ε_x , ε_y , and ε_z for the x -, y -, and z -directed polarizations, respectively. These axes are then known as the principal axes. Let us consider a uniform plane wave propagating along one of the principal axes, say, the z -direction. The wave will then generally contain both x - and y -components of the fields. It can be decomposed into two waves, one having an x -directed electric field and the other having a y -directed electric field. These component waves travel individually in the anisotropic medium as though it is isotropic, but with different phase velocities since the effective permittivities are different. In view of this, the phase relationship between the two waves, and hence the polarization of the composite wave, changes with distance along the direction of propagation. Also, when they encounter a discontinuity, the component waves undergo reflection and transmission by different amounts. We shall illustrate by means of an example.

Example 9.12 Propagation of a uniform plane wave along a principal axis of an anisotropic dielectric

Let us consider a uniform plane wave of frequency 1500 MHz incident from free space ($z < 0$) normally onto an anisotropic perfect dielectric medium ($z > 0$), characterized by the permittivity matrix

Propagation along a principal axis

$$[\varepsilon] = \varepsilon_0 \begin{bmatrix} 4 & 0 & 0 \\ 0 & 9 & 0 \\ 0 & 0 & 4 \end{bmatrix}$$

and $\mu = \mu_0$. We wish to discuss the reflected and transmitted waves for several cases of incident waves.

Case 1. The incident wave has only an x -component of \mathbf{E} as given by

$$\mathbf{E}_i = E_0 \cos(3 \times 10^9 \pi t - 10\pi z) \mathbf{a}_x$$

Then the effective permittivity of the anisotropic medium is $4\varepsilon_0$, and from (4.146) and (4.147), $\bar{\Gamma} = -\frac{1}{3}$ and $\bar{\tau} = \frac{2}{3}$. The reflected and transmitted wave electric fields are

$$\begin{aligned} \mathbf{E}_r &= -\frac{E_0}{3} \cos(3 \times 10^9 \pi t + 10\pi z) \mathbf{a}_x \\ \mathbf{E}_t &= \frac{2E_0}{3} \cos(3 \times 10^9 \pi t - 20\pi z) \mathbf{a}_x \end{aligned}$$

where we have made use of the fact that for the transmitted wave, the phase constant is $\omega\sqrt{\mu_0 \cdot 4\varepsilon_0} = 2\omega\sqrt{\mu_0\varepsilon_0} = 2 \times 10\pi = 20\pi$.

Case 2. The incident wave has only a y -component of \mathbf{E} as given by

$$\mathbf{E}_i = E_0 \cos(3 \times 10^9 \pi t - 10\pi z) \mathbf{a}_y$$

Then the effective permittivity of the anisotropic medium is $9\epsilon_0$, and from (4.146) and (4.147), $\bar{\Gamma} = -\frac{1}{2}$ and $\bar{\tau} = \frac{1}{2}$. The reflected and transmitted wave electric fields are

$$\mathbf{E}_r = -\frac{E_0}{2} \cos(3 \times 10^9 \pi t + 10\pi z) \mathbf{a}_y$$

$$\mathbf{E}_t = \frac{E_0}{2} \cos(3 \times 10^9 \pi t - 30\pi z) \mathbf{a}_y$$

where we have made use of the fact that for the transmitted wave, the phase constant is $\omega\sqrt{\mu_0 \cdot 9\epsilon_0} = 3\omega\sqrt{\mu_0\epsilon_0} = 3 \times 10\pi = 30\pi$.

Case 3. The incident wave has both x - and y -components of \mathbf{E} and is linearly polarized, as given by

$$\mathbf{E}_i = E_1 \cos(3 \times 10^9 \pi t - 10\pi z) \mathbf{a}_x + E_2 \cos(3 \times 10^9 \pi t - 10\pi z) \mathbf{a}_y$$

Then from superposition of cases 1 and 2, the reflected and transmitted wave electric fields are given by

$$\mathbf{E}_r = -\frac{E_1}{3} \cos(3 \times 10^9 \pi t + 10\pi z) \mathbf{a}_x - \frac{E_2}{2} \cos(3 \times 10^9 \pi t + 10\pi z) \mathbf{a}_y$$

$$\mathbf{E}_t = \frac{2E_1}{3} \cos(3 \times 10^9 \pi t - 20\pi z) \mathbf{a}_x + \frac{E_2}{2} \cos(3 \times 10^9 \pi t - 30\pi z) \mathbf{a}_y$$

Note that \mathbf{E}_r is linearly polarized, although along a direction making an angle to that of the direction of polarization of \mathbf{E}_i . The polarization of \mathbf{E}_t , on the other hand, varies with z , since the phase difference between the x - and y -components of the electric field is $\Delta\phi = 10\pi z$. As the transmitted wave propagates in the z -direction, $\Delta\phi$ changes from zero at $z = 0$ to $\pi/2$ at $z = 0.05$ m to π at $z = 0.1$ m, and so on. Thus, the polarization changes from linear at $z = 0$ to elliptical for $z > 0$, becoming linear again at $z = 0.1$ m, but rotated by an angle as shown in Fig. 9.25, and so on.

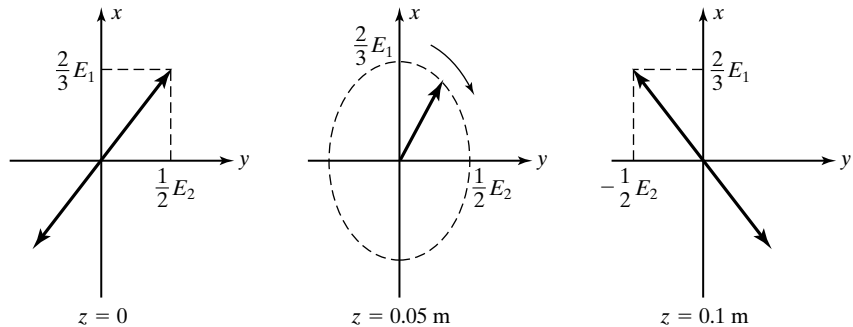


FIGURE 9.25

Change in polarization versus z of the transmitted wave electric field of Example 9.12.

The simple form of permittivity tensor given by (9.122) can be realized for certain anisotropic crystals by an appropriate choice of the coordinate system. If the permittivities ϵ_x , ϵ_y , and ϵ_z are all different, then the crystal is said to be *biaxial*. If two of the three are equal, then it is said to be *uniaxial*.

To generalize the observation in Example 9.12, the phase difference between the x - and y -components of \mathbf{E} in the anisotropic medium can be expressed as

Wave plates

$$\begin{aligned} \Delta\phi &= (\omega\sqrt{\mu_0\epsilon_x} - \omega\sqrt{\mu_0\epsilon_y})z \\ &= \frac{\omega}{c}(\sqrt{\epsilon_{rx}} - \sqrt{\epsilon_{ry}})z \\ &= \frac{2\pi}{\lambda_0}(n_x - n_y)z \end{aligned} \quad (9.123)$$

where λ_0 is the free-space wavelength, and n_x and n_y are the refractive indices. The result given by (9.123) is the basis behind *wave plates* or *retardation plates*. The word *retardation* refers to the fact that the phase of one of the two components lags that of the second component. If $\Delta\phi = 2m\pi$, where m is an integer, the plate is called a *full-wave plate*. If reflections from the surfaces of the plate are considered to be negligible, as is usually the case, then it can be seen that the state of polarization of the wave at the output plane of the plate is the same as that at the input plane. For $\Delta\phi = (2m + 1)\pi$ and $(2m + 1)\pi/2$, the arrangement corresponds to *half-wave plate* and *quarter-wave plate*, respectively. A half-wave plate results in a rotation of the direction of linear polarization, as illustrated in Fig. 9.25, which corresponds to $\Delta\phi = \pi$. Note that the direction has shifted by twice the angle that it initially makes with the x - (or y -) direction. A quarter-wave plate can transform a linearly polarized wave into a circularly polarized wave.

For a different example of an anisotropic medium than that characterized by (9.122), let us consider the \mathbf{D} to \mathbf{E} relationship of the form

Circular characteristic polarizations

$$\bar{\mathbf{D}} = \epsilon\bar{\mathbf{E}} + j\epsilon_0\gamma\bar{\mathbf{B}} \times \bar{\mathbf{E}} \quad (9.124)$$

which is exhibited by certain materials when placed in a static magnetic field \mathbf{B} , where γ is a constant depending on the material. For a uniform plane wave propagating in the z -direction, and $\bar{\mathbf{B}} = B_0\mathbf{a}_z$, we have

$$\begin{aligned} \bar{D}_x &= \epsilon\bar{E}_x - j\epsilon_0\gamma B_0\bar{E}_y \\ \bar{D}_y &= j\epsilon_0\gamma B_0\bar{E}_x + \epsilon\bar{E}_y \end{aligned}$$

To find the characteristic polarizations, we set $\bar{D}_x/\bar{D}_y = \bar{E}_x/\bar{E}_y$. Thus,

$$\frac{\epsilon\bar{E}_x - j\epsilon_0\gamma B_0\bar{E}_y}{j\epsilon_0\gamma B_0\bar{E}_x + \epsilon\bar{E}_y} = \frac{\bar{E}_x}{\bar{E}_y}$$

Solving for \bar{E}_x/\bar{E}_y , we get

$$\boxed{\frac{\bar{E}_x}{\bar{E}_y} = \pm j}$$

This result corresponds to equal amplitudes of E_x and E_y and phase differences of $\pm 90^\circ$. Thus, the characteristic polarizations are both circular, rotating in opposite senses as viewed along the z -direction.

The effective permittivities of the medium corresponding to the characteristic polarizations are

$$\begin{aligned} \frac{\bar{D}_x}{\bar{E}_x} &= \frac{\varepsilon \bar{E}_x - j\varepsilon_0\gamma B_0 \bar{E}_y}{\bar{E}_x} \\ &= \varepsilon - j\varepsilon_0\gamma B_0 \frac{\bar{E}_y}{\bar{E}_x} \\ &= \varepsilon \mp \varepsilon_0\gamma B_0 \quad \text{for } \frac{\bar{E}_x}{\bar{E}_y} = \pm j \end{aligned} \quad (9.125)$$

The phase constants associated with the propagation of the characteristic waves are

$$\boxed{\beta_{\pm} = \omega \sqrt{\mu(\varepsilon \mp \varepsilon_0\gamma B_0)}} \quad (9.126)$$

where the subscripts $+$ and $-$ refer to $\bar{E}_x/\bar{E}_y = +j$ and $\bar{E}_x/\bar{E}_y = -j$, respectively.

Let us now consider the electric field of the wave to be linearly polarized in the x -direction at $z = 0$, that is,

$$\mathbf{E}(0) = E_0 \cos \omega t \mathbf{a}_x \quad (9.127)$$

Then we can express (9.127) as the superposition of two circularly polarized fields having opposite senses of rotation in the xy -plane in the manner

$$\mathbf{E}(0) = \left(\frac{E_0}{2} \cos \omega t \mathbf{a}_x + \frac{E_0}{2} \sin \omega t \mathbf{a}_y \right) + \left(\frac{E_0}{2} \cos \omega t \mathbf{a}_x - \frac{E_0}{2} \sin \omega t \mathbf{a}_y \right) \quad (9.128)$$

The circularly polarized field inside the first pair of parentheses on the right side of (9.128) corresponds to

$$\frac{\bar{E}_x}{\bar{E}_y} = \frac{E_0/2}{-jE_0/2} = +j$$

whereas that inside the second pair of parentheses corresponds to

$$\frac{\bar{E}_x}{\bar{E}_y} = \frac{E_0/2}{jE_0/2} = -j$$

Assuming propagation in the positive z -direction, the field at an arbitrary value of z is then given by

$$\begin{aligned}
 \mathbf{E}(z) &= \left[\frac{E_0}{2} \cos(\omega t - \beta_+ z) \mathbf{a}_x + \frac{E_0}{2} \sin(\omega t - \beta_+ z) \mathbf{a}_y \right] \\
 &\quad + \left[\frac{E_0}{2} \cos(\omega t - \beta_- z) \mathbf{a}_x - \frac{E_0}{2} \sin(\omega t - \beta_- z) \mathbf{a}_y \right] \\
 &= \left[\frac{E_0}{2} \cos\left(\omega t - \frac{\beta_+ + \beta_-}{2} z - \frac{\beta_+ - \beta_-}{2} z\right) \mathbf{a}_x \right. \\
 &\quad \left. + \frac{E_0}{2} \sin\left(\omega t - \frac{\beta_+ + \beta_-}{2} z - \frac{\beta_+ - \beta_-}{2} z\right) \mathbf{a}_y \right] \\
 &\quad + \left[\frac{E_0}{2} \cos\left(\omega t - \frac{\beta_+ + \beta_-}{2} z + \frac{\beta_+ - \beta_-}{2} z\right) \mathbf{a}_x \right. \\
 &\quad \left. - \frac{E_0}{2} \sin\left(\omega t - \frac{\beta_+ + \beta_-}{2} z + \frac{\beta_+ - \beta_-}{2} z\right) \mathbf{a}_y \right] \\
 &= \left[E_0 \cos\left(\frac{\beta_- - \beta_+}{2} z\right) \mathbf{a}_x \right. \\
 &\quad \left. + E_0 \sin\left(\frac{\beta_- - \beta_+}{2} z\right) \mathbf{a}_y \right] \cos\left(\omega t - \frac{\beta_+ + \beta_-}{2} z\right)
 \end{aligned} \tag{9.129}$$

The result given by (9.129) indicates that the x - and y -components of the field are in phase at any given value of z . Hence, the field is linearly polarized for all values of z . The direction of polarization is, however, a function of z since $\tan^{-1}(E_y/E_x)$, the angle made by the field vector with the x -axis, is $[(\beta_- - \beta_+)/2]z$. Thus, the direction of polarization rotates linearly with z at a rate of $(\beta_- - \beta_+)/2$. This phenomenon is known as *Faraday rotation* and is illustrated with the aid of the sketches in Fig. 9.26. The sketches in any given column correspond to a fixed value of z whereas the sketches in a given row correspond to a fixed value of t . At $z = 0$, the field is linearly polarized in the x -direction and is the superposition of two counterrotating circularly polarized fields, as shown by the time series of sketches in the first column. If the medium is isotropic, the two counterrotating circularly polarized fields undergo the same amount of phase lag with z and the field remains linearly polarized in the x -direction, as shown by the dashed lines in the second and third columns. For the case of the anisotropic medium, the two circularly polarized fields undergo different amounts of phase lag with z . Hence, their superposition results in a linear polarization making an angle with the x -direction and increasing linearly with z , as shown by the solid lines in the second and third columns.

Faraday rotation

The phenomenon of Faraday rotation that we have just discussed forms the basis for a number of devices. A simple example is illustrated by the magneto-optical switch. The magneto-optical switch is a device for modulating a laser beam by switching an electric current on and off. The electric current generates

Magneto-optical switch

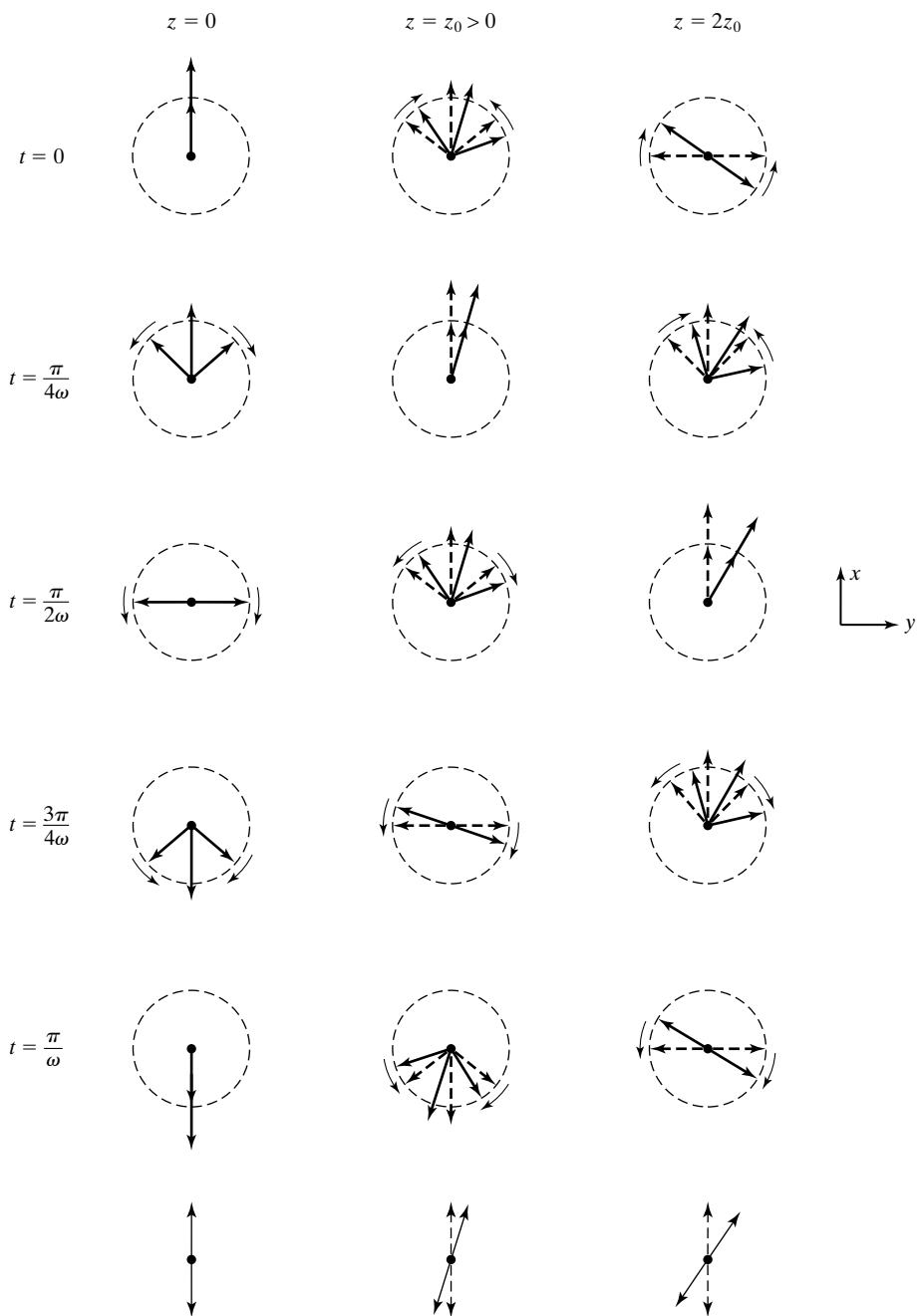


FIGURE 9.26 For illustrating the phenomenon of Faraday rotation.

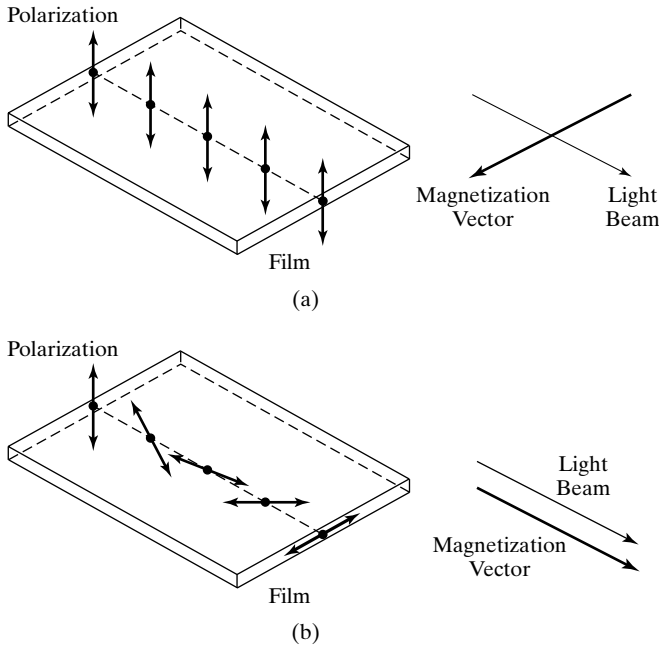


FIGURE 9.27
For illustrating the principle of operation of a magneto-optical switch.

a magnetic field that rotates the magnetization vector in a magnetic iron-garnet film on a substrate of garnet in the plane of the film through which a light wave passes. When it enters the film, the light wave field is linearly polarized normal to the plane of the film. If the current in the electric circuit is off, the magnetization vector is normal to the direction of propagation of the wave and the wave emerges out of the film without change of polarization, as shown in Fig. 9.27(a). If the current in the electric circuit is on, the magnetization vector is parallel to the direction of propagation of the wave, and the light wave undergoes Faraday rotation and emerges out of the film with its polarization rotated by 90° , as shown in Fig. 9.27(b). After it emerges out of the film, the light beam is passed through a polarizer, which has the property of absorbing light of the original polarization but passing through the light of the 90° -rotated polarization. Thus, the beam is made to turn on and off by the switching on and off of the current in the electric circuit. In this manner, any coded message can be made to be carried by the light beam.

K9.7. Anisotropic dielectric materials; Characteristic polarizations; Wave plates; Faraday rotation.

D9.11. At $\lambda_0 = 0.633 \mu\text{m}$, the refractive indices of mica are given by $n_x = 1.594$ (fast axis) and $n_y = 1.599$ (slow axis). Find the following: **(a)** the minimum thickness of a mica sheet to act as a half-wave plate; **(b)** the number of wavelengths undergone by the wave in the thickness of the plate for the x -polarization; and **(c)** the number of wavelengths undergone by the wave in the thickness of the plate for the y -polarization.

Ans. **(a)** $63.3 \mu\text{m}$; **(b)** 159.4; **(c)** 159.9.

SUMMARY

In this chapter, we extended the treatment of the parallel-plate waveguide to the rectangular waveguide, which is a metallic pipe of rectangular cross section. By considering a rectangular waveguide of cross-sectional dimensions a and b , we discussed transverse electric, or TE, modes, as well as transverse magnetic or TM modes, and learned that although TE $_{m,n}$ modes can include values of m or n equal to zero, TM $_{m,n}$ modes require that both m and n be nonzero, where m and n refer to the number of one-half sinusoidal variations of the fields along the dimensions a and b , respectively. The cutoff wavelengths for the TE $_{m,n}$ or TM $_{m,n}$ modes are given by

$$\lambda_c = \frac{1}{\sqrt{(m/2a)^2 + (n/2b)^2}}$$

The mode that has the largest cutoff wavelength or the lowest cutoff frequency is the dominant mode, which here is the TE $_{1,0}$ mode.

By placing perfect conductors in two transverse planes of a rectangular waveguide separated by an integer multiple of one-half the guide wavelength, we introduced the cavity resonator, which is the microwave counterpart of the lumped parameter resonant circuit encountered in low-frequency circuit theory. For a rectangular cavity resonator having dimensions a , b , and d , the frequencies of oscillation for the TE $_{m,n,l}$ or TM $_{m,n,l}$ modes are given by

$$f_{\text{osc}} = \frac{1}{\sqrt{\mu\epsilon}} \sqrt{\left(\frac{m}{2a}\right)^2 + \left(\frac{n}{2b}\right)^2 + \left(\frac{l}{2d}\right)^2}$$

where l refers to the number of one-half sinusoidal variations of the fields along the dimension d .

Next we introduced the cylindrical waveguide, which is a metallic pipe of cylindrical cross section. We learned that guided modes in the cylindrical waveguide are characterized by field variations in the radial direction in accordance with Bessel functions and sinusoidal variations in the angular direction. The modes are designated as TE $_{n,m}$ and TM $_{n,m}$, where the first subscript refers to the angular variations and the second to the radial variations. The TE $_{1,1}$ mode is the dominant mode. We also discussed the cylindrical cavity resonator formed by placing perfect conductors in two transverse planes of the guide, as in the case of the rectangular cavity resonator.

We then considered losses in waveguides and resonators and discussed by means of examples the determination of the attenuation constant for a propagating mode in a waveguide and the Q factor, a measure of frequency selectivity, for an oscillating mode in a resonator.

Proceeding further, we introduced the optical fiber, which consists typically of a core and a cladding having circular cross sections. By assuming the cladding region to extend to infinity so that the situation corresponds to one of a cylindrical dielectric rod, we carried out the field analysis and learned that in addition to TE ($E_z = 0$) and TM ($H_z = 0$) modes, the fields correspond to the

so-called hybrid modes, designated HE and EH. For the hybrid modes, both E_z and H_z are not equal to zero; however, for the HE modes, H_z is predominant, whereas for the EH modes, E_z is predominant. In fact, the dominant mode is the $HE_{1,1}$ mode, having no cutoff. For single-mode operation at a given wavelength λ_0 , the condition is given by

$$V = \frac{2\pi a}{\lambda_0}(\text{NA}) < 2.405$$

where a is the radius of the core, and NA is the numerical aperture given by

$$\text{NA} = \sqrt{n_1^2 - n_2^2}$$

n_1 and n_2 being the refractive indices of the core and the cladding, respectively. For weak guidance ($n_1 \approx n_2$), the modes are designated LP, with $LP_{0,1}$ mode corresponding to the $HE_{1,1}$ mode.

We then extended our discussion of dispersion in the previous chapter to the propagation of a signal with a pulse envelope, to study the phenomenon of pulse broadening in a dispersive medium. In particular, we considered a signal with a Gaussian pulse envelope and derived the expression for the *pulse broadening parameter*, which governs the pulse spread with distance in the medium. Following a brief discussion of the types of dispersion in optical waveguides, we derived the expression for the pulse broadening parameter for the case of material dispersion and discussed dispersion characteristics due to material dispersion in fused silica.

Next we turned our attention to two related topics, interference and diffraction, which are both based on superposition of waves. Although the distinction is not sharp, interference usually applies to the interaction of only a few light beams with one another, whereas diffraction usually pertains to the superposition of a large number, even a continuous distribution, of beams. We discussed interference by considering (a) the two-beam interference experiment of Thomas Young and (b) multiple-beam interference due to plane wave incidence obliquely on a plane dielectric slab, the latter arrangement constituting a model for the Fabry–Perot etalon or interferometer. For diffraction, we introduced the Huygens–Fresnel principle, according to which each point on a wavefront generates a spherical wave, and illustrated its application by considering the example of a plane wave incident on a circular aperture in a screen. By investigating diffraction along the axis of the aperture, we discussed briefly Fresnel versus Fraunhofer diffraction.

Finally, we discussed the topic of wave propagation in an anisotropic medium. By considering the example of a uniform plane wave that is incident normally along a principal axis of a uniaxial crystal, thereby resulting in the characteristic polarizations to be linear, we illustrated the principle behind wave plates or retardation plates. By means of another example of an anisotropic medium for which the characteristic polarizations are circular, we introduced Faraday rotation, which is the phenomenon of rotation of the direction of polarization of

a linearly polarized wave as it propagates in the medium, and discussed the operation of a magneto-optical switch, a device employing Faraday rotation for modulating a light beam.

REVIEW QUESTIONS

- Q9.1.** Discuss the nomenclature associated with the modes of propagation in a rectangular waveguide.
- Q9.2.** Explain the relationship between the cutoff wavelength and the dimensions of a rectangular waveguide based on the phenomenon at cutoff.
- Q9.3.** Briefly outline the procedure for deriving the expressions for TE mode fields in a rectangular waveguide.
- Q9.4.** Compare and contrast TE and TM modes in a rectangular waveguide.
- Q9.5.** What is the dominant mode? Which one of the rectangular waveguide modes is the dominant mode?
- Q9.6.** Why is the dimension b of a rectangular waveguide generally chosen to be less than or equal to one-half the dimension a ?
- Q9.7.** What is a cavity resonator?
- Q9.8.** How do the dimensions of a rectangular cavity resonator determine the frequencies of oscillation of the resonator?
- Q9.9.** Briefly outline the procedure for deriving the expressions for the TE and TM mode fields in a cylindrical waveguide.
- Q9.10.** Compare and contrast TE and TM modes in a cylindrical waveguide.
- Q9.11.** Which one of the cylindrical waveguide modes is the dominant mode?
- Q9.12.** Discuss the basis for the computation of power loss associated with slightly imperfect conductors making up the walls of a waveguide.
- Q9.13.** Briefly outline the procedure for determining the attenuation constant for a propagating mode in a waveguide with slightly imperfect conductors.
- Q9.14.** How is the Q factor of a resonator defined? Briefly outline the procedure for the determination of the Q factor of a cavity resonator with slightly imperfect conductors.
- Q9.15.** Provide a brief description of the optical fiber.
- Q9.16.** Outline the steps involved in obtaining the guidance condition for a wave along a cylindrical dielectric rod surrounded by a cladding region extending to infinity.
- Q9.17.** What are hybrid modes? Why do they arise for guided waves in an optical fiber but not for those in a cylindrical metallic waveguide?
- Q9.18.** Discuss the condition for single-mode operation of an optical fiber.
- Q9.19.** Discuss the heuristic explanation for pulse broadening in a dispersive medium.
- Q9.20.** Outline the analysis for a signal with a Gaussian envelope for studying pulse broadening in a dispersive medium.
- Q9.21.** Discuss the *pulse broadening parameter* associated with the propagation of a signal with Gaussian envelope in a dispersive medium.
- Q9.22.** Briefly discuss the types of dispersion in optical waveguides.
- Q9.23.** Outline the derivation of the pulse broadening parameter for material dispersion.

- Q9.24.** Discuss the *dispersion coefficient* associated with material dispersion, by considering the example of fused silica.
- Q9.25.** What is interference? Under what condition(s) do two waves not produce interference?
- Q9.26.** Describe Young's two-beam interference experiment.
- Q9.27.** Discuss the phenomenon of multiple-beam interference resulting from the incidence of a uniform plane wave obliquely on a plane dielectric slab and its application to the Fabry–Perot etalon.
- Q9.28.** What is diffraction? Compare and contrast the phenomenon of diffraction with the principle of geometrical optics.
- Q9.29.** Describe the Huygens–Fresnel principle for the solution of a diffraction problem.
- Q9.30.** Using the example of diffraction along the axis of a circular aperture in a plane screen, discuss Fresnel versus Fraunhofer diffraction.
- Q9.31.** When does a wave propagate in an anisotropic medium without change in its polarization?
- Q9.32.** Discuss the principle behind wave plates, providing specific examples.
- Q9.33.** What is Faraday rotation? When does Faraday rotation take place in an anisotropic medium?
- Q9.34.** Consult appropriate reference books and list three applications of Faraday rotation.
- Q9.35.** What is a magneto-optical switch? Discuss its operation.

PROBLEMS

Section 9.1

- P9.1. Finding propagating modes and their characteristics for a rectangular waveguide.** For a rectangular waveguide of dimensions $a = 3.75$ cm and $b = 1.25$ cm, and having a dielectric of $\epsilon = 6.25\epsilon_0$ and $\mu = \mu_0$, find all propagating modes for $f = 5000$ MHz, and, for each mode, find the values of β_z , λ_g , v_{pz} , and η_g .
- P9.2. Design of a square waveguide for $TM_{1,1}$ mode propagation.** Consider propagation of TM waves of frequency $f = 6000$ MHz in an air-dielectric waveguide of square cross section ($b = a$). Find the range of a for which the $TM_{1,1}$ mode propagates with a 20% safety factor ($f > 1.20f_c$) but also such that f is at least 20% below the f_c of the next higher-order mode.
- P9.3. Application of transmission-line analogy to a rectangular waveguide system.** A rectangular waveguide of dimensions $a = 3$ cm and $b = 1.5$ cm has a dielectric discontinuity, as shown in Fig. 9.28. A $TE_{1,0}$ wave of frequency 6000 MHz is incident on the discontinuity from the free-space side. **(a)** Find the SWR in the free-space section. **(b)** Find the length and the permittivity of a quarter-wave section required to achieve a match between the two media. Assume $\mu = \mu_0$ for the quarter-wave section.

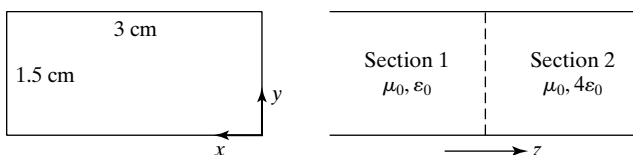


FIGURE 9.28

For Problem P9.3.

P9.4. Application of transmission-line analogy to a rectangular waveguide system. A rectangular waveguide of dimensions $a = 4$ cm and $b = 2$ cm has dielectric discontinuity, as shown in Fig. 9.29. A $TM_{1,1}$ wave of frequency 10,000 MHz is incident on the discontinuity from the free-space side. **(a)** Find the SWR in the free-space section. **(b)** Find the length and the permittivity of a quarter-wave section required to achieve a match between the two media. Assume $\mu = \mu_0$ for the quarter-wave section.

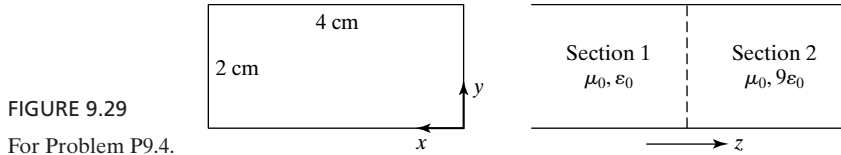


FIGURE 9.29
For Problem P9.4.

P9.5. Alternated-section transformer matching arrangement in a rectangular waveguide system. Consider the use of the alternated-section transformer arrangement (see Problem P7.23) to achieve a match between two sections of a rectangular waveguide, as shown in Fig. 9.30. Find the minimum values of l_2 and l_3 in centimeters to achieve the desired match for $TE_{1,0}$ mode at a frequency $f = 6000$ MHz.

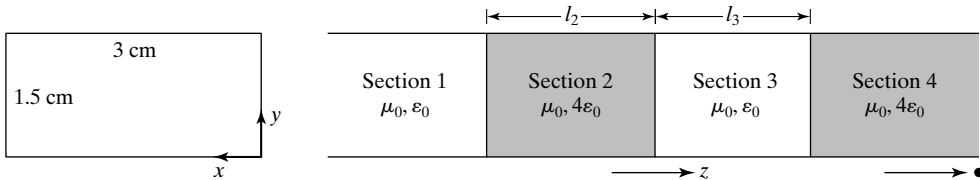


FIGURE 9.30
For Problem P9.5.

P9.6. Transparency of dielectric slab in an air–dielectric rectangular waveguide. A dielectric slab of thickness 4 cm and permittivity $2.25\epsilon_0$ exists in an air–dielectric rectangular waveguide of dimensions $a = 3$ cm and $b = 1.5$ cm, as shown in Fig. 9.31. Find the lowest frequency for which the dielectric slab is

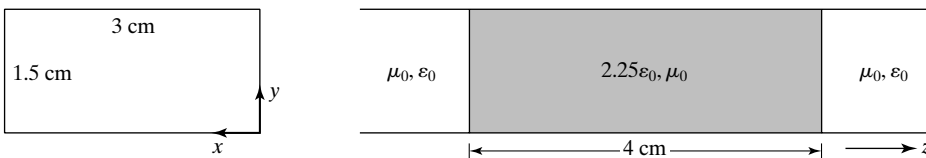


FIGURE 9.31
For Problem P9.6.

transparent (i.e., allows complete transmission) for $TE_{1,0}$ mode propagation in the waveguide.

- P9.7. Finding the frequencies of oscillation for a rectangular cavity resonator.** For a rectangular cavity resonator having the dimensions $a = 2.5$ cm, $b = 2$ cm, and $d = 5$ cm, and filled with a dielectric of $\epsilon = 2.25\epsilon_0$ and $\mu = \mu_0$, find the five lowest frequencies of oscillation. Identify the mode(s) for each frequency.
- P9.8. Finding the frequencies of oscillation for a cubical cavity resonator.** For an air-dielectric cubical cavity resonator having the dimensions $a = b = d = 5$ cm, find the three lowest frequencies of oscillation. Identify the mode(s) for each frequency.

Section 9.2

- P9.9. Finding propagating modes and their characteristics for a cylindrical waveguide.** For a cylindrical waveguide of radius $a = 3$ cm and having a dielectric of $\epsilon = 2.25\epsilon_0$ and $\mu = \mu_0$, find the propagating modes for a signal of frequency 5.0 GHz. For each of the propagating modes, find and tabulate the values of f_c , λ_c , λ_g , v_{pz} , and η_g , as in Table 9.4.
- P9.10. Finding cutoff frequencies for a cylindrical sector waveguide.** An air-dielectric waveguide has the cross section shown in Fig. 9.32. For the radius $a = 3$ cm, determine the lowest two cutoff frequencies and identify the corresponding modes.

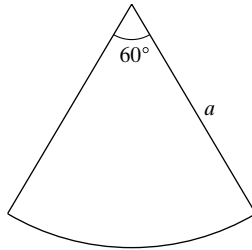


FIGURE 9.32
For Problem P9.10.

- P9.11. Alternated-section transformer matching arrangement in a cylindrical waveguide system.** Consider the use of the alternated-section transformer arrangement (see Problem P7.23) to achieve a match between two sections of a cylindrical waveguide, as shown in Fig. 9.33. Find the minimum values of l_2 and

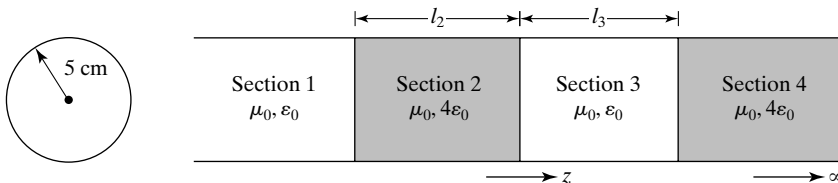


FIGURE 9.33
For Problem P9.11.

l_3 in centimeters to achieve the desired match for $TE_{1,1}$ mode at a frequency $f = 3$ GHz.

- P9.12. Alternated-section transformer matching arrangement in a cylindrical waveguide system.** Repeat Problem P9.11 for $TM_{0,1}$ mode.
- P9.13. Finding the frequencies of oscillation for a cylindrical cavity resonator.** A cylindrical cavity resonator is formed by placing two perfectly conducting sheets 4 cm apart in the cross-sectional planes of the cylindrical waveguide of Problem P9.9. Find the five lowest frequencies of oscillation and identify the mode(s) of oscillation for each frequency.
- P9.14. A cylindrical cavity resonator with three sections.** Consider $TE_{n,m}$ modes bouncing between the walls $z = 0$ and $z = 2d$ of a cylindrical cavity resonator of radius a with the end regions $0 < z < t$ and $(2d - t) < z < 2d$ filled with a nonmagnetic ($\mu = \mu_0$), perfect dielectric of permittivity ϵ_1 , and the region $t < z < (2d - t)$ filled with a nonmagnetic, perfect dielectric of permittivity ϵ_2 . **(a)** Obtain the condition for oscillation. **(b)** Compute the lowest resonant frequency for $a = 5$ cm, $d = 2$ cm, $t = 1$ cm, $\epsilon_1 = 4\epsilon_0$, and $\epsilon_2 = \epsilon_0$.

Section 9.3

- P9.15. Attenuation constant for TEM wave in a parallel-plate guide with imperfect conductors.** For a parallel-plate waveguide with imperfect but good conductors of conductivity σ and spacing a , show that the attenuation constant α_c for TEM wave propagation along the guide is $1/\sigma\delta a\eta$. Compute the value of α_c for $a = 5$ cm, $f = 5000$ MHz, copper plates, and air-dielectric.
- P9.16. Attenuation constant for TE wave in a parallel-plate guide with imperfect conductors.** Repeat Problem P9.15 for TE wave propagation to show that α_c is equal to $2(f_c/f)^2/[\sigma\delta a\eta\sqrt{1 - (f_c/f)^2}]$ and compute the value of α_c for the data specified in that problem and for the $TE_{1,0}$ mode.
- P9.17. Q factor of parallel-plate resonator with imperfect conductors.** For a parallel-plate resonator consisting of two infinite, plane, perfectly conducting plates in

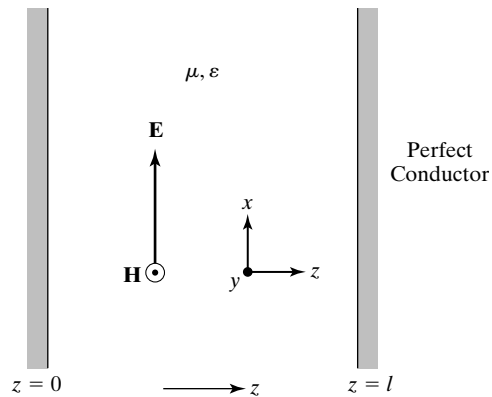


FIGURE 9.34
For Problem P9.17.

the $z = 0$ and $z = l$ planes and separated by a perfect dielectric, as shown in Fig. 9.34, the electric and magnetic fields are given by

$$\mathbf{E} = E_0 \sin \frac{n\pi z}{l} \sin \frac{n\pi t}{l\sqrt{\mu\epsilon}} \mathbf{a}_x$$

$$\mathbf{H} = \frac{E_0}{\sqrt{\mu/\epsilon}} \cos \frac{n\pi z}{l} \cos \frac{n\pi t}{l\sqrt{\mu\epsilon}} \mathbf{a}_y$$

where $n = 1, 2, 3, \dots$ (a) Show that the energy stored in the resonator per unit area of the plates is $\frac{1}{4}\delta E_0^2 l$. (b) If the plates are made of imperfect but good conductors, show that the Q of the resonator is $l/2\delta$. (c) Compute the value of Q for the fundamental mode of oscillation ($n = 1$), for $l = 1$ cm, assuming air-dielectric and copper plates.

- P9.18. Q factor of parallel-plate resonator with lossy dielectric and imperfect conductors.** For the parallel-plate resonator of Problem P9.17, assume that the dielectric is slightly lossy with conductivity $\sigma_d \ll \omega\epsilon$. (a) Assuming the plates to be perfect conductors, show that the Q of the resonator is given by $Q_1 = \omega\epsilon/\sigma_d$. (b) If in addition to the slightly lossy dielectric, the plates are made up of imperfect but good conductors, show that the Q of the resonator is given by

$$\frac{1}{Q} = \frac{1}{Q_1} + \frac{1}{Q_2}$$

where Q_1 is as given in part (a) and Q_2 is equal to $l/2\delta$, as in Problem P9.17.

- P9.19. Q factor for $\text{TM}_{m,n,l}$ mode in a cubical cavity resonator.** Obtain the expression for the Q factor for $\text{TM}_{m,n,l}$ ($l \neq 0$) mode in a cubical cavity resonator of sides a and show that it is equal to $a/4\delta$.

Section 9.4

- P9.20. Derivation of characteristic equation for guidance of hybrid modes in an optical fiber.** Supply the missing steps in the derivation of the characteristic equation (9.81) for the case of $l \neq 0$ from the boundary conditions $\bar{E}_{z1} = \bar{E}_{z2}$, $\bar{H}_{z1} = \bar{H}_{z2}$, $\bar{E}_{z1}/\bar{H}_{\phi1} = \bar{E}_{z2}/\bar{H}_{\phi2}$, and $\bar{E}_{\phi1}/\bar{H}_{z1} = \bar{E}_{\phi2}/\bar{H}_{z2}$ at $r = a$.
- P9.21. Consistency of guidance conditions for optical fiber modes with boundary conditions.** Show that the guidance conditions (9.79)–(9.81) are consistent with the boundary conditions for r -components of the fields given by (9.77c), (9.77d), (9.78c), and (9.78d).
- P9.22. Numerical aperture of an optical fiber.** Assume that a wave is incident from air onto the core of an optical fiber at an angle θ_a , as shown by the cross-sectional view in Fig. 9.35. Show that the maximum allowable value of θ_a for guiding of the wave in the core by total internal reflection is given by

$$\sin [\theta_a]_{\max} = \sqrt{n_1^2 - n_2^2}$$

which is defined to be the numerical aperture (NA) of the optical fiber. This provides the physical interpretation for NA.

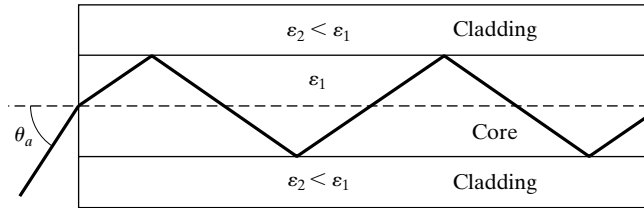


FIGURE 9.35
For Problem P9.22.

- P9.23. Alternate characteristic equation for guidance of hybrid modes in an optical fiber.** Supply the missing steps in the derivation of (9.86) from (9.81) by using (9.85a)–(9.85d). [Hint: Use (9.85b) and (9.85c) for the left side of (9.81) and (9.85a) and (9.85d) for the right side of (9.81).]
- P9.24. Maximum value of core radius for single-mode propagation in an optical fiber.** For an optical fiber with core and cladding refractive indices $n_1 = 1.50$ and $n_2 = 1.40$, find the maximum value of a/λ_0 for single-mode operation.

Section 9.5

- P9.25. Minimizing pulse half-width for a Gaussian-enveloped signal in a dispersive medium.** With reference to the result given by (9.96), show that there is an optimum pulse half-width for which the transmitted pulse half-width at a given value of z is minimized. Find the expression for this optimum pulse half-width and the corresponding transmitted pulse half-width.
- P9.26. Pulse spread due to intermodal dispersion in an optical fiber.** A measure of the pulse spread due to intermodal dispersion is provided by the difference in travel times between the longest ray path and the shortest ray path. Show that this difference per unit distance along the fiber is approximately equal to Δ/c , where $\Delta = (n_1 - n_2)$.
- P9.27. Propagation of a signal with Gaussian envelope in an optical fiber.** A signal with a Gaussian pulse envelope of half-width 5 ps propagates in an optical fiber made of fused silica with the characteristics shown in Fig. 9.18. If the wavelength of the signal is $0.8 \mu\text{m}$, obtain approximate values for (a) the time taken by the signal to propagate 1 km and (b) the half-width of the Gaussian pulse envelope of the signal at the distance of 1 km.

Section 9.6

- P9.28. Satisfaction of certain relations by Fresnel coefficients.** Verify that the Fresnel coefficients given in Section 8.5 satisfy (9.112a) and (9.112b) for both cases of the polarization of \mathbf{E}_i : (a) perpendicular and (b) parallel. Further show that (9.112b) is consistent with conservation of power flow normal to the dielectric slab.
- P9.29. Limiting frequency resolution of Fabry–Perot etalon.** Assume that the limiting frequency resolution of the Fabry–Perot etalon is defined as the separation between the two frequencies at which I_t/I_i is $\frac{1}{2}$. Then, assuming further

that this frequency difference is small compared to the frequency range, $\Delta f = c/(2nd \cos \theta_t)$, between two adjacent peaks of the interference pattern for fixed d and θ_t , show that it is equal to $\Delta f/F$.

- P9.30. Boundary between Fresnel and Fraunhofer diffraction regions.** The boundary between the Fresnel and Fraunhofer diffraction regions is determined by the maximum allowable departure of the phase of the waves emanating from the aperture and arriving at the observation point (and hence, vice versa) from that of a plane wave. For a maximum allowable departure of $\pi/8$, which is the value used in practice, show by considering the circular aperture that the boundary between the two regions is $2D^2/\lambda$, where D is the diameter of the hole.

Section 9.7

- P9.31. Propagation of a uniform plane wave along a principal axis of an anisotropic dielectric.** For all three cases in Example 9.12, find the expressions for the incident, reflected, and transmitted wave magnetic fields.
- P9.32. Angle between \mathbf{E} and \mathbf{H} for plane-wave propagation in an anisotropic medium.** Show that for plane wave propagation in an anisotropic medium, the angle between \mathbf{E} and \mathbf{H} is not in general equal to 90° . For the anisotropic medium of Example 9.12, find the angle between \mathbf{E} and \mathbf{H} at $z = 0+$, for $E_2 = E_1 = E_0$ in case 3.
- P9.33. Normal incidence of a uniform plane wave on an anisotropic perfect dielectric.** Medium 1 ($z < 0$) is free space, whereas medium 2 ($z > 0$) is a nonmagnetic ($\mu = \mu_0$), anisotropic perfect dielectric characterized by

$$[\boldsymbol{\varepsilon}] = \varepsilon_0 \begin{bmatrix} 6.25 & 0 & 0 \\ 0 & 2.25 & 0 \\ 0 & 0 & 6.25 \end{bmatrix}$$

For a uniform plane wave having the electric field

$$\mathbf{E}_i = E_0[\cos(6\pi \times 10^8 t - 2\pi z) \mathbf{a}_x + \sin(6\pi \times 10^8 t - 2\pi z) \mathbf{a}_y]$$

incident on the interface $z = 0$ from medium 1, find the following: **(a)** the reflected wave electric and magnetic fields; and **(b)** the transmitted wave electric and magnetic fields.

- P9.34. Normal incidence of a uniform plane wave on an anisotropic perfect dielectric.** Medium 1 ($z < 0$) is free space, whereas medium 2 ($z > 0$), is a nonmagnetic ($\mu = \mu_0$) anisotropic perfect dielectric characterized by

$$[\boldsymbol{\varepsilon}] = \varepsilon_0 \begin{bmatrix} 8 & 2 & 0 \\ 2 & 5 & 0 \\ 0 & 0 & 4 \end{bmatrix}$$

A uniform plane wave having the electric field

$$\mathbf{E}_i = E_0 \cos(6\pi \times 10^9 t - 20\pi z) \mathbf{a}_x$$

is incident on the interface $z = 0$ from medium 1. Obtain the reflected and transmitted wave electric and magnetic fields.

P9.35. Uniform plane-wave propagation through an anisotropic perfect dielectric slab.

In Fig. 9.36, medium 2 is a nonmagnetic ($\mu = \mu_0$), anisotropic perfect dielectric characterized by

$$[\boldsymbol{\varepsilon}] = \varepsilon_0 \begin{bmatrix} 4 & 0 & 0 \\ 0 & 16 & 0 \\ 0 & 0 & 4 \end{bmatrix}$$

A circularly polarized uniform plane wave having the electric field

$$\mathbf{E}_i = E_0 [\cos(6\pi \times 10^9 t - 2\pi z) \mathbf{a}_x + \sin(6\pi \times 10^9 t - 2\pi z) \mathbf{a}_y]$$

is incident normally onto medium 2 from medium 1. **(a)** Find the minimum value of L , the thickness of medium 2, for which the reflected wave is linearly polarized. **(b)** Find the reflected wave electric field for the value of L in (a). **(c)** Find the minimum value of L for which there is no reflected wave.

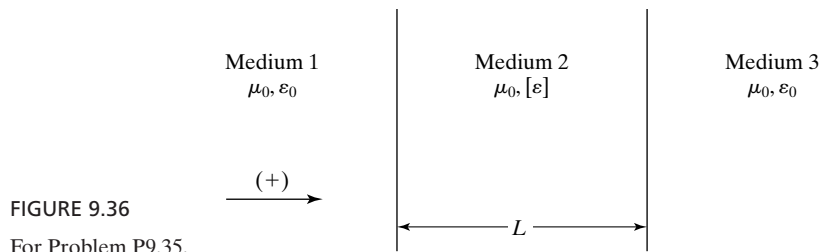


FIGURE 9.36
For Problem P9.35.

P9.36. Faraday rotating power of anisotropic medium with circular characteristic polarizations. Show that for $\gamma B_0 \ll \varepsilon/\varepsilon_0$, the Faraday rotating power $(\beta_- - \beta_+)/2$ of the medium characterized by (9.124) is approximately equal to $\pi\gamma B_0/(\lambda_0 \sqrt{\varepsilon/\varepsilon_0})$.

REVIEW PROBLEMS

R9.1. Number of propagating modes in a square waveguide. Show that for a waveguide of square cross section ($a = b$), the number of propagating modes at a frequency f many times the cutoff frequency of the dominant mode is approximately equal to $2\pi\mu\varepsilon f^2 a^2$.

- R9.2. Minimizing SWR in a rectangular waveguide system using a quarter-wave section.** A rectangular waveguide system consisting of two sections is shown in Fig. 9.37. For $TE_{1,0}$ waves of frequency 5000 MHz incident from Section 1 onto the discontinuity, find the SWR in Section 1. It is desired to minimize the SWR in Section 1 by placing a $\lambda_g/4$ section of $\epsilon = 4\epsilon_0$ and $\mu = \mu_0$ at a distance d to the left of the discontinuity. **(a)** What is the length of the $\lambda_g/4$ section? **(b)** Using the Smith chart, find the minimum value of d and the value of the minimum SWR to the left of the $\lambda_g/4$ section.

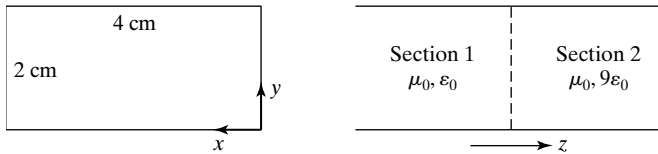


FIGURE 9.37
For Problem R9.2.

- R9.3. Frequencies of oscillation for a cylindrical sector cavity resonator.** Consider an air-dielectric cavity resonator made up by placing conductors in the $z = 0$ and $z = d$ planes of the waveguide of Problem P9.10. Determine the two lowest frequencies of oscillation for $a = 3$ cm and $d = 5$ cm, and identify the corresponding modes.
- R9.4. Attenuation constant for TM wave in a parallel-plate guide with imperfect conductors.** Repeat Problem P9.15 for TM wave propagation to show that α_c is equal to $2/[\sigma\delta a\eta\sqrt{1 - (f_c/f)^2}]$ and compute the value of α_c for the data specified in that problem and for the $TM_{1,0}$ mode.
- R9.5. Maximum value of core radius for single-mode propagation in an optical fiber.** For an optical fiber with core and cladding refractive indices $n_1 = 3.503$ and $n_2 = 3.5$, find the maximum value of the core radius for single-mode operation at $\lambda_0 = 1.2$ μm .
- R9.6. Pulse broadening due to material dispersion in a single-mode optical fiber.** A light-emitting diode at the wavelength 0.9 μm with spectral width 25 nm excites a single-mode fiber made of fused silica with the characteristics shown in Fig. 9.18. Find the approximate pulse width after broadening due to material dispersion over a distance of 1 km.
- R9.7. Diffraction of a uniform plane wave by a circular disk.** Consider the arrangement complementary to that in Example 9.11, that is, a circular disk of radius a having its center at the origin and illuminated by a plane wave of electric field intensity E_0 . Obtain the expression for the diffracted field along the axis of the disk and show that the intensity is a constant, independent of distance from the center of the disk. (*Hint:* Use the fact that for two complementary screens placed together in the same plane, no aperture exists so that no diffraction results.)
- R9.8. Uniform plane wave propagation through an anisotropic perfect dielectric slab.** In Fig. 9.38, medium 2 is a nonmagnetic ($\mu = \mu_0$), anisotropic perfect dielectric characterized by

$$[\epsilon] = \epsilon_0 \begin{bmatrix} 8 & 2 & 0 \\ 2 & 5 & 0 \\ 0 & 0 & 9 \end{bmatrix}$$

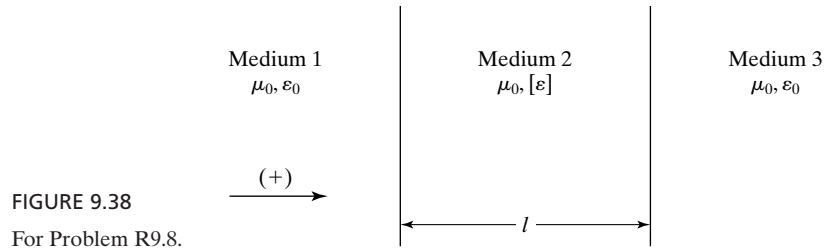


FIGURE 9.38
For Problem R9.8.

For a uniform plane wave with the electric field

$$\mathbf{E}_i = E_0 \mathbf{a}_x \cos(6\pi \times 10^8 t - 2\pi z)$$

incident on medium 2 normally on medium 1, find the following: **(a)** the reflected wave electric and magnetic fields if the thickness l of medium 2 is $\frac{1}{4}$ m and **(b)** the minimum value of l for which medium 2 is transparent for the incident wave.